USAFTPS-TIM-20A-04

Event-Based Sensor Visual-Inertial Odometry System: Have T-Rex

U S A F T P S

ANTHONY LUBY, Capt, USAF
Project Manager / Flight Test Engineer

MACIEJ HATTA, Maj, RCAF
Project Test Pilot

BRICE CASTANET, Def Civ, DGA
Project Flight Test Engineer

JASON SHANK, Maj, USAF
Project Test Pilot

KEVIN HAND, Maj, ANG
Project Test Pilot

KALYN TUNG, Capt, USAF
Project Flight Test Engineer

NOVEMBER 2020

FINAL TECHNICAL INFORMATION MEMORANDUM

UNITED STATES AIR FORCE TEST PILOT SCHOOL
AIR FORCE TEST CENTER
EDWARDS AIR FORCE BASE, CALIFORNIA
AIR FORCE MATERIEL COMMAND
UNITED STATES AIR FORCE

This technical information memorandum, (USAFTPS-TIM-20A-04) Project *Have T-Rex* was submitted under job order number MT20A400 by the Commandant, USAF Test Pilot School, Edwards AFB, California 93524-6843.

Prepared by:

ANTHONY S. LUBY, Capt, USAF
Project Manager / Flight Test Engineer

BRICE A. CASTANET, Def Civ, DGA
Project Engineer

KEVIN J. HAND, Maj, ANG
Project Pilot

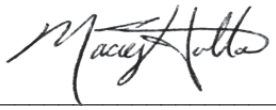

MACIEJ HATTA, Maj, RCAF
Project Pilot

JASON C. SHANK, Maj, USAF
Project Pilot

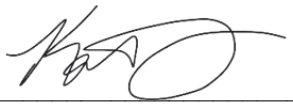

KALYN A. TUNG, Capt, USAF
Project Engineer

This memorandum has been reviewed and is approved for publication:

KOPRIVA.MICHAEL.J.1368049103 Digitally signed by KOPRIVA.MICHAEL.J.1368049103 Date: 2020.12.04 12:55:29 -08'00'

MICHAEL J. KOPRIVA, NH-03, DAF
Project Staff Advisor

CHIAWEI N. LEE, NH-03, DAF
TMP Director, USAF Test Pilot School

VANHOY.DAVID.L.1229799688 Digitally signed by VANHOY.DAVID.L.1229799688 Date: 2021.01.22 12:45:40 -08'00'

DAVID L. VANHOY, NH-04, DAF
Technical Director, USAF Test Pilot School

PABON.SEBRINA.L.1015514848 Digitally signed by PABON.SEBRINA.L.1015514848 Date: 2021.01.20 12:31:00 -08'00'

SEBRINA L. PABON, Col, USAF
Commandant, USAF Test Pilot School

REPORT DOCUMENTATION PAGE

Form Approved
OMB No. 0704-0188

PLEASE DO NOT RETURN YOUR FORM TO THE ABOVE ORGANIZATION.

1. REPORT DATE *(DD-MM-YYYY)*	**2. REPORT TYPE**	**3. DATES COVERED** *(From - Through)*
07-12-2020	Final Technical Information	08 Sept – 21 Sept 2020

4. TITLE AND SUBTITLE

Event-Based Sensor Visual-Inertial Odometry System:
Have T-Rex

5A. CONTRACT NUMBER

5B. GRANT NUMBER

5C. PROGRAM ELEMENT NUMBER

6. AUTHOR(S)
Hand, Kevin J, Major, USAF
Hatta, Maciej, Major, RCAF
Shank, Jason C, Major, USAF
Luby, Anthony S, Captain, USAF
Tung, Kalyn A, Captain, USAF
Castanet, Brice A, Def Civ, DGA

5D. PROJECT NUMBER
MT20A4000

5E. TASK NUMBER

5F. WORK UNIT NUMBER

7. PERFORMING ORGANIZATION NAME(S) AND ADDRESS(ES)
Air Force Test Center
412th Test Wing
USAF Test Pilot School
Edwards AFB CA 93524-6485

8. PERFORMING ORGANIZATION REPORT NUMBER

USAFTPS-TIM-20A-04

9. SPONSORING / MONITORING AGENCY NAME(S) AND ADDRESS(ES)
Dr. Robert Leishman
2950 Hobson Way
Wright-Patterson Air Force Base, OH 45433-7765

10. SPONSOR/MONITOR'S ACRONYM(S)

11. SPONSOR/MONITOR'S REPORT NUMBER(S)

12. DISTRIBUTION / AVAILABILITY STATEMENT
DISTRIBUTION A. Unlimited distribution. See disclaimer on cover.

13. SUPPLEMENTARY NOTES
SC: 012100 CA: 412th Test Wing Edwards AFB CA Print this document in COLOR.

14. ABSTRACT

This report presents the results of Project Have T-Rex, an evaluation of an event-based sensor (EBS) for event-based visual inertial odometry (EVIO) in a RASCAL pod on an F-16D. The LDTO was the AFTC. The ETO was the USAF TPS. The USAF TPS, Class 20A, conducted 13 test flights totaling 21.4 hours at Edwards AFB, California, from 08 to 21 September 2020. The overall test objective was to determine EVIO algorithm accuracy and collect data to support ongoing target detection and tracking algorithm development All objectives were met.

15. SUBJECT TERMS
Key words or phrases identifying major concepts in the report.
EVIO (Event-based Visual Inertial Odometry), EBS (Event Based Sensor), AltNav (Alternative Navigation), RASCAL (Reconfigurable Airborne Sensor, Communications, and Laser), F-16D

16. SECURITY CLASSIFICATION OF:			**17. LIMITATION OF ABSTRACT**	**18. NUMBER OF PAGES**	**19A. NAME OF RESPONSIBLE PERSON**
a. REPORT	**b. ABSTRACT**	**c. THIS PAGE**			Dr. Robert Leishman
U	U	U	Same as Report	98	**19B. TELEPHONE NUMBER (INCLUDE AREA CODE)** 937-255-3636 x4755

STANDARD FORM 298 (REV. 8-98)
PRESCRIBED BY ANSI STD. Z39.18

This page was intentionally left blank.

EXECUTIVE SUMMARY

This report presents the performance and results of an airborne event-based sensor for event-based visual inertial odometry under the project name *Have T-Rex*. Testing was requested by the Autonomy & Navigation Technology Center, Air Force Institute of Technology, Wright-Patterson Air Force Base, Ohio (AFIT/ANT). The lead developmental test organization was the Air Force Test Center, Edwards AFB, California. The executing test organization was the 412th Test Wing. Testing was conducted at Edwards AFB, California, by the United States Air Force Test Pilot School, Class 20A as part of a student Test Management Project. Testing was conducted from 8 September 2020 to 21 September 2020 and consisted of 21.4 flight test hours (13 sorties) in the F-16, serial number 87-0377, and 2.2 flight test support hours (2 sorties) in a T-38C as an airborne target.

The Global Position System (GPS) was the linchpin of military and commercial position, navigation, and timing applications. The performance of GPS navigation was reliant upon reliable, unobstructed reception of low power satellite signals. These signals can be easily jammed or spoofed. The AFIT Autonomy and Navigation Technology Center has invested in a variety of alternative navigation solutions to mitigate this risk. Event-based sensor visual-inertial odometry (EVIO) navigation was one such research area. Visual odometry uses cameras mounted on a vehicle to estimate its motion by identifying and tracking image features over time. Motion estimation accuracy was limited by the performance of the camera as low frames-per-second capture rates can miss critical information between frames, especially during rapid movement. Alternatively, cameras with very high capture rates require far more processing power.

The system under test (SUT) included event-based sensors (EBS) and an inertial measurement unit (IMU) in a reconfigurable airborne sensor, communications, and laser (RASCAL) pod flown on an F-16D to improve visual odometry performance. An EBS operates on a hardware implementation of intensity change detection. This operating concept increases temporal resolution and dynamic range with low power requirements, making it advantageous for rapid motion and low/varying ambient lighting conditions. The SUT's navigation algorithm processed EBS imagery to identify feature motion, supplemented with IMU data, through a Kalman Filter to predict the aircraft's position, velocity, and attitude. The SUT algorithm was not yet implemented for in-flight navigation estimation; all navigation estimates were performed post-flight.

The overall test objective was to determine EVIO algorithm accuracy and collect data to support ongoing target detection and tracking algorithm development. There were four specific test objectives: demonstrate the SUT functionality to produce a navigation solution, determine the accuracy of the navigation solution through varying flight conditions, collect operationally representative flight profile data, and collect target tracking data for future research.

Data were collected at varying altitudes (200 feet to 20,000 feet Above Ground Level) and ground speeds (250 to 520 knots), over varying terrain (sagebrush desert, urban, mountainous, lakebed), and ambient lighting conditions (day, dawn/dusk, and night). Additionally, maneuvers in pitch and roll were executed to determine the impact of dynamic maneuvering. Lastly, data were collected against airborne and ground moving targets.

The data collected showed no conclusive trends in the accuracy of the SUT in response to line of sight rate, ambient lighting conditions, terrain, or dynamic maneuvering. The persistent extremely large solution errors prevented proper investigation of how these factors influenced SUT performance. The team recommended to investigate and correct EVIO algorithm accuracy deficiencies before continuing flight test. The results show the system under test was unable to produce a reliable or useful navigational solution in the tested configurations. The results also showed that the system was able to detect airborne and ground moving targets; however, further analysis would be required to develop a target tracking algorithm.

This page was intentionally left blank.

TABLE OF CONTENTS

LIST OF ILLUSTRATIONS

LIST OF TABLES

This page was intentionally left blank.

INTRODUCTION

This report presents the performance and results of an airborne event-based sensor for event-based visual inertial odometry under the project name *Have T-Rex*. Testing was requested by the Autonomy & Navigation Technology Center, Air Force Institute of Technology, Wright-Patterson Air Force Base, Ohio. The lead developmental test organization was the Air Force Test Center, Edwards AFB, California. The executing test organization was the 412th Test Wing. Testing was conducted at Edwards AFB, California, by the United States Air Force Test Pilot School, Class 20A as part of a student Test Management Project. Testing was conducted from 8 September 2020 to 21 September 2020 and consisted of 21.4 flight test hours (13 sorties) in the F-16, serial number 87-0377, and 2.2 flight test support hours (2 sorties) in a T-38C as an airborne target.

BACKGROUND

U.S. military navigation methods were highly reliant on Global Positioning System (GPS) signals and processing to achieve the highest level of accuracy. With ever increasing threats from adversaries to these signals, AFIT/ANT invested in developing navigation solutions that offered similar accuracy to GPS and were less susceptible to jamming or spoofing.

A potential solution was visual odometry (VO), the use of visual data to estimate position and attitude change over time. VO solutions used cameras to collect imagery, then software algorithms detected and tracked features to estimate motion relative to those points of interest. An advantage of VO was that it was a passive technology that could not be easily jammed. VO could be limited by low camera sampling rates, or by the high computational processing requirements of high sampling rates. Low sampling rates caused large movements between frames or blurring of features, increasing motion estimate uncertainty. Fixed camera frame rates also limited the dynamic range of the resulting image, with particular shortcomings in high and low light conditions.

Event-based sensors (EBS) were a visual sensor technology that asynchronously responded to changes in light intensity at individual pixels, as opposed to traditional frame-based cameras that measured the absolute intensity for all pixels in every image. Events were triggered by movement in the frame, or from the camera's movement relative to the scene. EBS achieved higher temporal fidelity over a high dynamic range, up to 140 dB, compared to the 60 dB achievable by traditional frame-based cameras, according to *High Speed and High Dynamic Range Video With an Event Camera* (reference 2).

In *Smart Features for Dynamic Vision Sensors* (reference 3), previous flight testing of event-based visual inertial odometry (EVIO) systems consisted of a 14-foot unmanned aerial vehicle (UAV) that flew approximately 800 feet above ground level at 60-80 knots. The previous test resulted in approximately 86 meters of navigation estimate error after a 1,000 meters of flight in 41 seconds. This test program flew the system on a high performance aircraft in varying ambient lighting conditions to capture the most stressing VO conditions of rapid motion and low light as well as collected data for future moving targeting tracking indicators analysis.

TEST ITEM DESCRIPTION

The system under test (SUT) for this program was an AFIT/ANT developed event-based visual inertial odometry hardware and algorithm that used an event-based camera and inertial measurement unit (IMU) to estimate a vehicle's 6 degrees-of-freedom motion and attitude. The hardware components were contained in a Reconfigurable Airborne Sensor, Communications, and Laser (RASCAL) pod and flown on a F-16D. The SUT algorithms were not implemented to estimate aircraft navigation / states real-time. EBS and IMU data were processed post-flight to generate aircraft navigation estimates and compared to truth time, space,

position, information (TSPI) data. The post-flight processing was performed in the computer lab on the second floor of the Test Pilot School. The SUT generated a time tag from the GPS antenna; GPS was not used for navigation estimates. The IMU was aligned prior to take-off and received no in-flight updates. Figure 1 **Have T-Rex RASCAL Pod System Architecture**depicts the overall pod system architecture. Figure 2 **SUT Cameras within the RASCAL Pod** shows the internal cameras mounted inside the RASCAL pod. See appendix D for additional internal RASCAL pod layout.

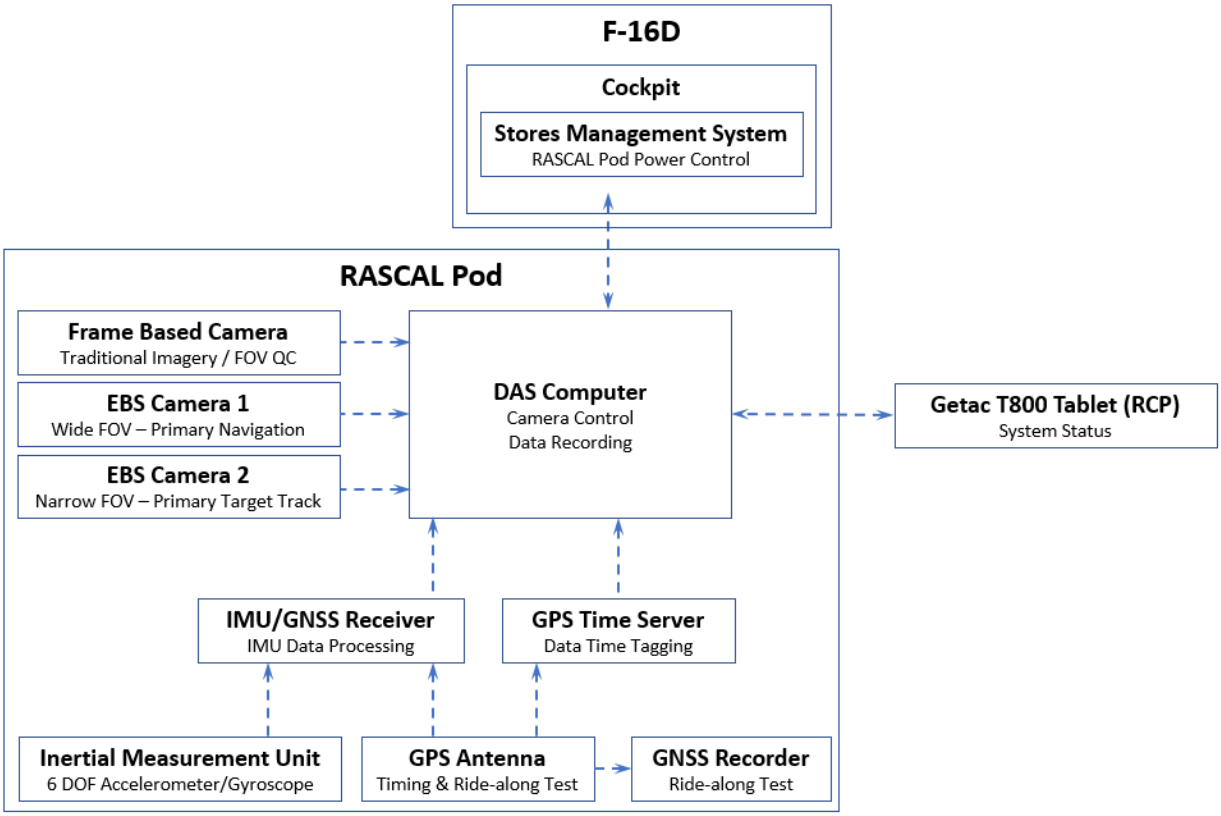

Figure 1 Have T-Rex RASCAL Pod System Architecture

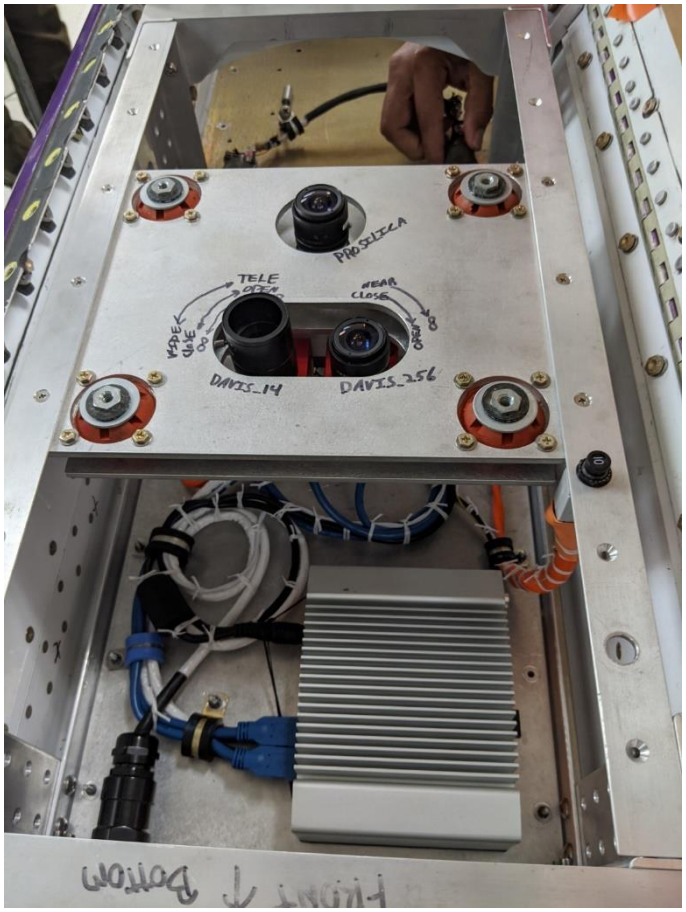

Figure 2 SUT Cameras within the RASCAL Pod

EVENT BASED SENSOR

The RASCAL pod contains two commercial off the shelf DAVIS346 EBS cameras produced by iniVation AG, appendix F, which operated in the visible spectrum with a resolution of 346 x 260 pixels. The optics on the cameras were different to achieve specific fields of view; however, the sensors were the same. The relatively low resolution sensor drove lower altitude test points to resolve expected ground features for tracking. The primary EBS camera for EVIO had a field of view of 90° x 67° while the EBS camera for target detection and tracking algorithm development had a narrower field of view of 30° x 23°. Field of view orientation is shown in Figure 3 **EBS FOV Orientation**, with the wider field of view of each camera oriented along the longitudinal axis.

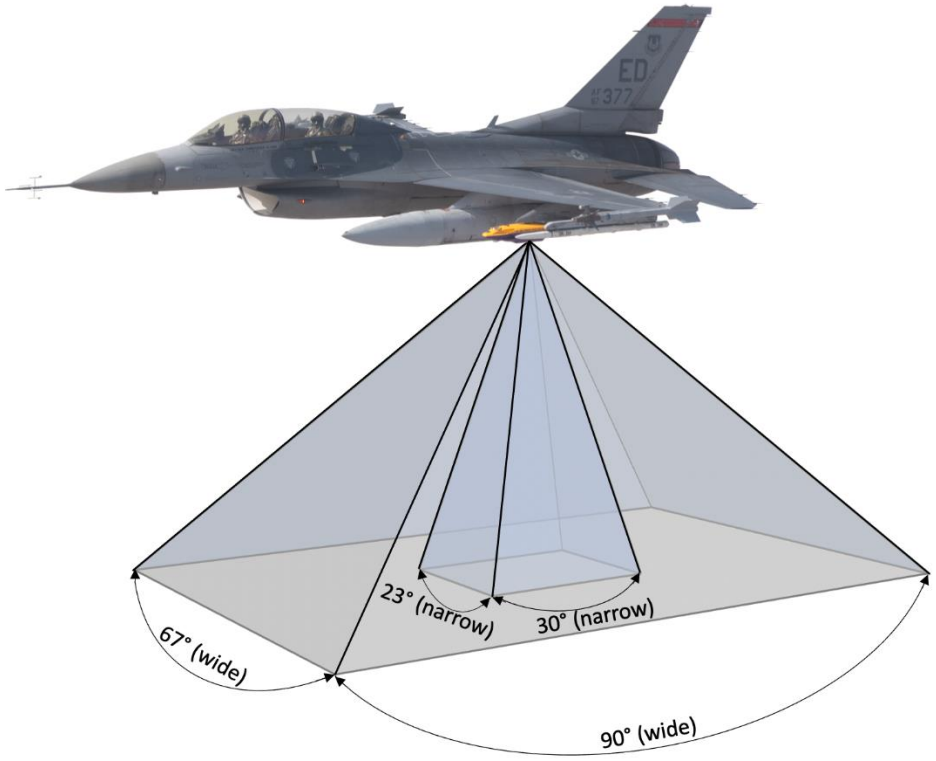

Figure 3 EBS FOV Orientation

Unlike traditional frame based cameras that synchronously measure light intensity at all pixels to generate an image at a set frame rate (e.g. 30 frames per second), each pixel in an EBS asynchronously reports changes in light intensity. Asynchronous operation and implementing change detection via hardware rather than software improves temporal resolution and dynamic range over traditional frame based cameras. Output data rate correlates to motion and scene spatial content, with rapid motion or highly textured scenes resulting in higher data rates compared to uniform scenes or low line of sight rates. Figure 4 **Event-Based Sensor Pixel Output Example**illustrates the output behavior of an EBS pixel. Each dot is an event that is encoded with the time, pixel location, and the sign of brightness change. The "on" and "off" define the type of change, "on" being an increase in intensity and "off" a decrease in intensity. In flight pictures shown in Figure 5 **Example Traditional Frame-Based Image (top) and Event-Based Sensor Output (bottom)** demonstrated this concept and highlighted the intensity changes compared to a traditional frame-based image.

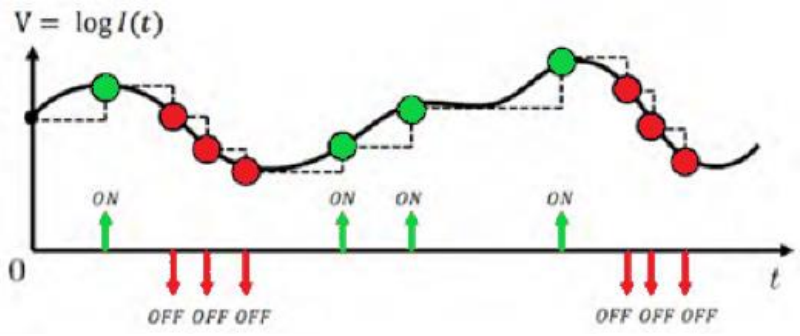

Figure 4 Event-Based Sensor Pixel Output Example

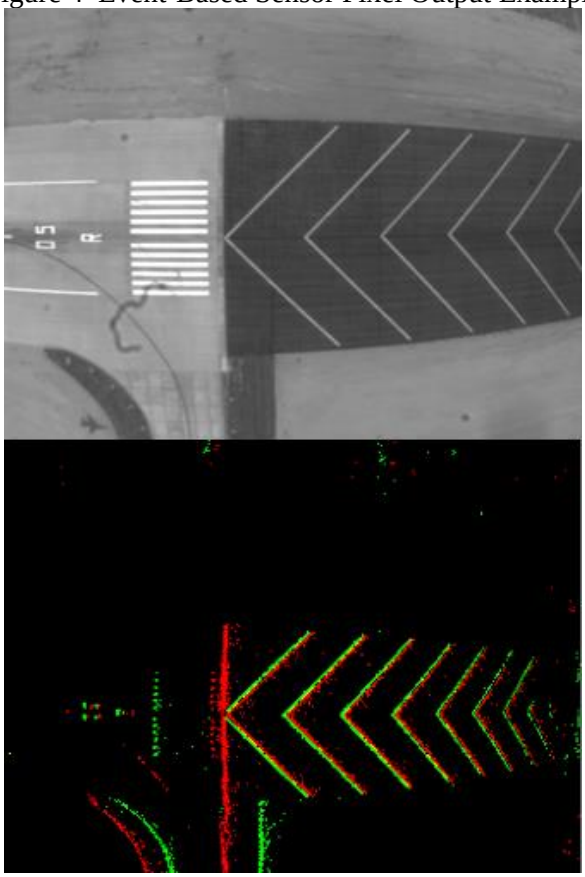

Figure 5 Example Traditional Frame-Based Image (top) and Event-Based Sensor Output (bottom)

ALGORITHM OPERATION

The event stream output of EBS cameras required the development of data processing algorithms to realize EVIO. Utilizing the EBS event stream directly would have required completely new processing techniques to discern features and estimate motion, but there was an extensive body of research in visual odometry using traditional frame based imagery that AFIT/ANT used as the basis for their algorithm. This test supported research along multiple lines of development, and the algorithm implemented in the SUT is summarized in Figure 6 **Post-Processing Navigation Estimate Software Architecture**below.

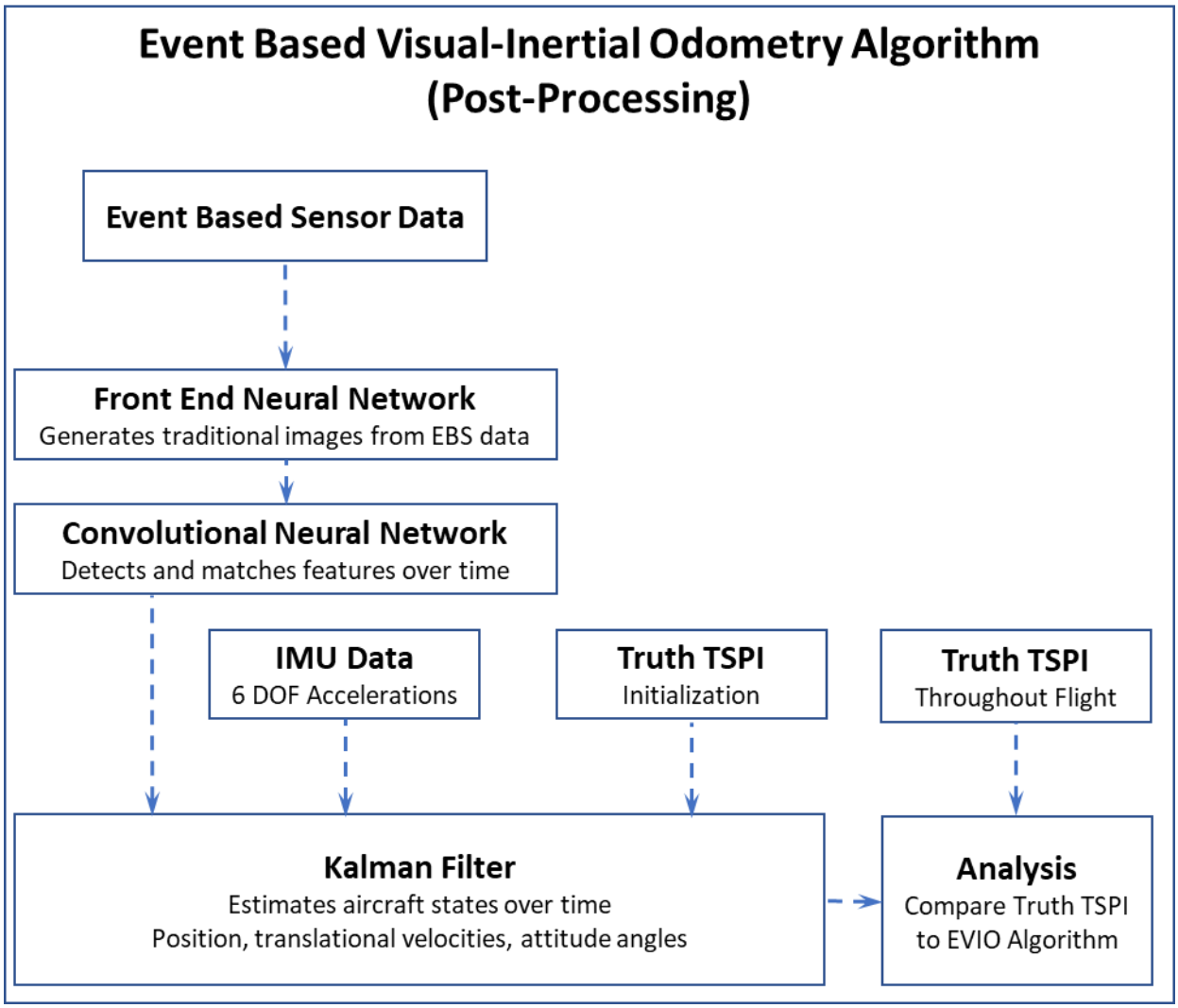

Figure 6 Post-Processing Navigation Estimate Software Architecture

The SUT implemented a recurrent convolutional neural network serially to generate traditional image frames from the EBS event data stream. This enabled the use of existing frame based visual odometry algorithms. A second neural network within the Kalman filter estimated aircraft motion by tracking features in the images generated by the first network over time. *What Is a Neural Network?* (reference 5) described a neural network as an adaptive system defined by the structure of nodes and the weights that connect them. The neural network broke down the input into layers of abstraction. Its behavior was defined by the way its individual nodes were connected and by the weights of those connections. These weights were automatically adjusted during training according to a specific learning rule until the artificial neural network performed the desired task correctly. It could be trained using many examples to recognize patterns in images.

The front end recurrent-convolutional neural network developed by Rebecq et. al (reference 2) took the events from the event based sensor, which were encoded with the time, pixel location, and change in polarity to generate image frames at a comparable rate of >5,000 frames per second. Although this was the theoretical frame rate, the actual system generated 20 frames per second (20 Hz) due to Kalman filter algorithm design limitations. The neural network integrated over a stream of events to predict an image

based on the previous state. The neural network used supervised training on 1,000 simulated sequences of event data with corresponding ground truth videos, in addition to using post-processing to normalize the output images to increase the contrast in low contrast images. The front end neural network was not trained for this specific SUT. Rebecq et. al (reference 2) provided the trained neural network based on event data simulated from Microsoft Common Objects in Context 2014 images which were then used to reconstruct the actual Microsoft Common Objects in Context 2014 images. No aerial or overhead imagery was used to train the neural network.

Usage of the neural network to convert EBS data to traditional images allowed AFIT to leverage existing computer vision and visual odometry research while retaining the dynamic range advantages of EBS. An example image frame generated from event data compared to a traditional frame-based camera is depicted in Figure 7 **Example Traditional Frame-Based Image (left), Event-Based Sensor Output (center), and Neural Network Event-Based Sensor Image Reconstruction (right)**.

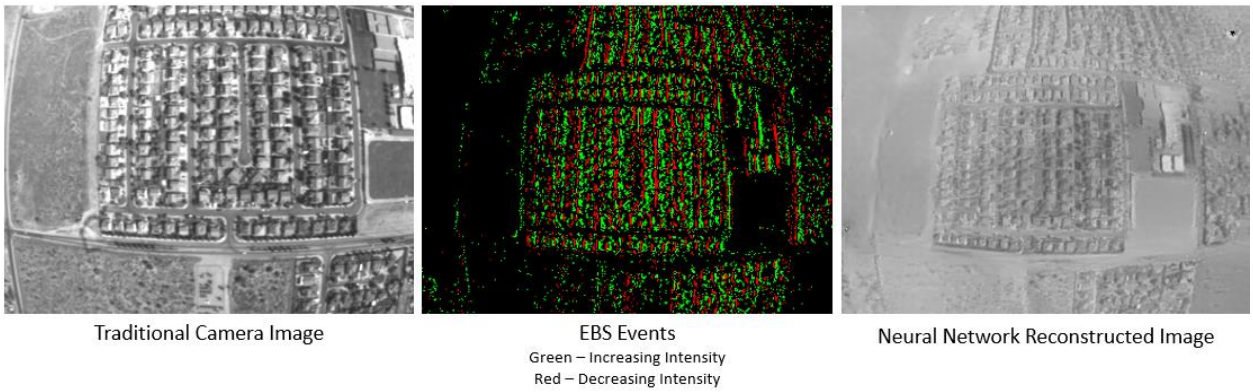

Figure 7 Example Traditional Frame-Based Image (left), Event-Based Sensor Output (center), and Neural Network Event-Based Sensor Image Reconstruction (right)

The front-end neural network generated image frames were then passed to a convolutional neural network to perform visual feature detection and tracking. The feature tracking neural network was trained during previous test efforts using synthetic datasets, the Microsoft Common Objects in Context 2014 computer vision dataset, and constructed image frames from the small UAV flight test referenced in Smart Features (reference 3).

The motion of the tracked features between frames was used to estimate aircraft motion by the Multi State Constrained Kalman Filter. This Kalman filter was used to estimate the camera's motion. The aircraft motion estimates were augmented with IMU data in the filter based on a Bayesian state predictor. Kaleb Nelson described in *Event-based Visual-Inertial Odometry on a Fixed-Wing Unmanned Aerial Vehicle (thesis)* (reference 6) how the Kalman Filter was implemented and accounted for accelerometer and gyroscope biases.

Since both VO and IMU provided estimates of relative motion, the starting truth position and attitude from the Time-Space Position Information (TSPI) were required to initialize the navigation state estimates.

PILOT-VEHICLE INTERFACE (PVI)

A PVI in the form of a Getac T800 tablet computer was used during ground operations. It was directly connected to the RASCAL pod via Ethernet cable, and used to initialize the camera and IMU, control data recording, and monitor pod status through a Graphical User Interface (GUI). The PVI operated only pre- and post-taxi from a ground crew connection to monitor pod alignment status.

RASCAL POD

The Reconfigurable Airborne Sensor, Communications, and Laser (RASCAL) pod was a modified SUU-20 weapons dispenser developed by the USAF Test Pilot School. It was a mature flight-rated external store that was used to house a variety of flight instrumentation systems and sensors, and was designed to allow for short lead-time and low-cost modifications to a flight test pod. The RASCAL pod had a current SEEK EAGLE flight clearance, *FC A2909-02: USAF Test Pilot School Reconfigurable Airborne Sensor, Communications, and Laser (RASCAL)-7 Pod with Ethernet Modification on F-16C/D Blocks 25-52 Aircraft* (reference 4), and was approved to operate up to specified aircraft flight limits. The EBS, IMU, and visual camera hardware components were installed in a RASCAL pod, shown in Figure 8 **RASCAL Pod**.

Figure 8 RASCAL Pod

These components recorded data to a solid-state hard drive, which was downloaded via an Ethernet port post-flight. Two EBS and a traditional, frame-based camera were fixed to look straight down through optical windows at the bottom of the RASCAL pod. The cameras all pointed at body-fixed nadir. The traditional frame-based camera was designed for use in-flight for situational awareness and post-flight to verify that the field of view captured the features of interest. The RASCAL pod operated on aircraft 28V power supplied through the aircraft's hardpoint.

F-16D AND ADVANCED RANGE DATA SYSTEM (ARDS) POD

The SUT was flown on an F-16D. The F-16D was a highly maneuverable, multi-role aircraft capable of performing from -2.5g to 7.3g, 200 KCAS to 550 KCAS, 1.2 Mach, and surface to 50,000' MSL. It was loaded with captive air training missiles on stations 1 and 9, an ARDS pod on station 2, a RASCAL Pod on station 3, 370 gal wing tanks on stations 4 and 6, and a common range integrated instrumentation system (CRIIS) pod on station 8.

Truth TSPI used for aircraft state initialization and solution accuracy comparison post-flight was provided by an ARDS pod. It recorded TSPI data throughout the time of flight. The ARDS TSPI was accurate to 3 m (reference 7).

TEST OBJECTIVE

The overall test objective was to determine EVIO algorithm accuracy and collect data to support ongoing EVIO and target detection / tracking algorithm development. The specific test objectives were:

1. Demonstrate navigation solution functionality.
2. Determine navigation solution accuracy as a result of varying flight conditions.
3. Collect operationally representative profile data.
4. Collect imagery, IMU data, and TSPI of ground-moving and airborne targets.

There were no evaluation criteria for this test program. The overall test objective was met.

CONSTRAINTS

Wildfires throughout California and in R-2508 created significant smoke obscurations and resulted in temporary flight restrictions in the western Sidewinder corridor. The smoke presented issues with a discernible horizon during dynamic maneuvering test points. This reduced the amount of test points collected from a desired of 15 runs to the actual 6 runs performed for the dynamic maneuvering runs. The test objectives were still met.

The aperture on the narrow field of view EBS was broken before the last flight, which was intended to be an airborne target data flight. All of the test points were successfully completed on the first airborne target flight, so the test objective was met. However, additional airborne target data was collected using the wider field of view EBS.

TEST AND EVALUATION

The overall test objective was to determine EVIO algorithm accuracy and collect data to support ongoing target detection and tracking algorithm development. There were four specific test objectives: demonstrate the SUT functionality to produce a navigation solution, determine the accuracy of the navigation solution through varying flight conditions, collect operationally representative flight profile data, and collect target tracking data for future research.

The SUT included EBS and an IMU in a RASCAL pod flown on an F-16D to improve visual odometry performance. An EBS operates on a hardware implementation of intensity change detection. This operating concept increases temporal resolution and dynamic range with low power requirements, making it advantageous for rapid motion and low/varying ambient lighting conditions. The SUT's navigation algorithm processed EBS imagery to identify feature motion, supplemented with IMU data, through a Kalman Filter to predict the aircraft's position, velocity, and attitude. The SUT algorithm was not yet implemented for in-flight navigation estimation; all navigation estimates were performed post-flight.

The data collected showed no conclusive trends in the accuracy of the SUT in response to line of sight rate, ambient lighting conditions, terrain, or dynamic maneuvering. The persistent extremely large solution errors prevented proper investigation of how these factors influenced SUT performance. Investigate and correct EVIO algorithm accuracy deficiencies before continuing flight test. The results show the system under test was unable to produce a reliable or useful navigational solution in the tested configurations. The results also showed that the system was able to detect airborne and ground moving targets; however, further analysis would be required to develop a target tracking algorithm.

Due to the low technological maturity of the cameras and algorithms, there were no evaluation criteria for this test.

NAVIGATION SOLUTION FUNCTIONALITY

The specific test objective was to demonstrate navigation solution functionality. This was accomplished in conjunction with follow on objectives and testing.

Test Methods and Conditions

In order to demonstrate the capability of the SUT to generate a navigation solution, greater than five minutes of flight EBS imagery and IMU data were collected and post-processed as this was the first full-scale flight test of the SUT hardware and algorithm. These data were collected from every flight. Test team members on the ground connected the Getac tablet to the pod via Ethernet to initialize the SUT sensors and begin the IMU alignment process. The ground crew disconnected the tablet and the pilot taxied the aircraft to complete IMU alignment. An unobstructed ramp area was used to perform a figure-eight required for the IMU alignment, then the pilot taxied back to parking so that the ground crew could verify successful alignment on the tablet and begin data recording. The SUT recorded sensor data throughout the flight until post-flight engine shutdown. Ground power was applied to the aircraft post-flight to transfer data via Ethernet and clear the internal pod hard drive for subsequent data collection.

The SUT sensor data and the ARDS TSPI data were downloaded to dedicated data processing computers. The SUT algorithms were then used to generate navigation solution estimates over specific time segments as recorded by flight test engineer notes and F-16 data acquisition system events. No accuracy evaluation was conducted, but comparison to truth TSPI illustrated the mechanization of the SUT algorithms.

Navigation Solution Functionality Test Results

The system successfully produced a navigation solution; however, this solution was not useful. The data were analyzed over a total of 140 runs. Figure 9 **SUT Position, Velocity, and Attitude Estimates**shows position, velocity, and attitude estimates over time for a sample test run. This sample data were representative of all the runs completed. The algorithm used did not contain a physics based model of aircraft motion, and aircraft state estimates were not coupled to each other. For example, Figure 9 **SUT Position, Velocity, and Attitude Estimates**shows that although aircraft yaw estimates indicate an S-turn between approximately 20 degrees south of east and 25 degrees north of east, the lateral position and velocity estimates do not reflect any northerly motion. In actuality, the aircraft was flown straight and level at nearly constant groundspeed.

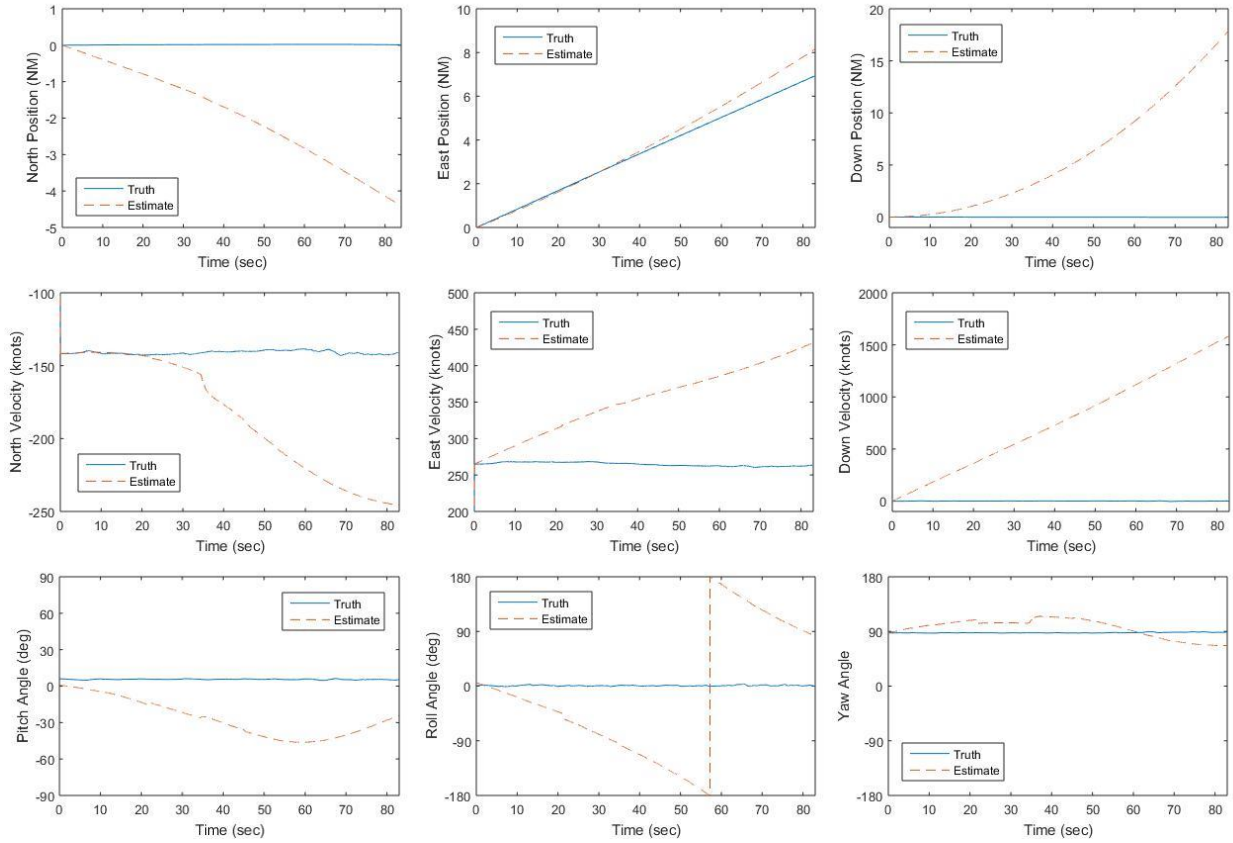

Figure 9 SUT Position, Velocity, and Attitude Estimates

NAVIGATION SOLUTION ACCURACY

The specific test objective was to determine the navigation solution accuracy as a result of varying flight conditions. This was accomplished by measuring the SUT accuracy as a function of line of sight rates, terrain features, ambient lightning conditions, and dynamic maneuvering.

Test Methods and Conditions

Constant system altitude and ground speed (GS) flight profiles were flown over the pre-planned geographic locations shown in figure 10. Ground runs were planned to obtain approximately 60 seconds of

data collection at high line of sight rates (LOSR). The flight profiles were repeated at a variety of GS and altitudes to isolate the impact of LOSR on EVIO navigation solution accuracy. Low altitude / high speed flight produced the highest line of sight rates and high altitude flight produced the lowest line of sight rates. High line of sight rate test points were flown at 1,500 ft height above target (HAT) and 450 knots GS. Medium line of sight rates were flown at 4,000 ft HAT and 300 knots GS. Low line of sight rates were flown at 7,000 ft HAT at 300 knots GS. Very high line of sight rates were flown at 650 ft AGL at 510 knots GS. Floor line of sight rates were flown at 300 ft AGL at 510 KCAS. Additional information on databands and the impact on dwell time is available in appendix A.

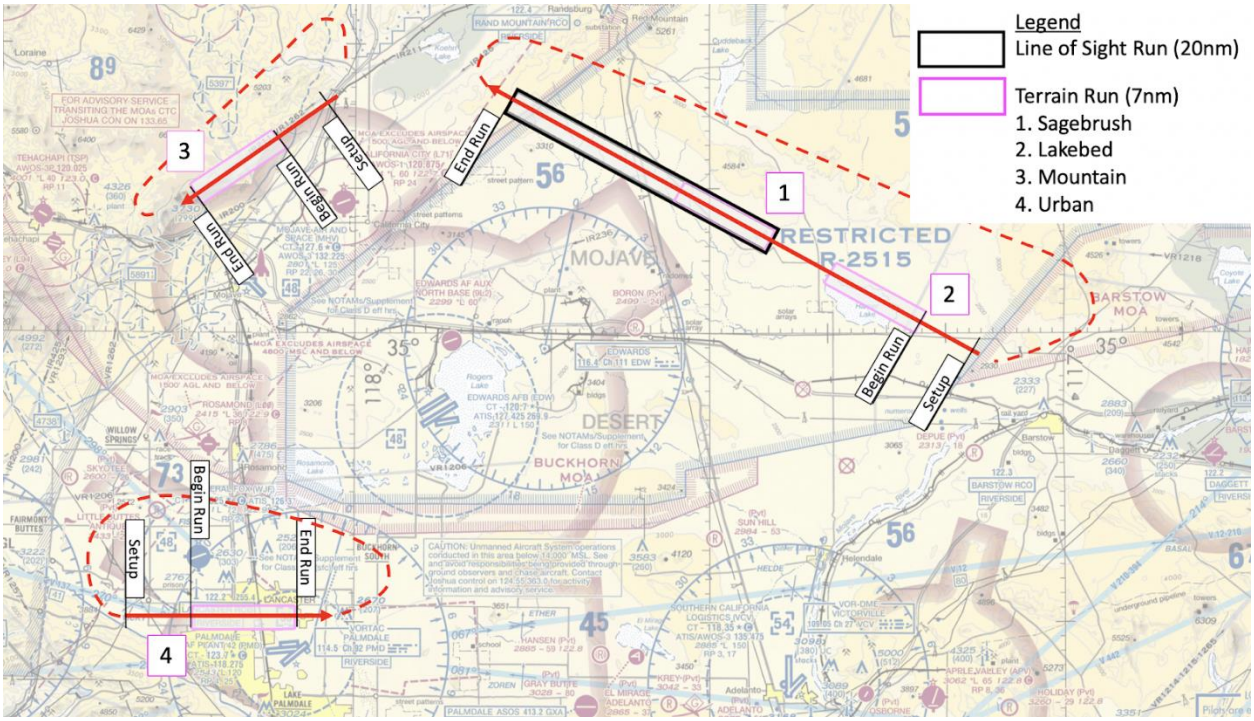

Figure 10 Example Ground Tracks (Line of Sight and Terrain Runs)

Line of sight rate was a function of ground speed and height above the terrain. Test points flown at constant system altitude over the same ground track resulted in variation of actual line of sight rate due to variation in terrain height. Classifications for the line of sight rates flown (floor, very high, high, medium, low, very low) are in appendix A. Accuracy for each run was calculated over a standardized ground distance to minimize bias due to terrain variation. Line of sight rate for each run was calculated as the dwell time for which a point feature remained in the field of view of the EBS camera:

$$L_{long} = 2 \times HAT \times \tan\left(\frac{FOV}{2}\right)(feet)$$

$$t_{dwell} = \frac{L_{long}}{Ground\ speed}(seconds)$$

Where L_{long} was the longitudinal distance across the ground within the FOV of the EBS sensor and HAT was the height above the terrain. The HAT for a ground run was a single elevation that was representative of the overall ground elevation along the ground run. Smaller values of t_{dwell} corresponded to higher line of sight rates. One value of terrain height was determined for each planned ground track for

analysis purposes to compare similar line of sight rate results across different terrains. An example of the planned flight path over varying terrain and the L_{long} is shown in figure 11.

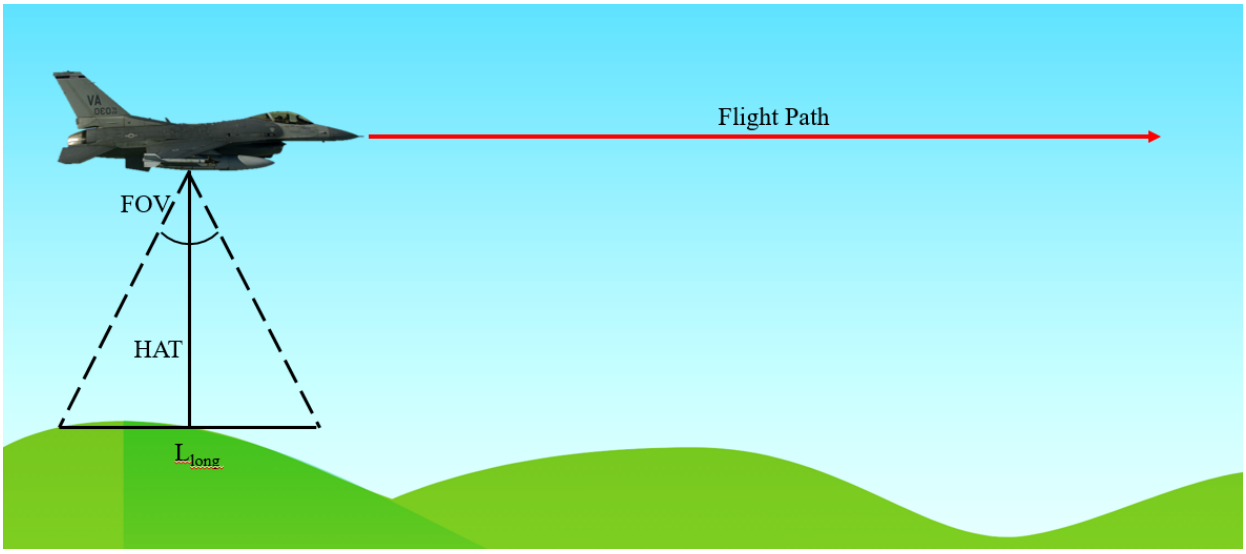

Figure 11 Example of Flight Path and FOV

Preflight planning of geographic locations and run-in headings provided the EBS sensors with consistent terrain features at the various system altitudes and GS. Flying constant above ground level (AGL) altitude and ground speed would present a constant line of sight rate. Constant system altitude profiles were flown for ease and consistency of execution, however, to minimize the impact of dynamic maneuvers which would be required to maintain constant AGL.

The same GS and height above terrains were repeated across the four terrain categories (urban, sagebrush desert, dry lakebed, and mountainous) to isolate the impact of terrain on navigation solution accuracy. Ground tracks of qualitatively uniform features were chosen to categorize the effect that each terrain's spatial feature size, spatial frequency, contrast, and geometric variety had on navigation solution accuracy. The bulk of the test program's data collection was performed during peak solar illumination hours from mid-morning to mid-afternoon, therefore illumination variation was considered negligible for comparisons across line of sight rates and terrains. Two sorties were flown through dusk until after the end of civil twilight. A racetrack was flown over the sagebrush desert terrain ground track to repeatedly revisit the same terrain at the same line of sight rate as solar illumination decreased. After the end of civil twilight, data collection was performed over the urban terrain ground track to capture artificial lighting.

The standardized ground tracks described above enabled the isolation of terrain, line of sight rate, and ambient lighting condition effects. In isolation, the 7 NM and 20 NM long ground tracks were not designed to provide insight into the long-term navigation performance of the SUT. Bulk processing of lengthier flight segments from both the repeated ground track data collections and operationally representative flight profiles were used to determine the long-term drift rate of the SUT's navigation solution.

The aircrew performed a series of dynamic maneuvers between 10,000-20,000 ft MSL over similar sagebrush terrain to examine the impact of changing aircraft attitudes and rates on the SUT. Each dynamic maneuver was preceded and followed by 30 seconds of straight and level flight to compare the maneuver's navigation solution impact to that of straight and level flight. The following sequence of maneuvers were performed six times across five sorties:

1. 120° bank to bank roll (5 second roll duration)
2. Aileron roll
3. Loop
4. Right (or left) level to slightly descending 180° turn, using incremental bank angles of 30° (level), 60° (level), and 90° (descending), pausing at each specified bank angle for 5 seconds
5. One climb consisting of incremental climb angles of 15°, 30°, and 45°, pausing at each specified climb angle for 5 seconds, followed by a nose high recovery to level flight

The Sidewinder low level route as defined by the R-2508 User's Handbook page 33 (reference 8) was flown for the long term drift rate test points. The low level route is depicted below in Figure 12 **Sidewinder Low Level Route**

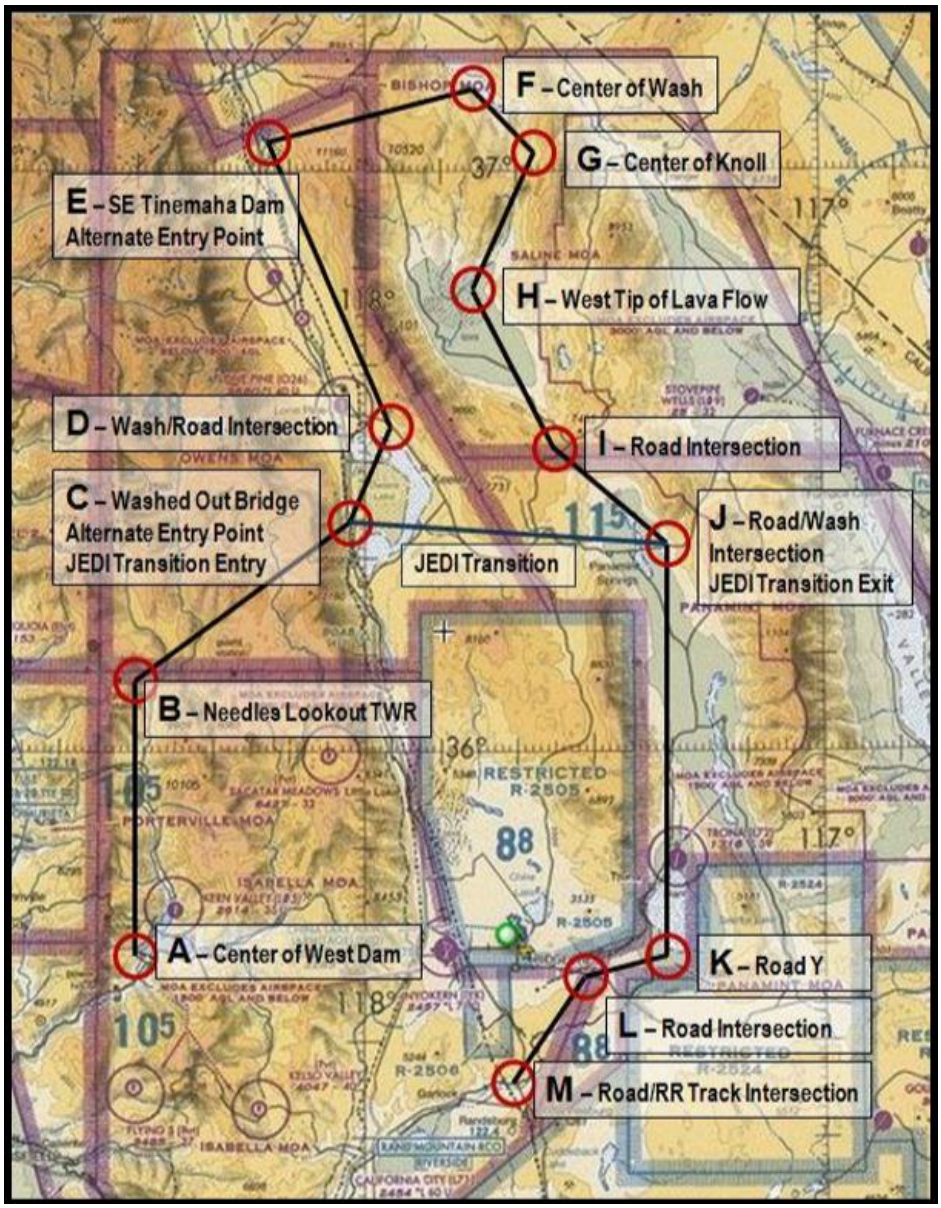

Figure 12 Sidewinder Low Level Route

Accuracy of SUT aircraft state estimates was determined by comparison to truth TSPI provided by an Advanced Range Data System (ARDS) pod. Root mean square error (RMSE) over standardized ground runs were calculated to determine the impact of LOSR, terrain, and ambient lighting conditions. A total of 147 runs were completed in support of this objective.

Image Reconstruction Anamolies

During the analysis of the front-end neural network image reconstructions, considerable artifacts were noted. These artifacts were seen across all test points and flight conditions. Figure 13 **Non-Physical Artifacts Consistently Generated by Front End Neural Network**shows non-physical artifacts that consistently appeared in the left and top right of image reconstructions across all sorties and terrain types. These artifacts, once present, continued to grow throughout the processed run. Artifacts would initially appear in the reconstructed images when overflying regions with repetitive terrain features or uniform terrains with very low spatial frequency content. Depending on the scene features and length of the run, the artifacts could grow to cover large portions of the field of view. Figure 14 **15 Second Progression of Front End Neural Network Artifacts (top) compared to the Same Areas from Traditional Camera Images (bottom)**also shows snapshots of an image reconstruction over a fifteen second period. Reconstructed images are above the corresponding traditional optical camera images for reference. The non-physical geometric pattern grows to encompass nearly the entire field of view. These features did not move over time and inserted false stationary feature tracks into the visual odometry Kalman filter. **Investigate the impact the artifacts have on navigation solution accuracy. (R1)**[1]

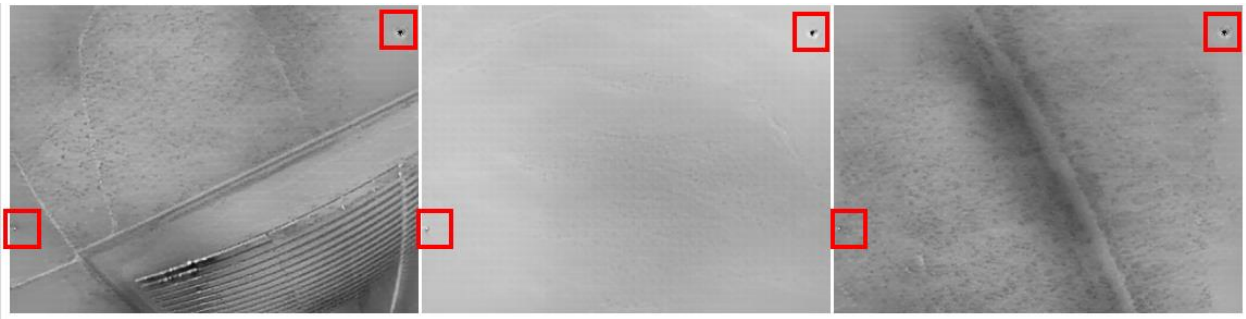

Figure 13 Non-Physical Artifacts Consistently Generated by Front End Neural Network

[1] Numerals following an R represent recommendation numbers.

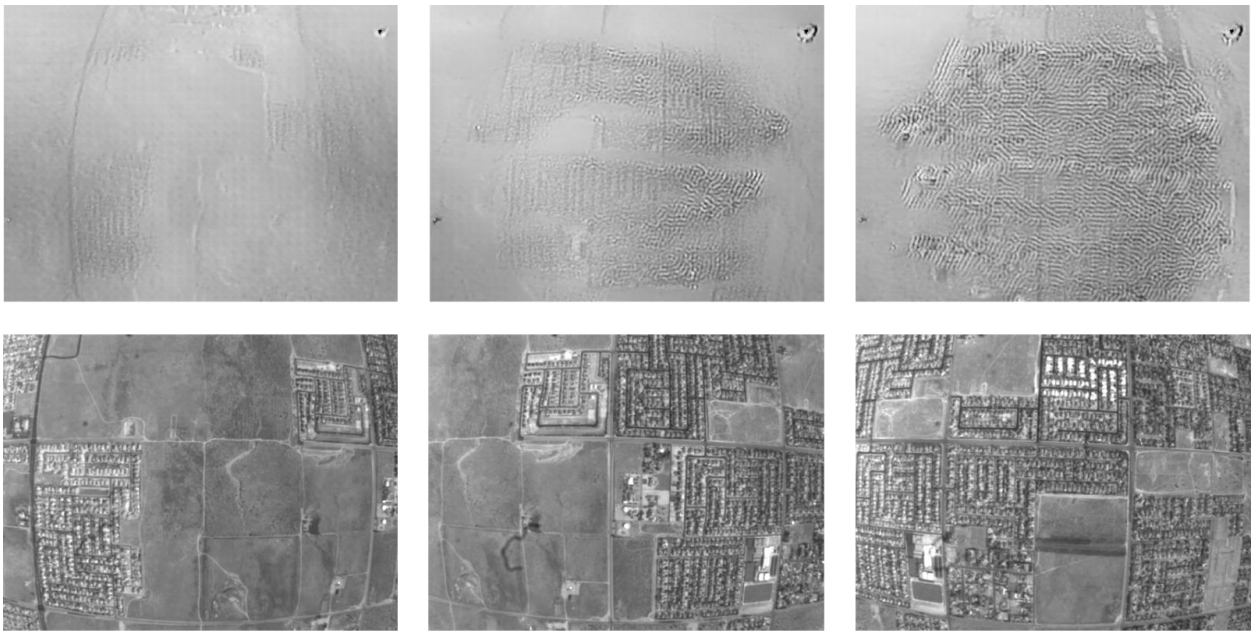

Figure 14 15 Second Progression of Front End Neural Network Artifacts (top) compared to the Same Areas from Traditional Camera Images (bottom)

Drift Rate Test Results

The lateral error was calculated as the Pythagorean distance between the truth TSPI and SUT estimated north/east position. The drift rate was defined as the final lateral error divided by the elapsed time of the processed run. The SUT's drift rate was greater than 850 NM/hr. The drift rate was calculated from a 43 minute operationally representative flight segment over the Sidewinder low level route. This data are located in appendix B, figure B-29**.** This was significantly higher than the 0.8 NM/hr for modern fighter inertial navigation specifications. The software used to separate the event data and IMU data from the raw data log was limited in the file size it could process. The longest flight segment it could process was approximately 45 minutes, depending on EBS data rates.

Accuracy Variance with Line of Sight Rate Test Results

The navigation estimation algorithm consistently produced accelerating vertical errors, resulting in total down axis errors in excess of 15 NM during straight and level test runs under 90 seconds. Figure 15 **Sample Navigation Estimate Down Error**depicts an example of the down error progression. The customer engineer indicated that the negligible motion about the lateral axis during straight and level flight provided minimal data to update the vertical navigation estimate, which resulted in unchecked vertical navigation solution drift. Due to this, and the knowledge that most of the runs were done at a constant altitude, the down direction results were not included in this accuracy data analysis.

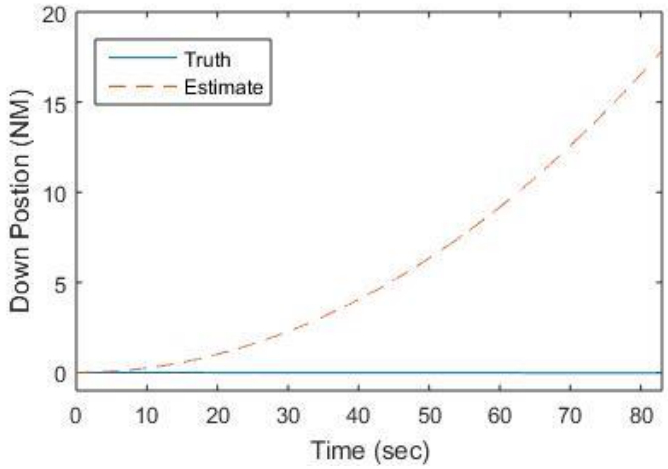

Figure 15 Sample Navigation Estimate Down Error

The SUT navigation accuracy ranged from 0.5 to 9 NM in error over the 20 NM runs over sagebrush desert terrain across all LOSR. The results show that accuracy decreased as LOSR decreased from high (t_{dwell} approximately 4 sec) to medium LOSR (t_{dwell} approximately 16 sec) (figure 16). Lateral velocity error varied from 39-289 knots and attitude RMSE ranged from 18-94 degrees across axes. Plots of error in the SUT estimates of aircraft state (attitude angles, position, and translational velocities) for each LOSR category as a function ground distance can be found in appendix B. There was no clear trend in navigation solution accuracy as a function of LOSR.

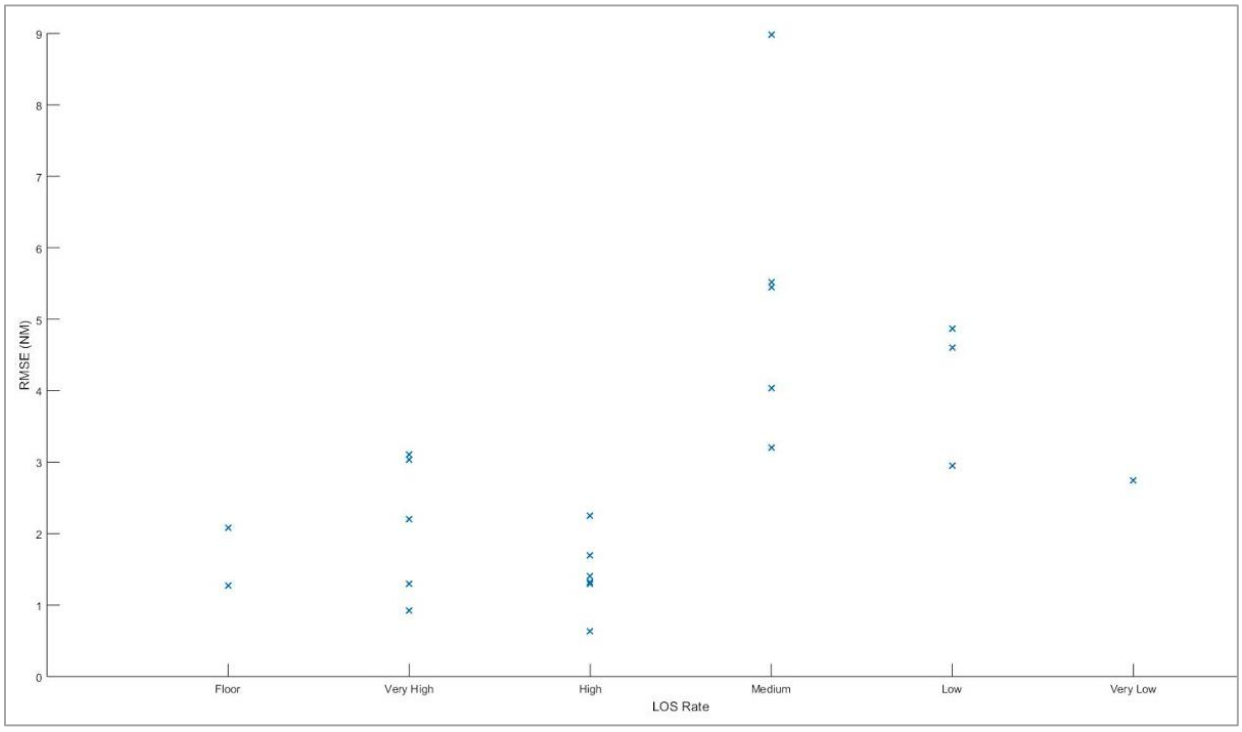

Figure 16 Lateral Distance RMSE for Varying LOS Rate Over 20 NM Sagebrush Runs

Accuracy Variance with Terrain Test Results

Lateral distance RMSE for differing terrain is shown below in Figure 17 **Lateral Distance RMSE for Different Terrain Over 7 NM Runs**7. RMSE over the standardized 7 NM runs was smallest over sagebrush and lakebed terrain with urban and mountain terrain 2-4x higher. Repeated, rectangular structural urban patterns posed a challenge to the image reconstruction neural network. Reconstructed image artifacts rapidly filled the field of view when overflying regular structures such as solar farms, homes, and industrial buildup (see **Error! Reference source not found.**4 above). The SUT navigation accuracy ranged from 0.5 to 3 NM over all terrains during the 7 NM runs. Plots of error in the SUT estimates of aircraft state (attitude angles, position, translational velocities) for each terrain category as a function of ground distance can be found in appendix B.

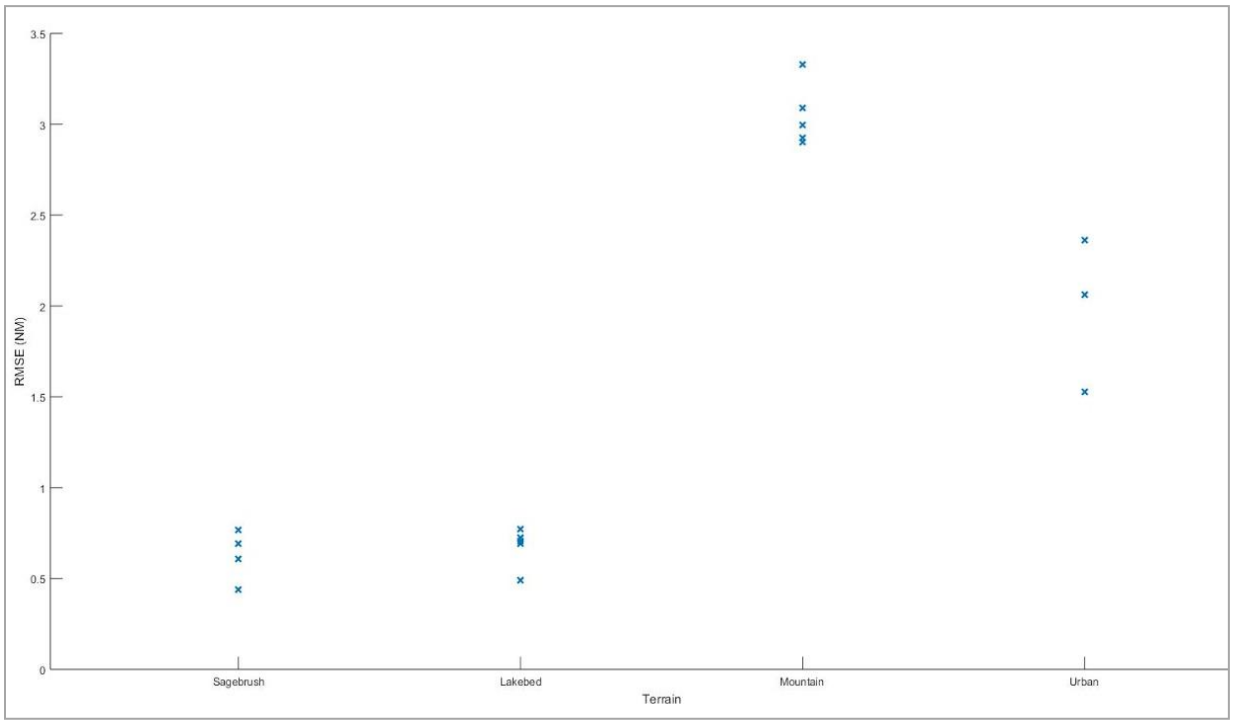

Figure 17 Lateral Distance RMSE for Different Terrain Over 7 NM Runs

Accuracy Variance with Ambient Lighting Conditions Test Results

Six runs over sagebrush were completed during daylight, and twenty were completed during dusk. Thirteen runs were completed at night over urban terrain and compared to the five runs completed during daylight.

The lateral RMSE during the 7 NM runs are depicted in figures 18 and 19. During sagebrush runs (Figure 18 **Sagebrush Daytime vs. Dusk Runs**8), the daytime RSME varied between 0.45 NM and 0.6 NM. At dusk, the RMSE was between 0.5 and 0.9 NM, and did not trend better or worse with decreasing ambient light. Figure 19 **Urban Daytime vs. Night Runs**shows the difference between daytime and nighttime runs over urban areas. The runs showed a RMSE of 1.5-2.5 NM during daytime and 1.3-2.1 NM at night. Additional data are attached in appendix B. The data did not clearly suggest that a trend existed in navigation solution accuracy as a function of ambient lighting conditions.

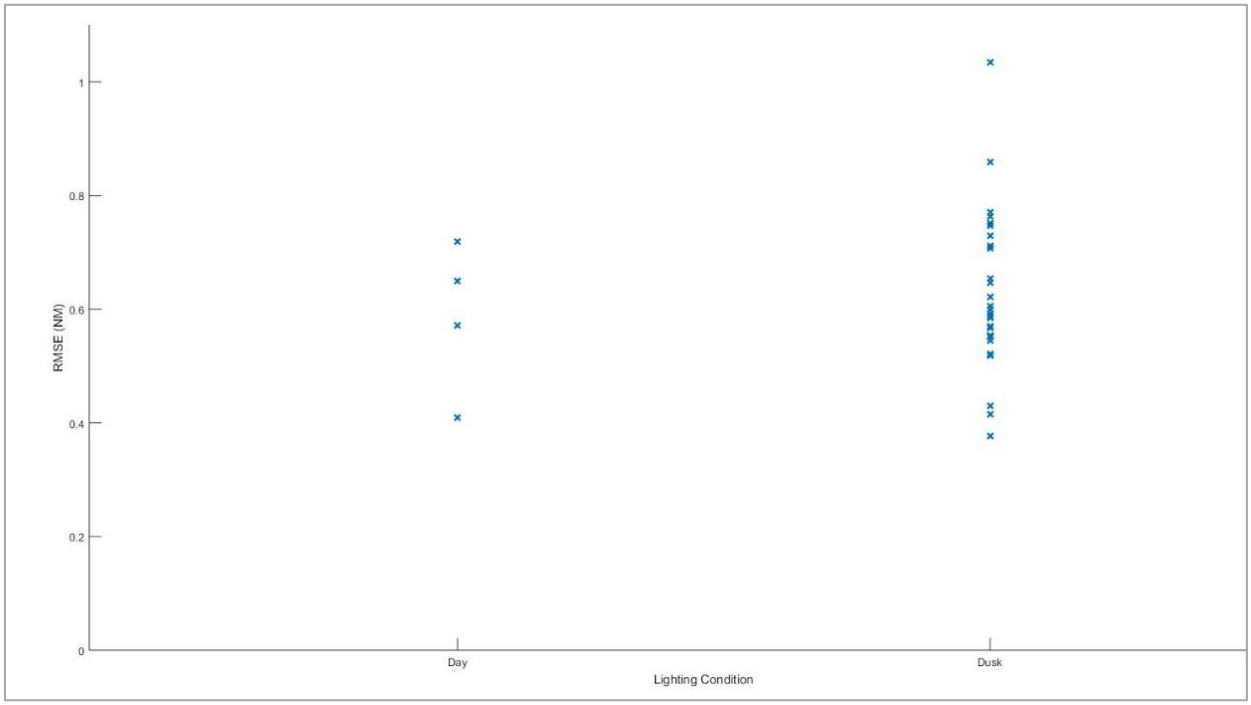

Figure 18 Sagebrush Daytime vs. Dusk Runs

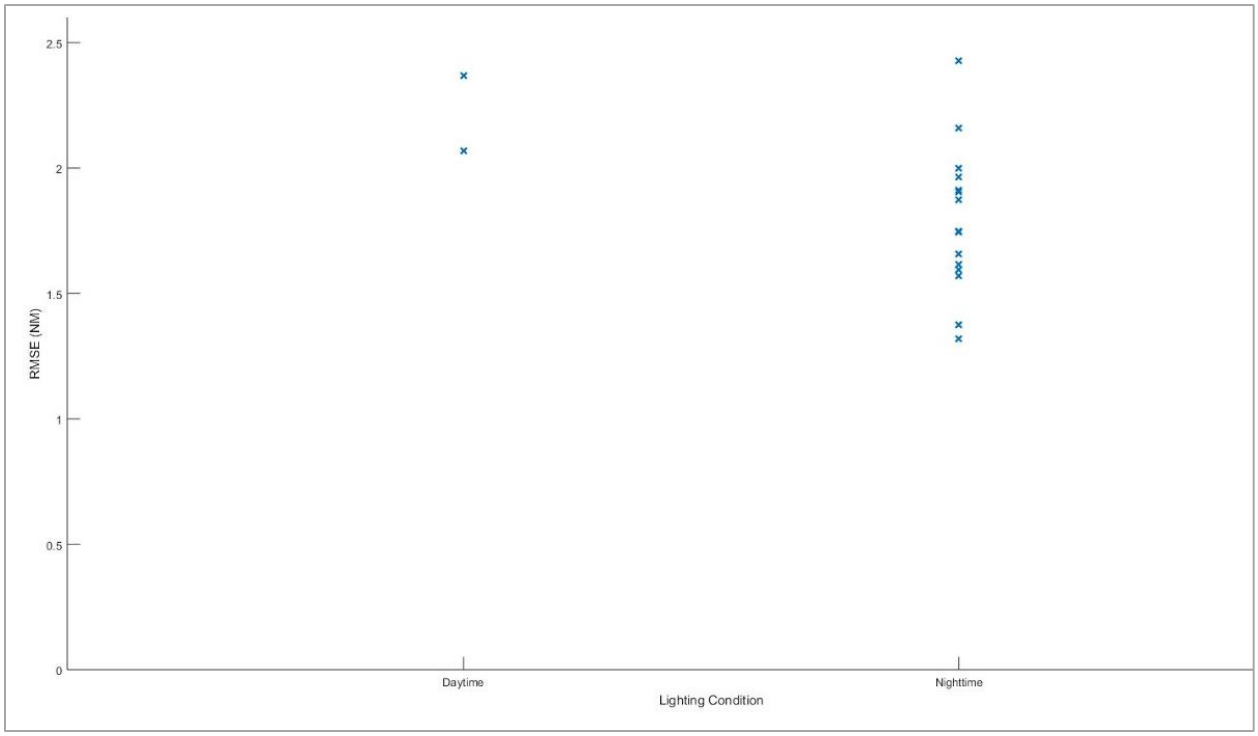

Figure 19 Urban Daytime vs. Night Runs

Accuracy Variance with Dynamic Maneuvering Test Results

Navigation solution accuracy during dynamic maneuvering was erratic and unpredictable. The camera was unable to distinguish ground features due to the low camera resolution and/or lack of horizon in some cases due to wildfire smoke. Figure 20 **Position, Velocity, and Orientation vs. Truth: Flight 1 Incremental Climb Dynamic Profile**shows sample navigation accuracy results for an incremental climb to 45° nose-high followed by an inverted nose-high recovery maneuver. The data from this run show a north error of 6 NM, an east error of 3 NM, and a down error of over 23 NM. The velocities showed a maximum north velocity difference of 350 knots north, 400 knots east, and 1,700 knots down at their greatest differences. The orientation maximum differences between this sample data and the truth orientation were 40 degrees pitch, 180 degrees in roll and 75 degrees in yaw. Additional flight results are in appendix B. The data show the SUT does not build an accurate reconstruction of the aircraft's states during dynamic maneuvers.

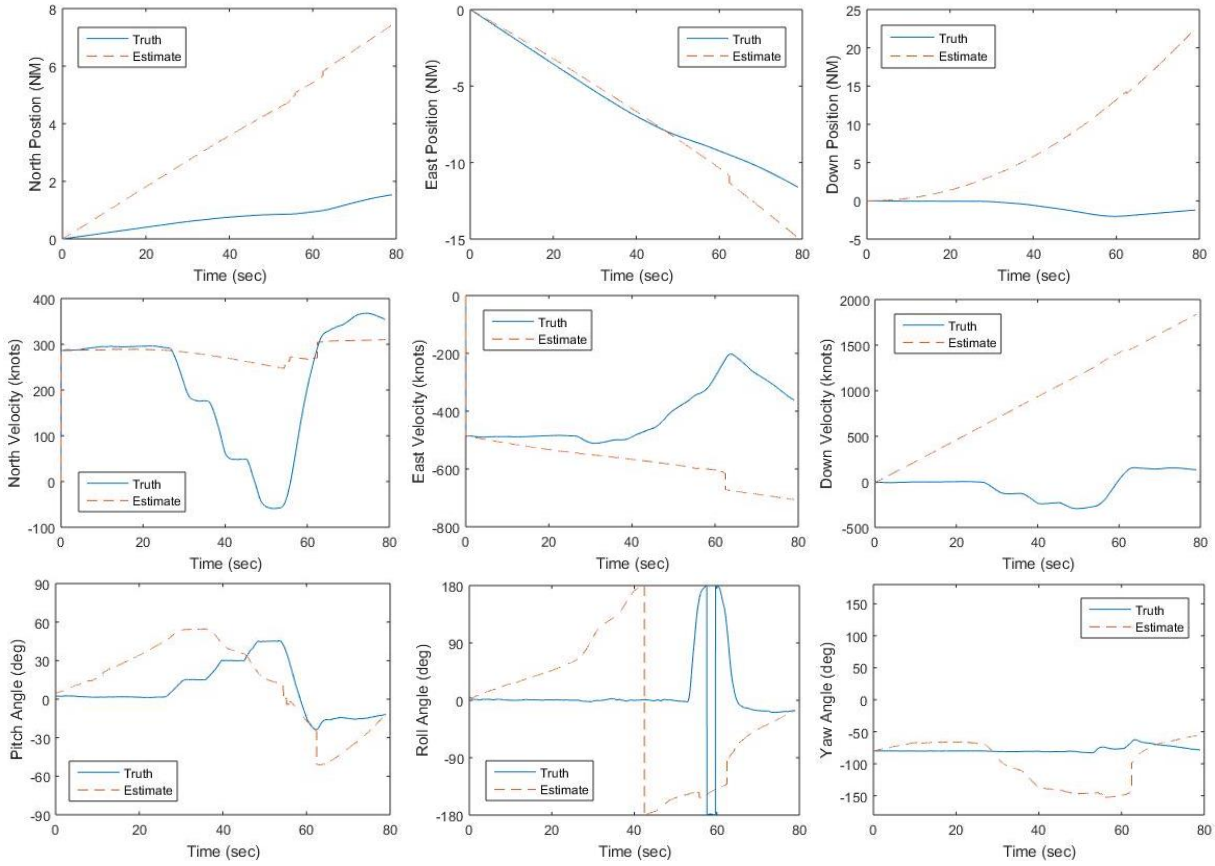

Figure 20 Position, Velocity, and Orientation vs. Truth: Flight 1 Incremental Climb Dynamic Profile

The data collected showed no conclusive trends in the accuracy of the SUT in response to LOSR, ambient lighting conditions, terrain, or dynamic maneuvering. The persistent extremely large solution errors prevented proper investigation of how these factors influenced SUT performance. **Investigate and correct EVIO algorithm accuracy deficiencies before continuing flight test. (R2)**

OPERATIONALLY REPRESENTATIVE PROFILE

The specific test objective was to collect operationally representative flight profile data.

Test Methods and Conditions

Operationally representative mission profiles were flown within the confines of the R-2508 complex, generally following the Sidewinder low-level route. The beginning of the mission was defined as passing 200 ft AGL after takeoff. The end of the mission was defined as passing 200 ft AGL on final approach. The mission profile included: climb, simulated air refueling (one hold pattern with 15 NM legs and 30 degrees of bank), a tactical let down, ingress, simulated bomb run, simulated battle damage assessment, and egress. Terrain varied many times between lakebed, sagebrush, and mountain landscapes. Event logs in the digital appendix denote the beginning of each major mission milestone, when transitioning between landscapes, and any other overflown features of interest (e.g. trains, sand dunes, etc.) to aid data analysis.

Test Results

EBS imagery, IMU truth data, and truth TSPI were collected across three operationally representative profiles. The sensor data and event logs are contained in the digital appendix for further analysis and future algorithm development. Figure 21 shows the SUT estimated navigation solution versus truth position over one operational run. The flight profile was executed within the confines of R-2508, while the SUT navigation estimate terminated northeast of Salt Lake City, UT. This run showed an error of over 500 NM north and 320 NM east of the truth final position. The additional runs in the digital appendix (appendix E) show similar results.

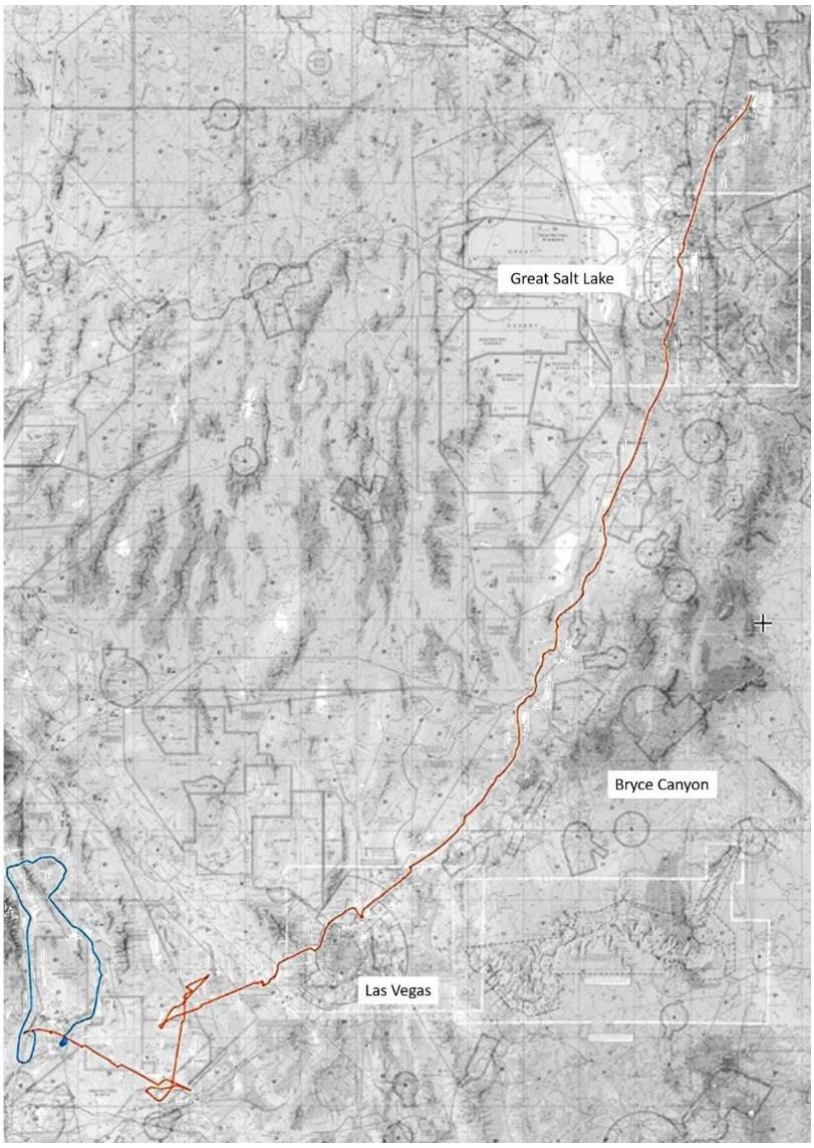

Figure 21 Operationally Relevant Profile Truth (Blue) vs. SUT Estimate Navigation Solution (Red)

EBS IMAGERY, IMU DATA, AND TSPI OF GROUND-MOVING AND AIRBORNE TARGETS

The specific test objective was to collect imagery, IMU data, and TSPI of ground-moving and airborne targets.

Test Methods and Conditions

The test aircraft overflew ground moving targets (approximately 13-15 ft in length) at constant altitude and ground speed. Due to the camera resolution limitations, a maximum height of 3,000 ft AGL was flown. Runs were repeated at varying airspeeds and altitudes in order to vary line of sight rates and target resolution. Two ground target vehicles were driven on public roadways while in Very High Frequency (VHF) radio contact with the aircraft. Commercial off the shelf GPS recorders captured target truth trajectory. The aircraft profile consisted of straight and level flight at the following conditions:

1. 500 ft AGL, 520 knots (9.10 pixel target dimensions)
2. 1,000 ft AGL, 500 knots (4.55 pixel target dimensions)
3. 1,500 ft AGL, 450 knots (3.02 pixel target dimensions)
4. 2,000 ft AGL, 400 knots (2.27 pixel target dimensions)
5. 2,500 ft AGL, 350 knots (1.82 pixel target dimensions)
6. 3,000 ft AGL, 300 knots (1.51 pixel target dimensions)

For the airborne target, the test aircraft maneuvered relative to a target T-38C at varying altitudes and attitudes. Due to the predicted camera resolution limitations, a maximum slant range of 3,000 ft was used. Truth TSPI for the target was recorded via the data acquisition system.

A vertical offset task commenced with the two aircraft in formation at 300 KCAS. The F-16D then climbed and took spacing to establish approximately 1 NM in trail and 1,000 ft high while the T-38C maintained original altitude, airspeed, and heading. The F-16D accelerated to 350 KCAS and overtook the T-38C, passing as close to overhead as possible to ensure the target remained in the EBS FOV. Once the T-38C drifted to approximately 1 NM in trail, the process reversed and the T-38C accelerated to 350 KCAS while the F-16D slowed to 300 KCAS. The T-38C then passed directly below the F-16D for similar FOV considerations. Once the F-16D regained visual of the T-38C over the nose, the maneuver was complete. The series of events are depicted in figure 22.

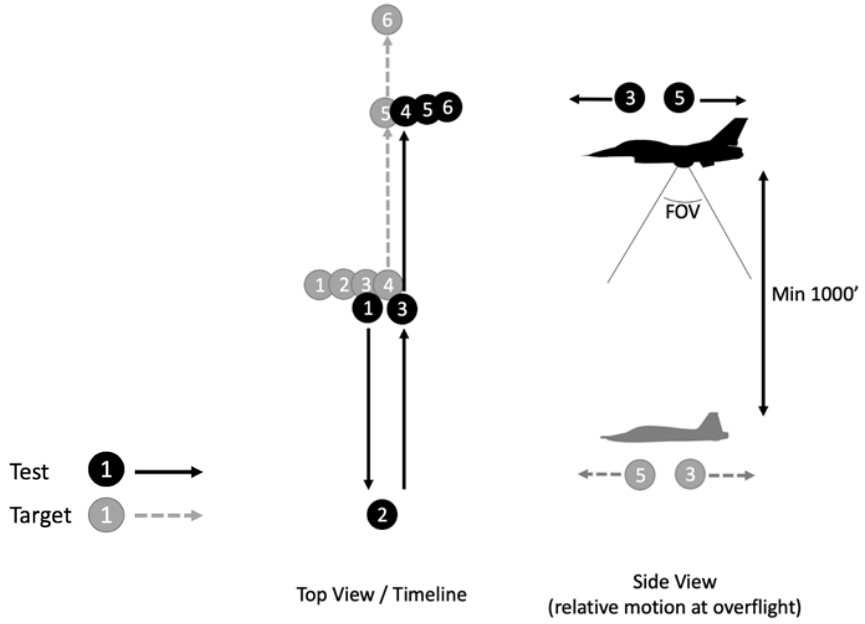

Figure 22 Vertical Offset Task Event Flow

A lateral offset (1G) task commenced with the two aircraft co-heading and line abreast, approximately 2,000 ft laterally spaced with the target T-38C stacked 1,000 ft high. The F-16D banked away from the T-38C by overbanking to 120° and maintaining 1G to minimize line-of-sight rate build-up while presenting the EBS FOV with a look-up target. Attitude was maintained for a minimum of 5 seconds, after which the F-16D rolled out to complete the maneuver. The series of events are depicted in figure 23.

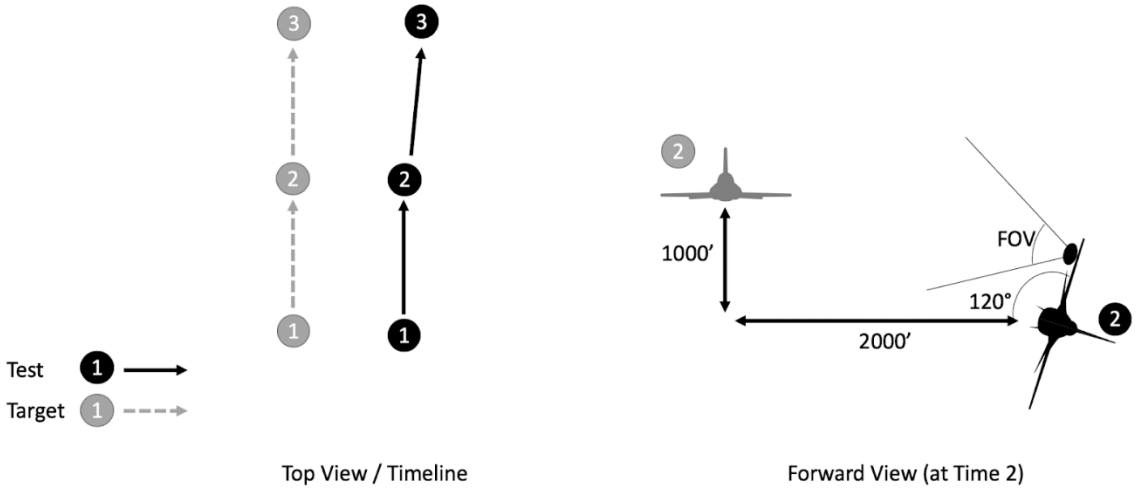

Figure 23 Lateral Offset Task (1G) Event Flow

A lateral offset (varying G) task provided varying line of sight rates to those of the previous 1G task. It commenced with the F-16D in a co-airspeed, co-heading, fighting wing position on the target at approximately 1,500 ft spacing. The F-16D then commenced a constant airspeed turn away from target at various combinations of bank and G levels to a heading change of 45°, followed by a reversal to co-heading to complete the maneuver. The maneuver was conducted in a level-turn, with under-banked and over-banked conditions to present a variety of changing backgrounds and clutter (look-down, horizon, and look-up) and line of sight rates (through varying G). Under and over-banked conditions were relative to 90° angle of bank (AOB) and stressed the lateral FOV limits of the EBS. Figure 24 **Lateral Offset Task (varying G) Event Flo**4 depicts all three banked cases.

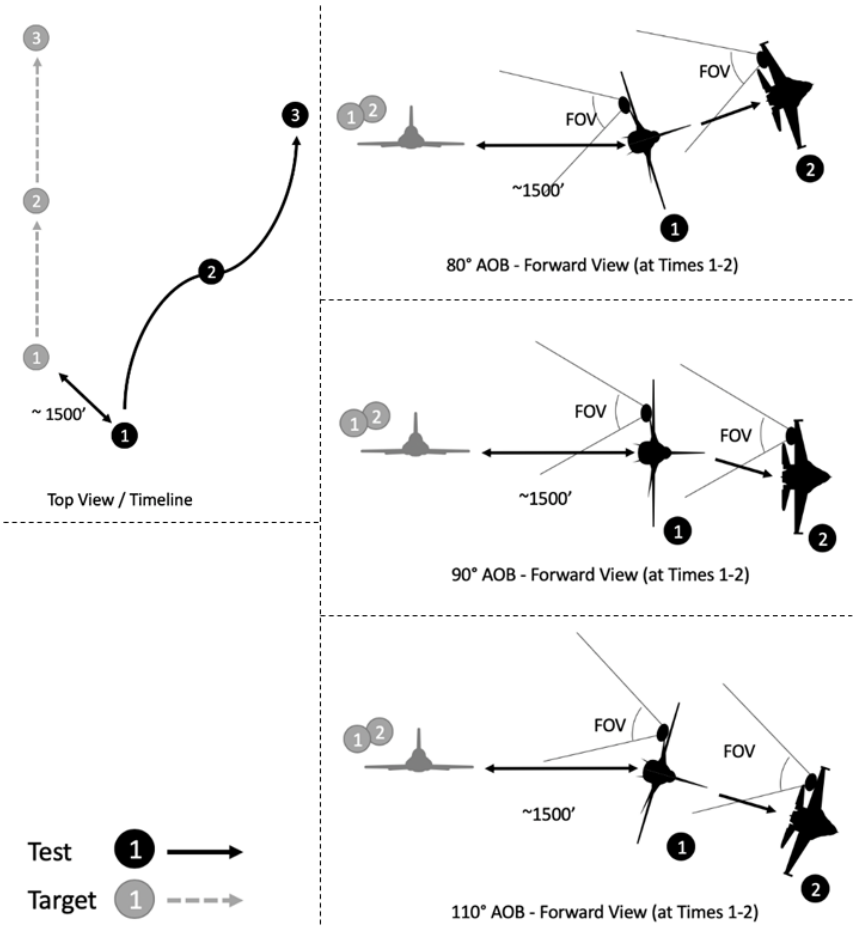

Figure 24 Lateral Offset Task (varying G) Event Flow

EBS Imagery, IMU Data, and TSPI of Ground-Moving Target

The EBS imagery, IMU data, and TSPI of ground-moving targets were collected and can be found in the digital appendix. Traditional and EBS images were inspected to ensure the target was captured in the FOV. Two passenger vehicles with TSPI were recorded in the event-based imagery for three runs each at low, medium, high, and very high line-of-sight rates. Figure 25 **Traditional and EBS Images of Moving Passenger Vehicle**5 and Figure **26 Traditional and EBS Images of Moving Tractor Trailer**6 show both the visual and raw EBS images from the wide and narrow FOV cameras with the ground moving target(s) highlighted.

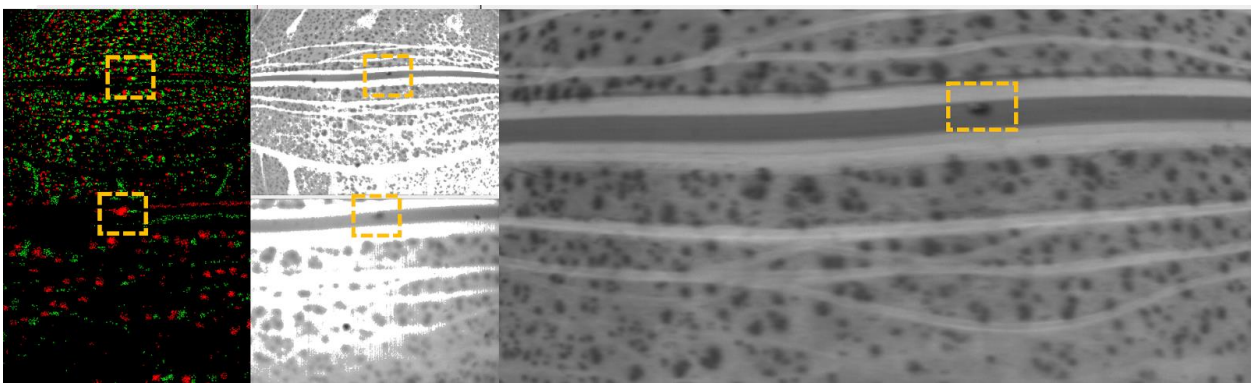

Figure 25 Traditional and EBS Images of Moving Passenger Vehicle

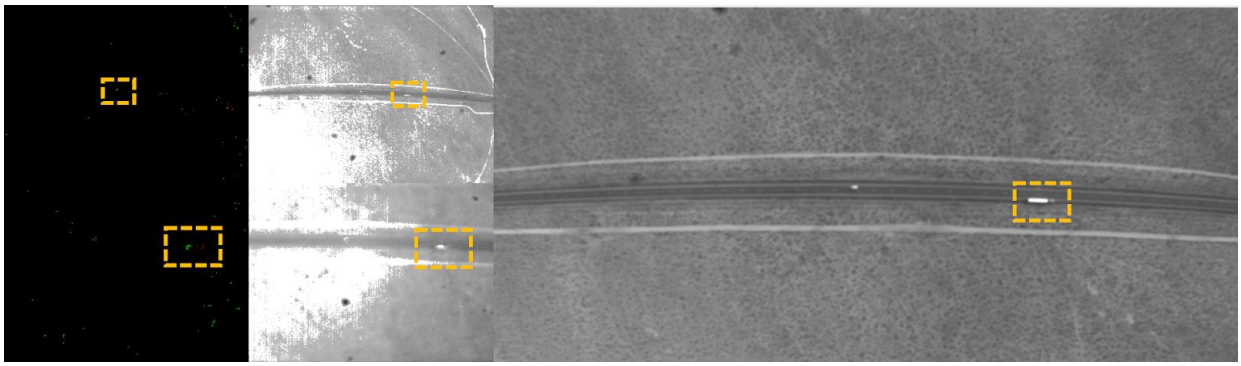

Figure 26 Traditional and EBS Images of Moving Tractor Trailer

Due to the low resolution of the EBS cameras, a cursory analysis revealed the maximum AGL altitude in which the ground targets triggered an EBS event was 1,500' AGL. TSPI data for the tractor trailer was unavailable as it was a target of opportunity and not instrumented.

EBS Imagery, IMU Data, and TSPI of Airborne Target

The EBS imagery, IMU data, and TSPI of an airborne target were collected. The EBS narrow FOV camera failed after sortie 10. This constrained data collection for the second airborne target collection sortie to the wide FOV camera only. However, data from the wide FOV EBS was used to supplement the data collection requirement.

Traditional and EBS images were inspected to ensure capture of the airborne target in the FOV during post-flight analysis. A T-38C with TSPI was recorded in the event-based imagery for multiple runs. A KC-135 was also recorded as a target of opportunity. Figure 27 **Traditional and EBS Images of T-38C**7 and Figure **28 Traditional and EBS Images of KC-135**8 show both the visual and raw EBS images with the airborne target highlighted. The EBS was capable of capturing moving targets, however, an algorithm did not exist that allowed for tracking the moving targets.

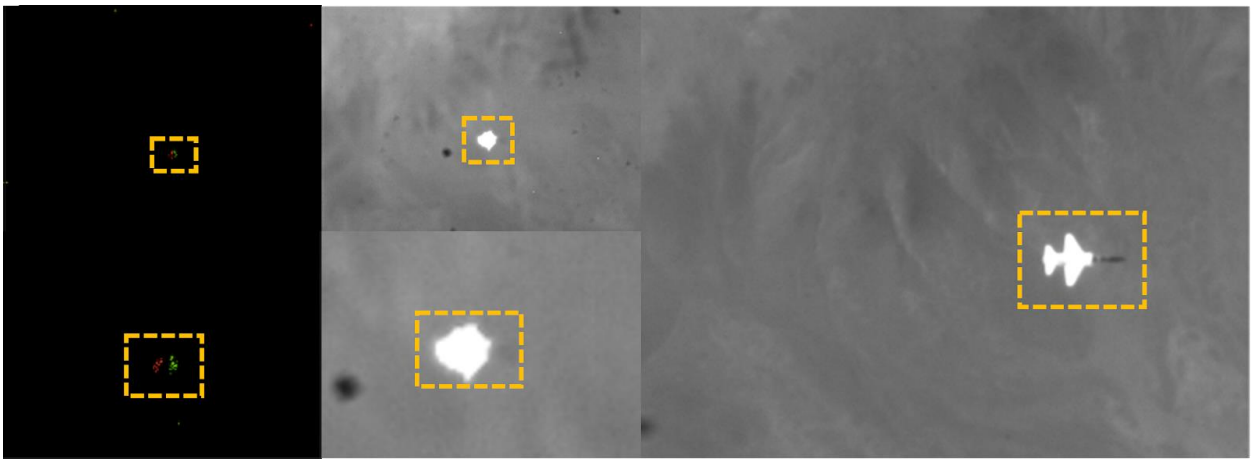

Figure 27 Traditional and EBS Images of T-38C

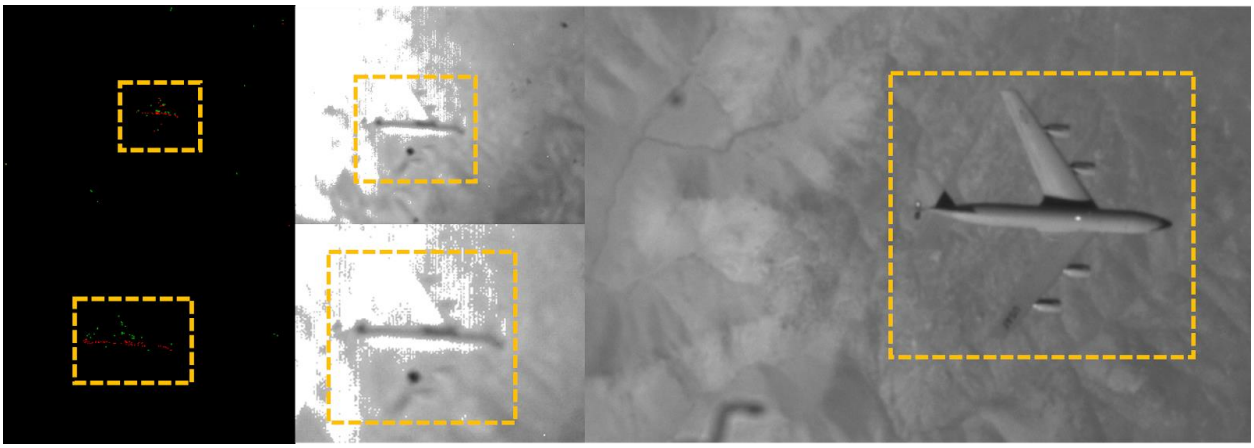

Figure 28 Traditional and EBS Images of KC-135

REFERENCES

1. *Event-Based Sensor Visual-Inertial Odometry System: Have T-Rex Test Plan,* USAF Test Pilot School, Edwards AFB, California, August 2020.

2. Rebecq, H. R., *High speed and high dynamic range video with an event camera,* IEEE Transactions on Pattern Analysis and Machine Intelligence, 2019.

3. Friedel, Zachary P., First Lieutenant, USAF, *Smart Features for Dynamic Vision Sensors,* IEEE/ION Position, Location and Navigation Symposium (PLANS) IEEE. 2020, pp. 973-978.

4. *USAF Test Pilot School Reconfigurable Airborne Sensor, Communications, and Laser (RASCAL)-7 Pod with Ethernet Modification on F-16C/D Blocks 25-52 Aircraft,* FC A2909-02, Air Force Life Cycle Management Center, Wright-Patterson AFB, Ohio 2016.

5. The MathWorks, Inc. *What Is a Neural Network?* Retrieved from MathWorks: https://www.mathworks.com/discovery/neural-network.html, 2020.

6. Nelson, Kaleb J., *Event-based visual-inertial odometry on a fixed-wing unmanned aerial vehicle (thesis),* Air Force Institute of Technology, Wright-Patterson AFB, Ohio, 2019.

7. *Sensor Accuracy Chart,* 412th Range Squadron, Edwards AFB, TSPI Range Office, 2020.

8. *R-2508 Complex User's Handbook,* R-2508 Central Coordinating Facility, Edwards AFB, California, January 2020.

This page was intentionally left blank

.

APPENDIX A – TEST CONDITION MATRIX

Overall test point execution is summarized in Table A1. Each unique profile run was assigned a test point run number for tracking purposes. Test sorties were identified in dedicated matrix columns with quantities of each profile run that was flown. For specific 20 NM and 7 NM profile runs, Tables A2 and A3 contain ground speed/altitude combinations and tolerances that determined the various line of sight rates tested, and were then binned into corresponding line of sight rate classifications. Additional details regarding pixel dwell times and refresh rates were also calculated to further characterize test points.

Table A1 Test Point Matrix.
Actual data points were encompassed within this test matrix databands.

STO/MOP & Test Point Run #	Maneuver / Conditions	Start Steerpoint	End Steerpoint	LOS Rate (Low/Med/High)	Test Point Priority	Min No. of Points (Success Criteria)	Desired No. of Points	Flt 1	Flt 2	Flt 3	Flt 4	Flt 5	Flt 6	Flt 7	Flt 8	Flt 9	Flt 10	Flt 11	Flt 12	Flt 13	Total	Start Altitude (ft AGL)	Altitude Tolerance (± ft of start alt)	Groundspeed Target (kts)	Groundspeed Tolerance (± kts)
STO 1	Demonstrate Navigation Solution Functionality																								
MOP 1.1	Navigation Solution Functionality																								
1	Any flight			Various	1	1	1	1		1	1	1	1	1	1	1	1	1	1	1	13	-	-	-	-
STO 2	Determine Navigation Solution Accuracy as a Result of Varying Flight Conditions																								
MOP 2.1	Drift Rate																								
2	Any flight			Various	1	1	3	1		1	1	1	1		1	1		1	1	1	10	-	-	-	-
MOP 2.2	EVIO Solution Accuracy Variance with Line of Sight Rate (20 nm runs)																								
3				Floor (200' AGL)	2	-	5		5					5							10	350	±150	510		
4				Very High	2	-	5		5					5							10	650		510		
5	Sagebrush	N35° 6.243'	N35° 15.620'	High	1	3	5				3			1.5	1						5.5	1,500		450	±30
6	Black Mountain	W117° 25.316'	W117° 46.753'	Med	1	3	5			0.5	1		1		3						5.5	4,000	±500	300	
7	287°M	2400 ft	3308 ft	Low	1	3	3				1				2						3	7,000		300	
8				Very Low	3	-	3									3					3	20,000 SALT	±1000	350**	±50
MOP 2.3	EVIO Solution Accuracy Variance with Terrain (7 nm runs)																								
9	Sagebrush	N35° 6.243'	N35° 9.564'	Med	1	3	5			1	1		1		3						6	4,000		300	
10	Black Mountain	W117° 25.316'	W117° 32.807'	High	2	-	5				3			1.5	1						5.5	1,500		450	
11	287°M	2400 ft	2764 ft	Low	2	-	3				1				2						3	7,000		300	
12	Lakebed	N35° 0.657'	N35° 4.056'	Med	1	3	5			1	1		1		3						6	4,000		300	
13	Harper Lake	W117° 12.731'	W117° 20.258'	High	2	-	5				3			1.5	1						5.5	1,500		450	
14	287°M	2053 ft	2032 ft	Low	2	-	3				1				2						3	7,000	±500	300	±30
15	Mountain	N35° 9.414'	N35° 13.225'	Med	1	3	5					3			2						5	4,000		300	
16	Isabella MOA	W118° 13.210'	W118° 6.319'	High	2	-	5						3		2						5	1,500		450	
17	044°M	5700 ft	3870 ft	Low	3	-	3						3								3	7,000		300	
18	Urban	N34° 40.545'	N34° 40.574'	Med	1	3	5	5													5	4,000		300	
19	Lancaster/Palmdale	W118° 13.115'	W118° 4.599'	High	2	-	5	5													5	1,500		450	
20	078°M	2385 ft	2423 ft	Low	3	-	3	3													3	7,000		300	
MOP 2.4	EVIO Solution Accuracy Variance with Ambient Lighting Conditions																								
21 / 9	Day from above	same as Sagebrush TP9		Med	1	3	5			1	1		1		3						6	4,000		300	
22	Dawn/Dusk	same as Sagebrush TP9		Med	1	3	5											5	15		20	4,000	±500	300	±30
23	Night	same as Urban TP18		Med	2	3	5											5	8		13	4,000		300	
MOP 2.5	EVIO Solution Accuracy Variance with Dynamic Maneuvering																								
24	Dynamic Profile	Airspace as required		Various	2	3	15	1	1	1			0.1			1	2				6.1	10-25K MSL	-	Various	-
STO 3	Collect Operationally Representative Profile Data																								
MOP 3.1	Record EBS Imagery, IMU Data, and TSPI of Operational Profile																								
25	Operational Profile	Isabella MOA and Sidewinder		Various	3	1	2					1	1				1				3	various	-	Various	-
STO 4	Collect Imagery, IMU Data, and TSPI of Ground-Moving and Airborne Targets																								
MOP 4.1	Record EBS Imagery, IMU Data, and TSPI of Ground-Moving Target																								
26	Ground-Moving	N35° 9.734'	N35° 11.910'	Various	4	1	3		19												19	Max 3000' AGL*	-	Various	-
MOP 4.2	Record EBS Imagery, IMU Data, and TSPI of Airborne Target																								
27	Airborne Target	Airspace as required		Various	4	1	3									3					3	6	10-15K MSL	-	250-350	-

Table A2 Line of Sight Classifications for 20 NM runs

Test Point Details

MOP:	LOS
Test Point Eval Leg Dist, D_{eval} [NM]:	20

Optical FOV Details

EBS FOV	FOV [°]	1/2 FOV [°]
FOV_{long}	90	45
FOV_{lat}	67	33.5

Event-Based Sensor FOV Details

EBS Focal Length	EBS Pixel Size	$IFOV$
[mm]	[um]	[°]
6	18.5	0.1767

Test Points in Priority Order

Line of Sight Classification and Tolerance Bands*	Ground Speed (GS)		HAT at start	Predicted FOV		Pixel Dwell Time in Frame	Time to Cover	Pixel Ground Distance	Pixel Refresh Rate	LOS Bin Label and t_{dwell} [sec]
	[knots]	[ft/sec]	[ft AGL]	L_{long} (fore/aft) [ft]	L_{lat} (left/right) [ft]	t_{dwell} along direction of travel (L_{long}) [sec]	Eval Leg, t_{eval} [min]	D_{pixel} [ft]	f_{pixel} [Hz]	
formulae:	*user defined*	$GS\left[\frac{NM}{hr}\right] \times \frac{6076\left[\frac{ft}{NM}\right]}{3600\left[\frac{sec}{hr}\right]}$	*user defined*	$2 \times HAT\ [ft] \times \tan\left(\frac{FOV_{long\ or\ lat}[°]}{2}\right)$		$\frac{L_{long}\ [ft]}{GS\left[\frac{ft}{sec}\right]}$	$60\left[\frac{min}{hr}\right] \times \frac{D_{eval}\ [NM]}{GS\left[\frac{NM}{hr}\right]}$	$2 \times HAT\ [ft] \times \tan\left(\frac{IFOV\ [°]}{2}\right)$	$\frac{GS\left[\frac{ft}{sec}\right]}{D_{pixel}\ [ft]}$	
(lowest LOS tolerance)	270	456	4500	9000	5957	19.75	4.4	13.88	32.84	**Medium LOS 10-20 sec**
Medium LOS	300	506	4000	8000	5295	15.80	4.0	12.33	41.05	
(highest LOS tolerance)	330	557	3500	7000	4633	12.57	3.6	10.79	51.61	
High (lowest LOS tolerance)	420	709	2000	4000	2648	5.64	2.9	6.17	114.95	**High LOS 2-10 sec**
High LOS	450	760	1500	3000	1986	3.95	2.7	4.63	164.22	
High (highest LOS tolerance)	480	810	1000	2000	1324	2.47	2.5	3.08	262.75	
Low (lowest LOS tolerance)	270	456	7500	15000	9928	32.92	4.4	23.13	19.71	**Low LOS 20-35 sec**
Low LOS	300	506	7000	14000	9266	27.65	4.0	21.58	23.46	
Low (highest LOS tolerance)	330	557	6500	13000	8605	23.34	3.6	20.04	27.79	
(lowest LOS tolerance)	480	810	800	1600	1059	1.97	2.5	2.47	328.43	**Very High LOS 1-2 sec**
Very High LOS	510	861	650	1300	860	1.51	2.4	2.00	429.49	
(highest LOS tolerance)	540	911	500	1000	662	1.10	2.2	1.54	591.18	
High (lowest LOS tolerance)	480	810	400	800	530	0.99	2.5	1.23	656.86	**Floor High LOS <1 sec**
Floor (Very Very High) LOS	510	861	300	600	397	0.70	2.4	0.93	930.56	
High (highest LOS tolerance)	540	911	200	400	265	0.44	2.2	0.62	1477.95	
Low (lowest LOS tolerance)	300	506	21000	42000	27799	82.95	4.0	64.75	7.82	**Very Low LOS >35 sec**
Very Low LOS	350	591	20000	40000	26475	67.71	3.4	61.67	9.58	
Low (highest LOS tolerance)	400	675	19000	38000	25152	56.29	3.0	58.58	11.52	

*Lowest LOS rates based on low airspeed/high altitude errors combined, and vice versa for highest LOS rates.

Table A3 Line of Sight Classifications for 7 NM runs

Test Point Details

MOP:	Terrain
Test Point Eval Leg Dist, D_{eval} [nm]:	7

Optical FOV Details

EBS FOV	FOV [°]	1/2 FOV [°]
FOV_{long}	90	45
FOV_{lat}	67	33.5

Event-Based Sensor FOV Details

EBS Focal Length	EBS Pixel Size	*IFOV*
[*mm*]	[*um*]	[°]
6	18.5	0.1767

Test Points in Priority Order

Line of Sight Classification and Tolerance Bands*	Ground Speed (*GS*)		*HAT* at start	Predicted FOV		Pixel Dwell Time in Frame	Time to Cover	Pixel Ground Distance	Pixel Refresh Rate	LOS Bin Label and t_{dwell} [sec]
	[*knots*]	[*ft/sec*]	[*ft AGL*]	L_{long} (fore/aft) [*ft*]	L_{lat} (left/right) [*ft*]	t_{dwell} along direction of travel (L_{lo} [*sec*]	Eval Leg, t_{eval} [*min*]	D_{pixel} [*ft*]	f_{pixel} [*Hz*]	
formulae:	*user defined*	$GS\left[\frac{NM}{hr}\right] \times \frac{6076.\left[\frac{ft}{NM}\right]}{3600.\left[\frac{sec}{hr}\right]}$	*user defined*	$2 \times HAT\ [ft] \times \tan\left(\frac{FOV_{long\ or\ lat}\ [°]}{2}\right)$		$\frac{L_{long}\ [ft]}{GS\left[\frac{ft}{sec}\right]}$	$60\left[\frac{min}{hr}\right] \times \frac{D_{eval}\ [NM]}{GS\left[\frac{NM}{hr}\right]}$	$2 \times HAT\ [ft] \times \tan\left(\frac{IFOV\ [°]}{2}\right)$	$\frac{GS\left[\frac{ft}{sec}\right]}{D_{pixel}\ [ft]}$	
(lowest LOS tolerance)	270	456	4500	9000	5957	19.75	1.6	13.88	32.84	**Medium LOS 10-20 sec**
Medium LOS	300	506	4000	8000	5295	15.80	1.4	12.33	41.05	
(highest LOS tolerance)	330	557	3500	7000	4633	12.57	1.3	10.79	51.61	
High (lowest LOS tolerance)	420	709	2000	4000	2648	5.64	1.0	6.17	114.95	**High LOS 2-10 sec**
High LOS	450	760	1500	3000	1986	3.95	0.9	4.63	164.22	
High (highest LOS tolerance)	480	810	1000	2000	1324	2.47	0.9	3.08	262.75	
Low (lowest LOS tolerance)	270	456	7500	15000	9928	32.92	1.6	23.13	19.71	**Low LOS 20-35 sec**
Low LOS	300	506	7000	14000	9266	27.65	1.4	21.58	23.46	
Low (highest LOS tolerance)	330	557	6500	13000	8605	23.34	1.3	20.04	27.79	

*Lowest LOS rates based on low airspeed/high altitude errors combined, and vice versa for highest LOS rates.

APPENDIX B – DATA ANALYSIS

The on-board processor created Lightweight Communications and Marshalling (LCM) files that contained the events, IMU, and timing data. During the flight, the FTE noted the UTC time that test runs began and ended. Post-flight, the UTC times were converted to Unix time and used to segment out a new LCM file for each test run from the LCM files created in flight. The ARDS truth position, velocity, and attitude were provided in a comma-separated values (.csv) file.

The LCM file and the truth .csv for each test run were processed using an AFIT provided code which separated the LCM file into a text file of the events stream, a .csv of the IMU data, and converted the ARDS truth file into a .csv that was formatted to be referenced by AFIT provided codes.

The events text file was processed through the front end neural network to reconstruct images based on the events. The images were output at a fixed rate of 20 Hz by the neural network.

The Kalman filter obtained the initial truth position from the truth .csv file, and processed the reconstructed images and IMU through the convolutional neural network to predict the changes in position, velocity, and attitude from the initial position.

The position estimations were converted from meters to nautical miles. The velocity estimations were converted from m/s to knots.

For all test points, the vertical velocity increased by over 2000 knots/min. The error of the vertical position and velocity estimations were far greater than in the other directions, so they were excluded from the majority of data analysis.

For the straight and level runs associated with determining the effects of terrain, LOS rate, and lighting, the truth north and east position values changed consistently and the velocities were constant, so the values were predictable. Additionally, the position and velocity estimates from the Kalman filter rapidly deviated from the truth values, so any variations in the truth values were not significant compared to the estimation error. To limit the number of plots and to simplify the data, the north and east positions and velocities were combined to create lateral position and vertical position using the equation below.

$$Lateral\ Postion = \sqrt{North\ Position^2 + East\ Position^2}$$

$$Lateral\ Velocity = \sqrt{North\ Velocity^2 + East\ Velocity^2}$$

The error for the estimations was calculated as:

$$Error = Truth - Estimate$$

For roll and yaw, errors greater in magnitude than 180° were corrected to stay within +/- 180°.

The root mean square errors for position, velocity, and attitude were calculated and used to compare runs. They were calculated over the run as

$$RMSE = \sqrt{\frac{\sum Error}{\#\ samples}}$$

For the dynamic maneuvering, the timings of the maneuvers varied in length, so the RMSE was not used. The truth and estimates for each parameter were plotted against each other and general behaviors were noted.

The median RMSE between the different LOSR shown in Table B1 showed that the high LOSR runs had the lowest overall RMSE in orientation for roll and pitch. However, the yaw RMSE showed the lowest overall RMSE for the medium LOSR. The data does not clearly support a conclusive statement that a trend existed showing one LOSR provided better performance than other LOSRs.

Table B1 Varying LOSR Orientation Median RMSE Results

LOS Rate	Roll RMSE (deg)	Pitch RMSE (deg)	Yaw RMSE (deg)
Very Low	72.1	31.8	68.5
Low	93.0	36.9	61.4
Med	93.3	36.0	50.2
High	66.7	18.5	58.1
Very High	91.5	45.6	71.9
Floor	81.5	42.2	72.2

Table B2 Varying LOSR Lateral Position and Velocity Median RMSE Results

LOS Rate	Lateral Position RMSE (NM)	Lateral Velocity RMSE (knots)
Very Low	2.88	179.66
Low	2.95	247.73
Med	5.45	288.49
High	1.29	145.43
Very High	2.20	39.04
Floor	2.08	76.26

The roll, pitch, and yaw median RMSE were consistent and do not prove a difference between the day and dusk runs over sagebrush as shown in Table B3. However, these runs still showed about a 100 degree roll RMSE, 44 degree pitch RMSE, and ~66 degree (average) yaw RMSE. These runs were performed at the same airspeeds and altitudes during the day and during civil twilight (dusk).

Table B3 Day and Dusk Orientation Median RMSE Results

Light	Roll RMSE (deg)	Pitch RMSE (deg)	Yaw RMSE (deg)
Day	99.7	43.2	68.7
Dusk	100.0	44.0	63.7

Table B4 Day and Dusk Lateral Position and Velocity Median RMSE Results

Light	Lateral Position RMSE (NM)	Lateral Velocity RMSE (knots)
Day	0.61	81.3
Dusk	0.62	69.6

The day and night runs over the city of Lancaster, CA provided similar results and did not show a significant difference in the lighting sources for the orientation error. Table B3 shows the orientation median RMSE for the runs.

Table B5 Day and Night Orientation Median RMSE Results

Light	Roll RMSE (deg)	Pitch RMSE (deg)	Yaw RMSE (deg)
Day	106.6	35.4	21.9
Night	105.5	31.6	20.7

Table B6 Day and Night Lateral Position and Velocity Median RMSE Results

Light	Lateral Position RMSE (NM)	Lateral Velocity RMSE (knots)
Day	2.09	117.5
Night	1.68	95.8

The runs over different terrain features and orientation median RMSE is shown in Table B4. The results do not show significantly different roll or pitch RMSE errors between the different landscapes. However, there are significant differences in the yaw RMSE with the feature-rich urban terrain showing the least error over the runs and the feature-less lakebed showing the worst errors.

Table B7 Terrain Orientation Median RMSE Results

Light	Roll RMSE (deg)	Pitch RMSE (deg)	Yaw RMSE (deg)
Sagebrush	99.7	43.2	68.7
Lakebed	96.9	45.0	73.6
Mountain	99.2	41.9	47.2
Urban	106.6	35.4	21.9

Table B8 Terrain Lateral Position and Velocity Median RMSE Results

Light	Lateral Position RMSE (NM)	Lateral Velocity RMSE (knots)
Sagebrush	0.61	81.3
Lakebed	0.69	64.9
Mountain	3.00	102.0
Urban	2.06	118.9

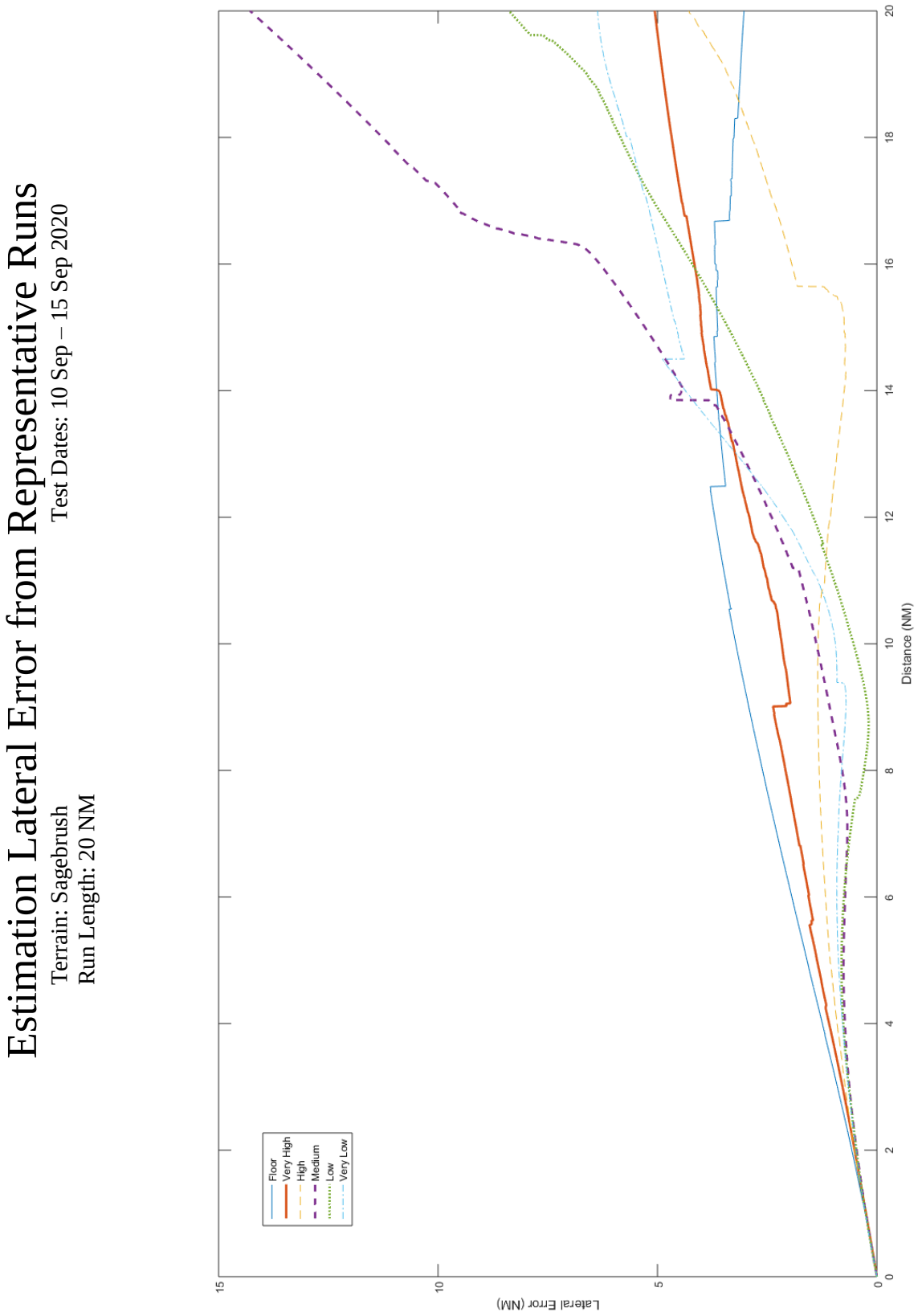

Figure B1 LOSR Effect on Lateral Position Error Over 20 NM Run Over Sagebrush

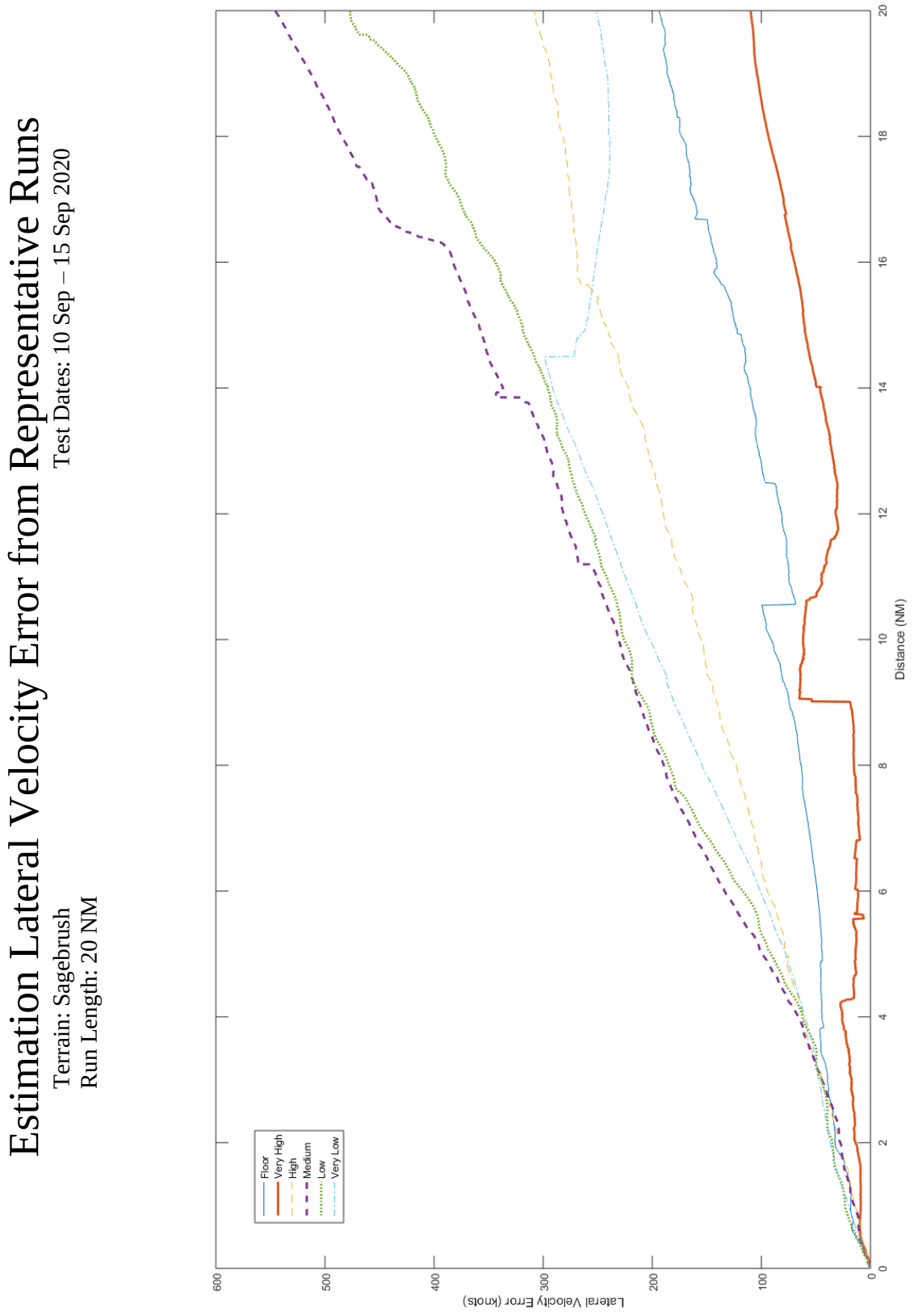

Figure B2 LOSR Effect on Lateral Velocity Error Over 20 NM Run Over Sagebrush

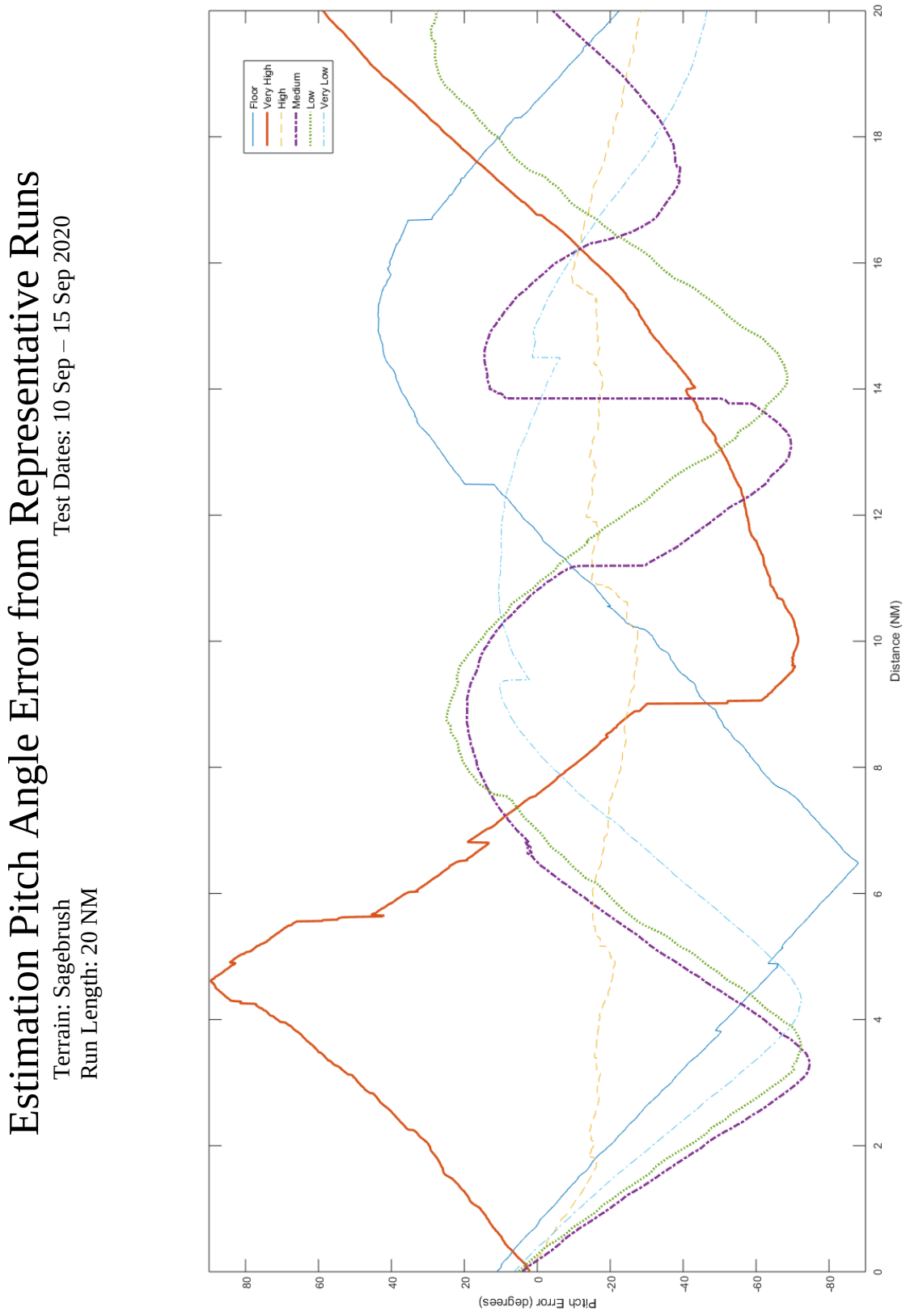

Figure B3 LOSR Effect on Pitch Angle Error Over 20 NM Run Over Sagebrush

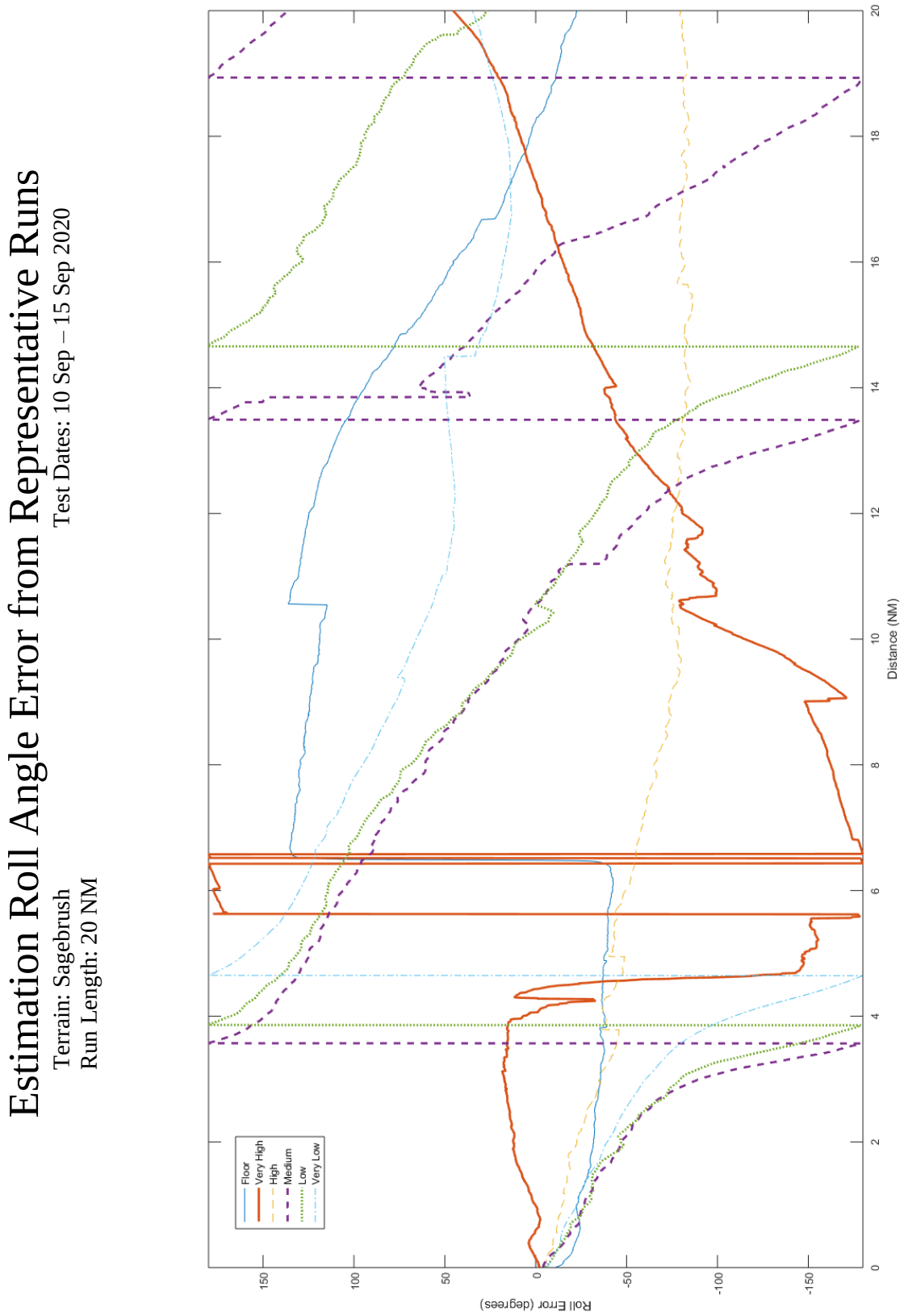

Figure B4 LOSR Effect on Roll Angle Error Over 20 NM Run Over Sagebrush

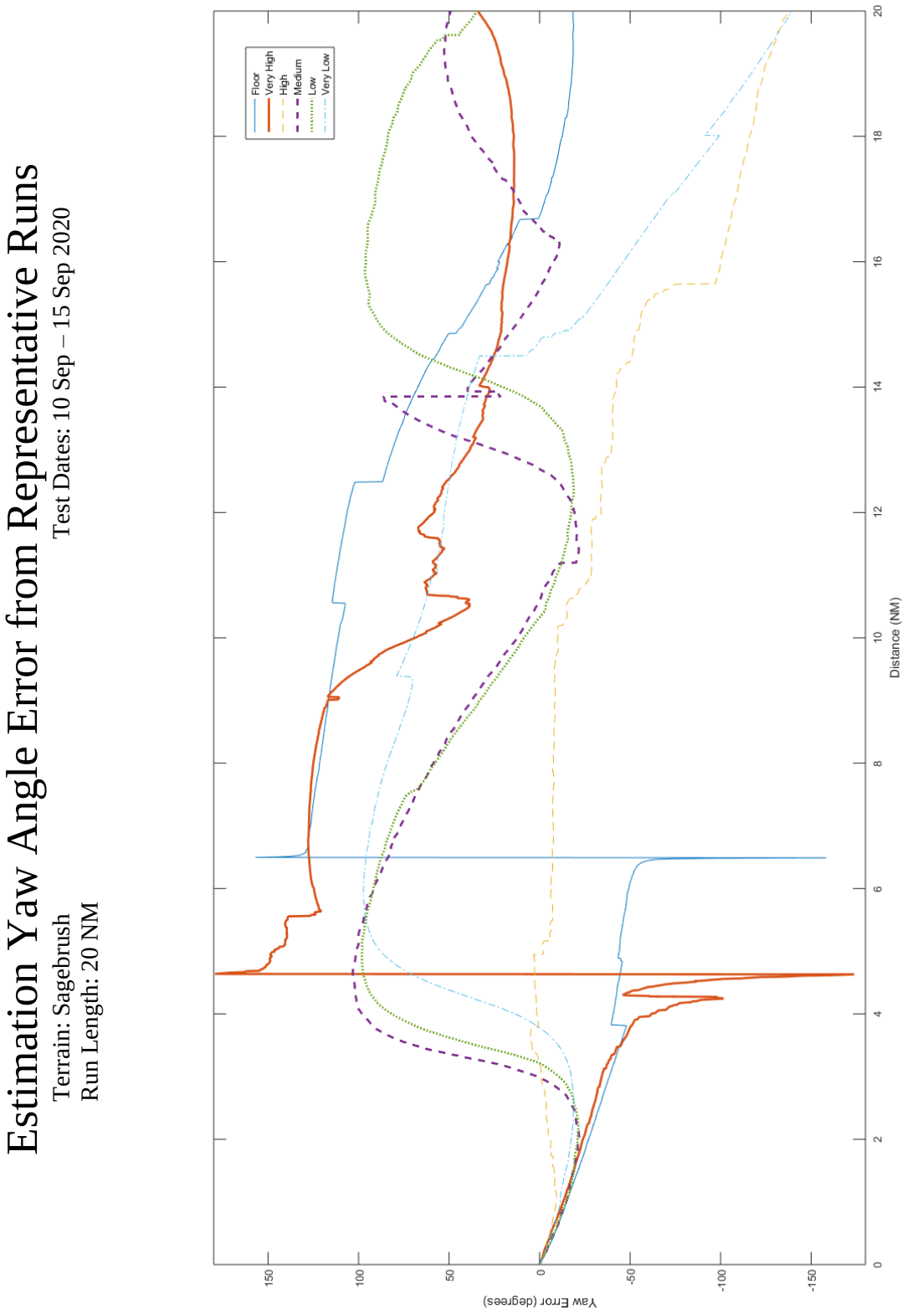

Figure B5 LOSR Effect on Yaw Angle Error Over 20 NM Run Over Sagebrush

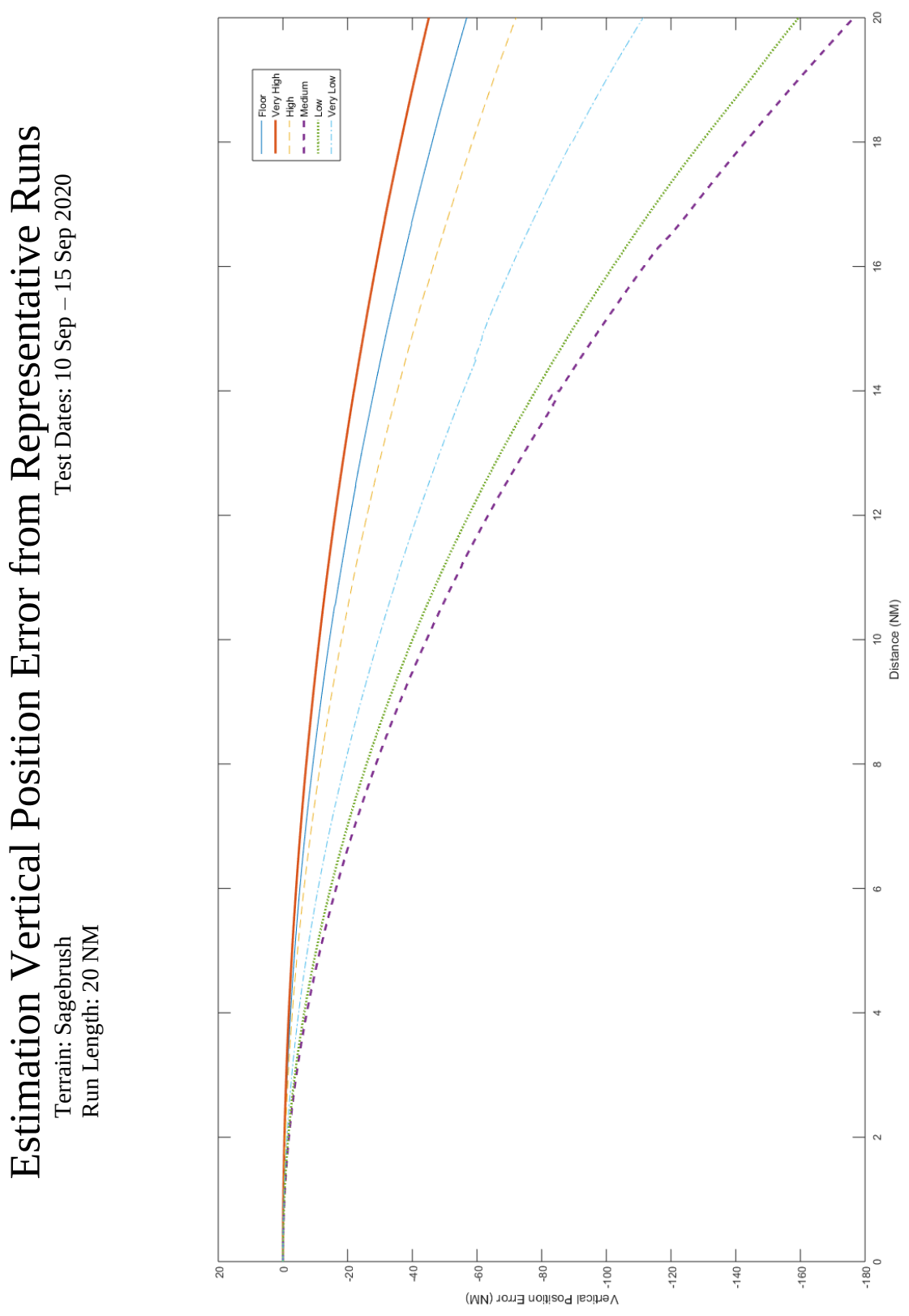

Figure B6 LOSR Effect on Vertical Error Over 20 NM Run Over Sagebrush

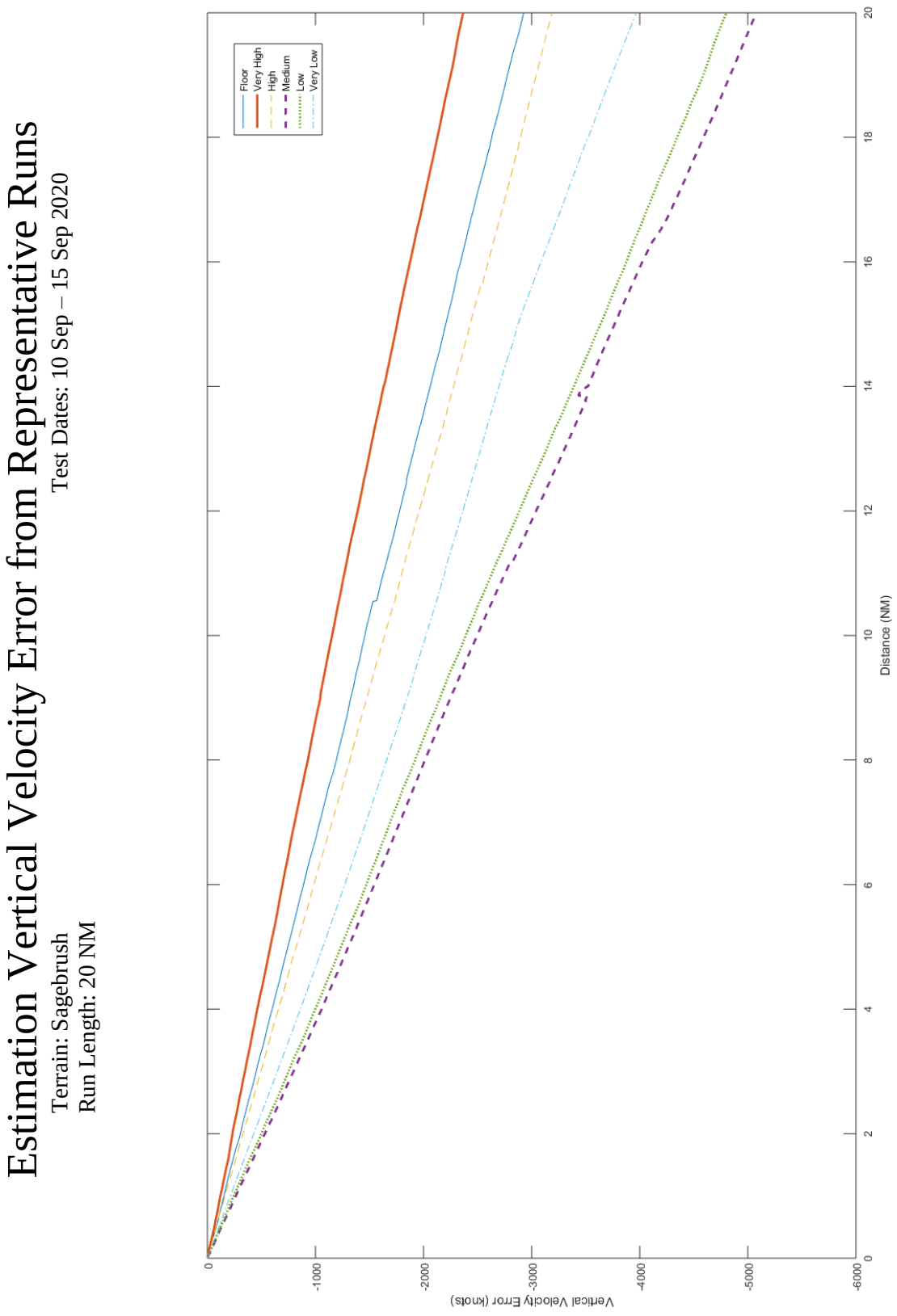

Figure B7 LOSR Effect on Vertical Velocity Error Over 20 NM Run Over Sagebrush

Estimation Lateral Position Error from Representative Runs

LOSR: Medium
HAT: 4,000 ft ± 500 ft
KGS: 300 ± 30

Test Dates: 9 Sep – 11 Sep 2020
Run Length: 7 NM

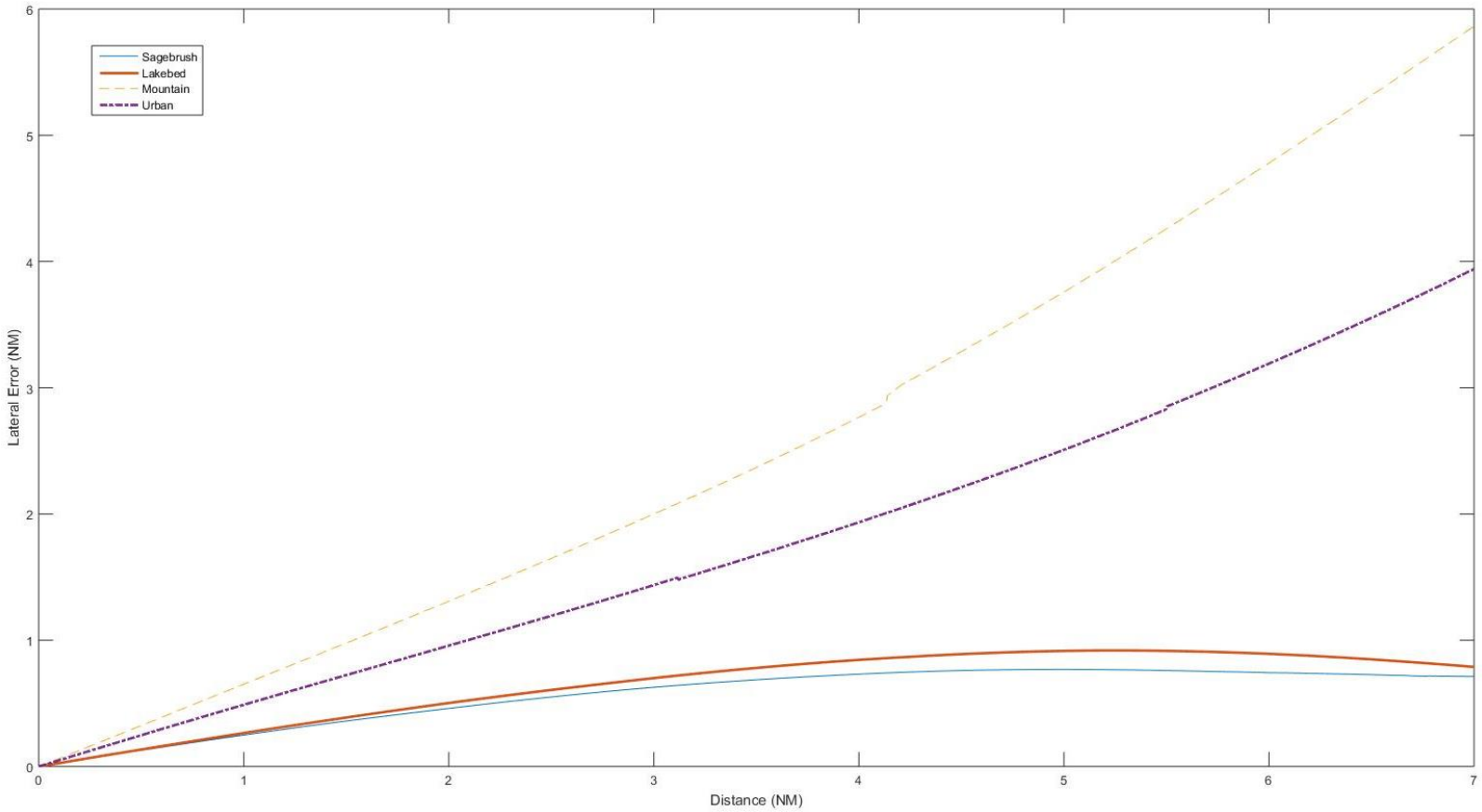

Figure B8 Terrain Effect on Lateral Position Error Over 7 NM Run

Estimation Lateral Velocity Error from Representative Runs

LOSR: Medium
HAT: 4,000 ft ± 500 ft
KGS: 300 ± 30

Test Dates: 9 Sep – 11 Sep 2020
Run Length: 7 NM

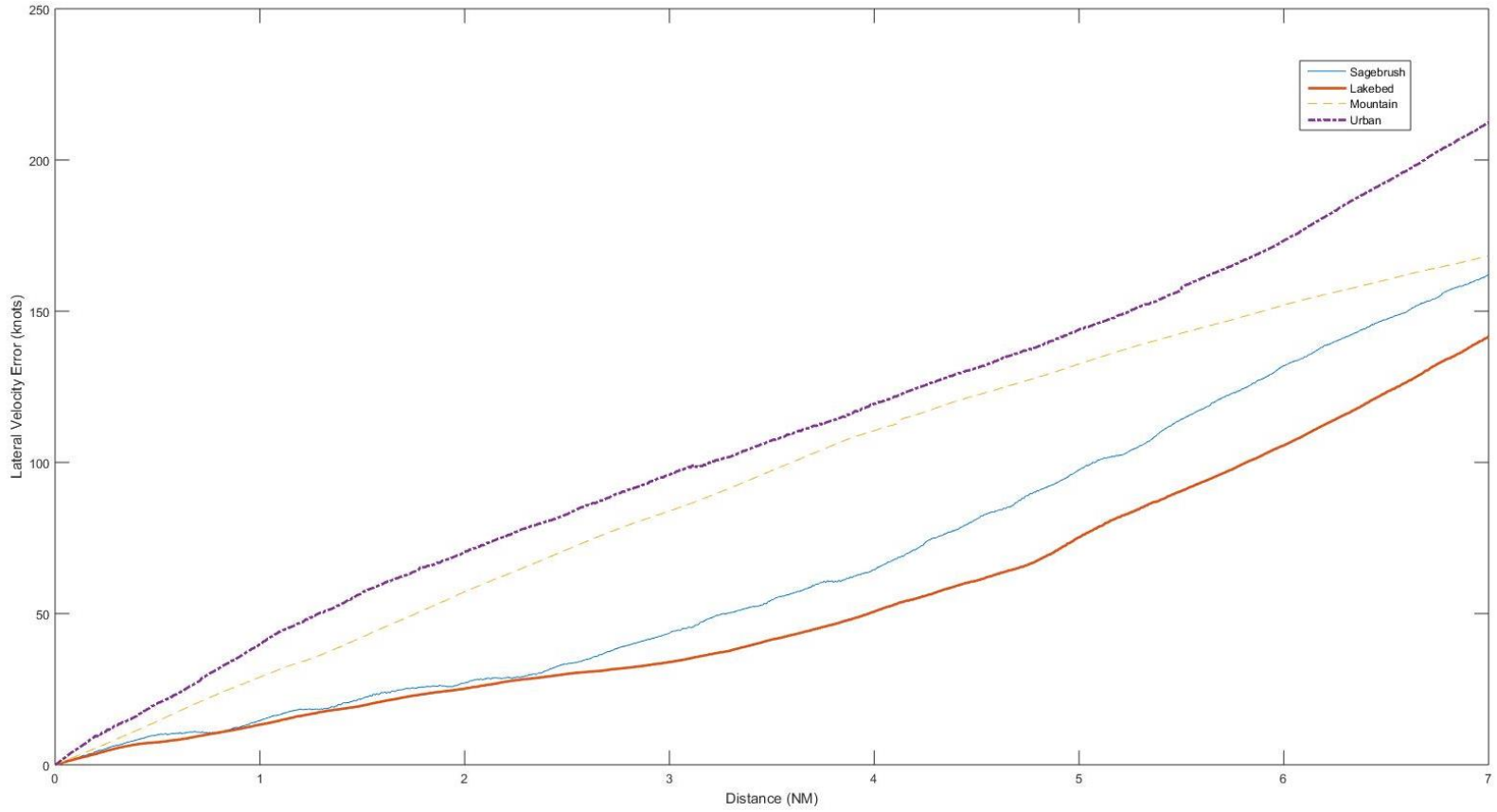

Figure B9 Terrain Effect on Lateral Velocity Error Over 7 NM Run

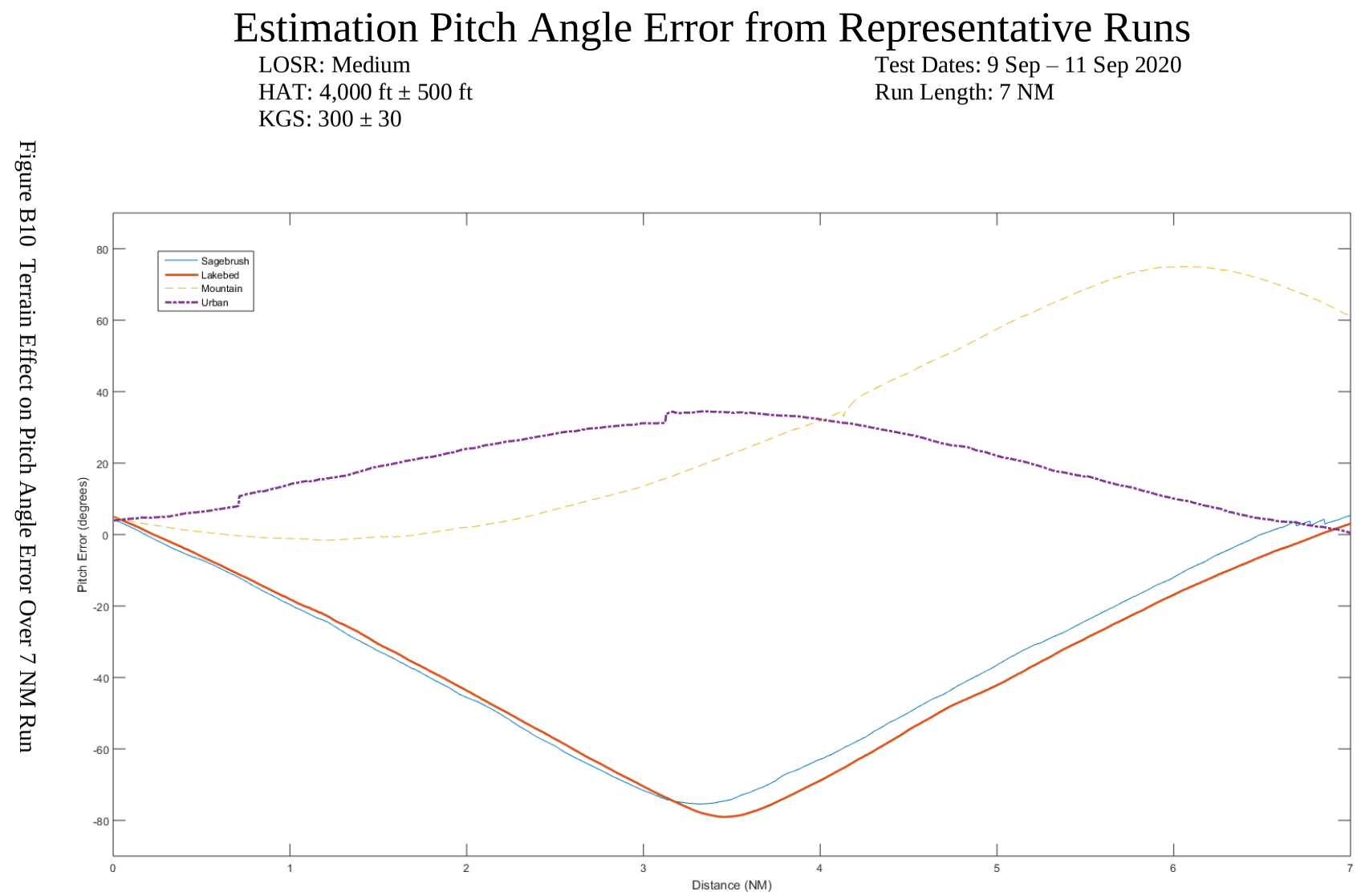

Figure B10 Terrain Effect on Pitch Angle Error Over 7 NM Run

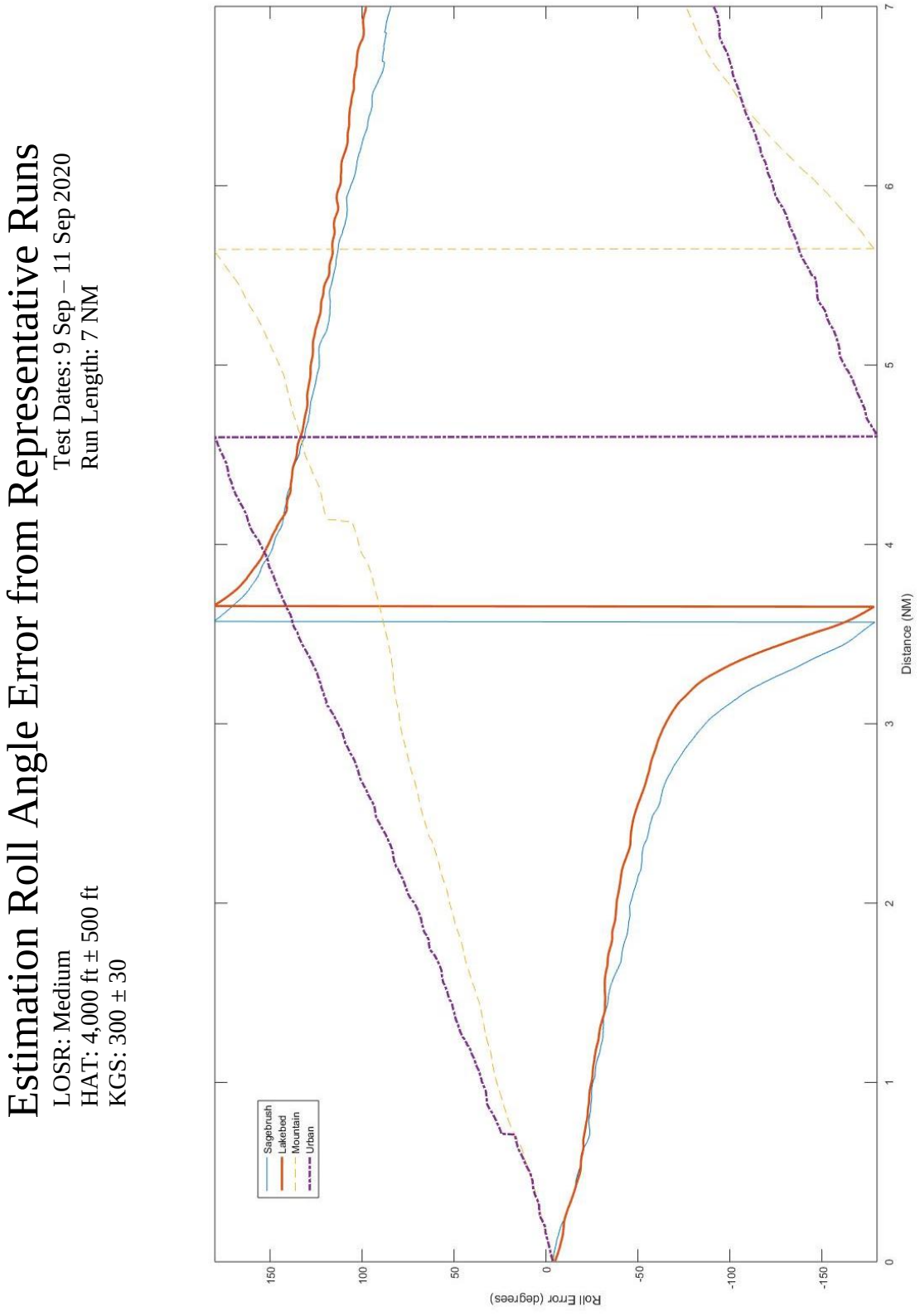

Figure B11 Terrain Effect on Roll Angle Error Over 7 NM Run

Estimation Yaw Angle Error from Representative Runs

LOSR: Medium
HAT: 4,000 ft ± 500 ft
KGS: 300 ± 30

Test Dates: 9 Sep – 11 Sep 2020
Run Length: 7 NM

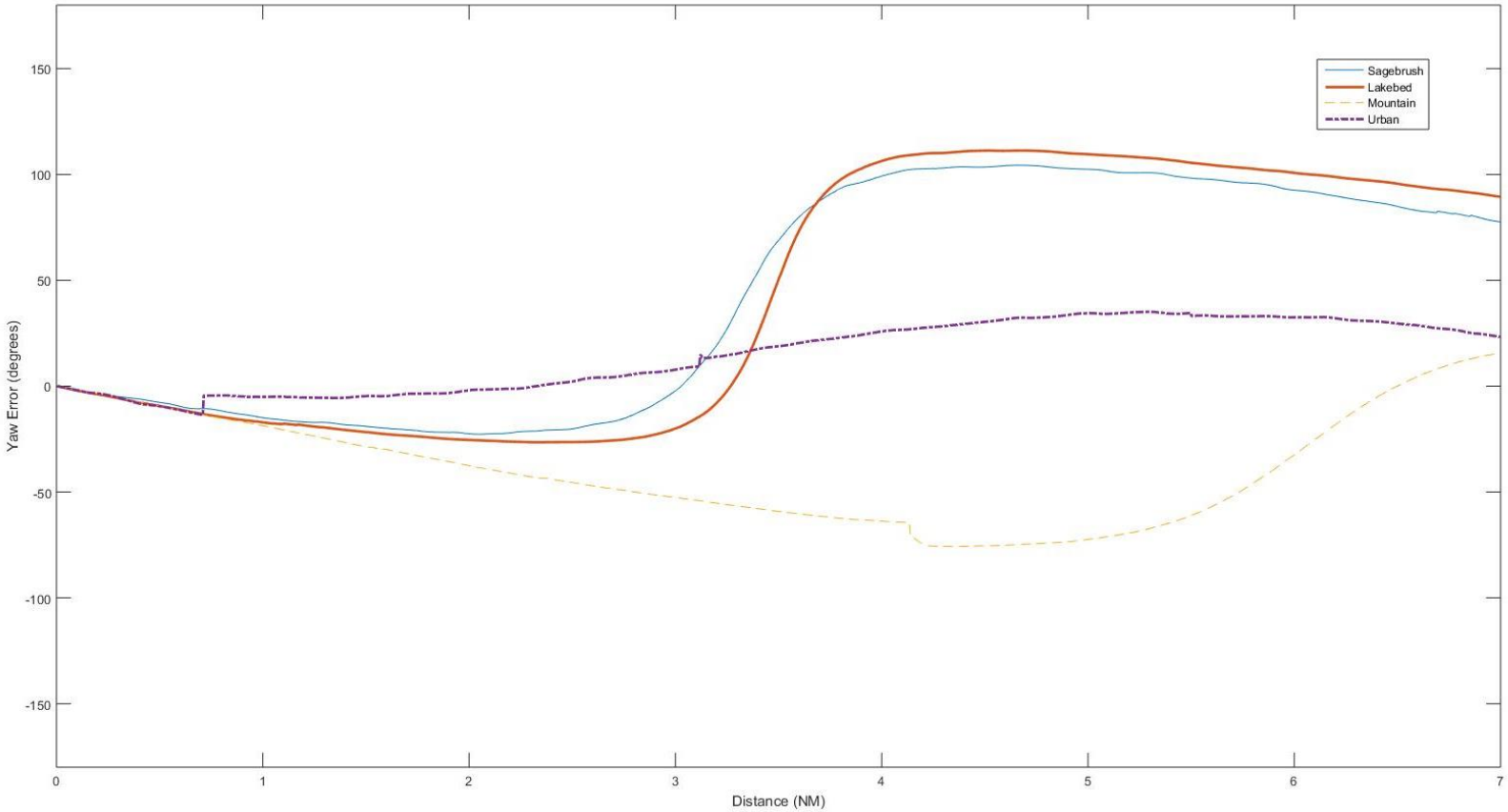

Figure B12 Terrain Effect on Yaw Angle Error Over 7 NM Run

Figure B13 Terrain Effect on Vertical Position Error Over 7 NM Run

Estimation Vertical Velocity Error from Representative Runs

LOSR: Medium
HAT: 4,000 ft ± 500 ft
KGS: 300 ± 30

Test Dates: 9 Sep – 11 Sep 2020
Run Length: 7 NM

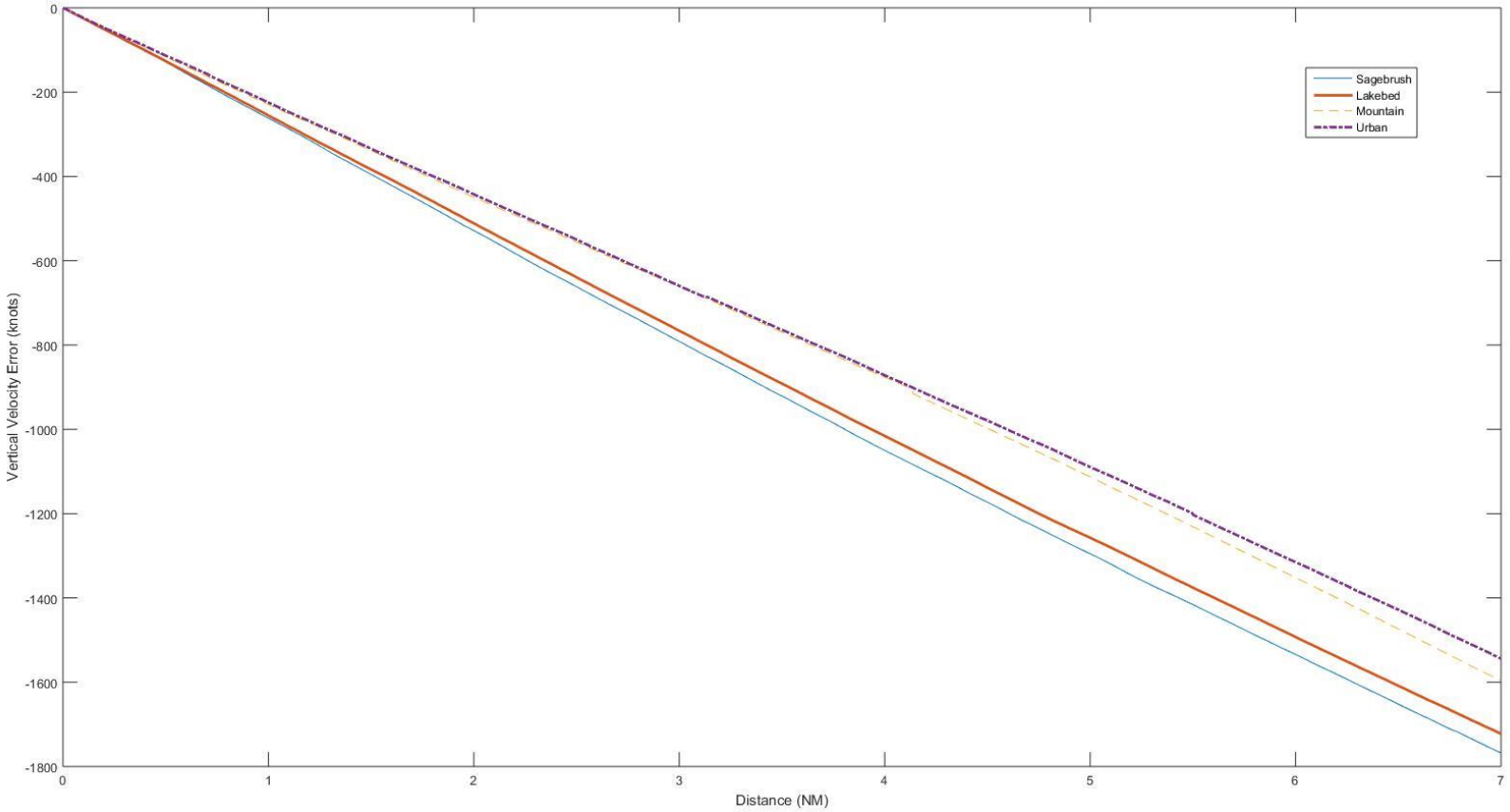

Figure B14 Terrain Effect on Vertical Velocity Error Over 7 NM Run

Estimation Lateral Position Error from Representative Runs

LOSR: Medium
HAT: 4,000 ft ± 500 ft
KGS: 300 ± 30

Test Dates: 10 Sep – 18 Sep 2020
Run Length: 7 NM
Terrain: Sagebrush

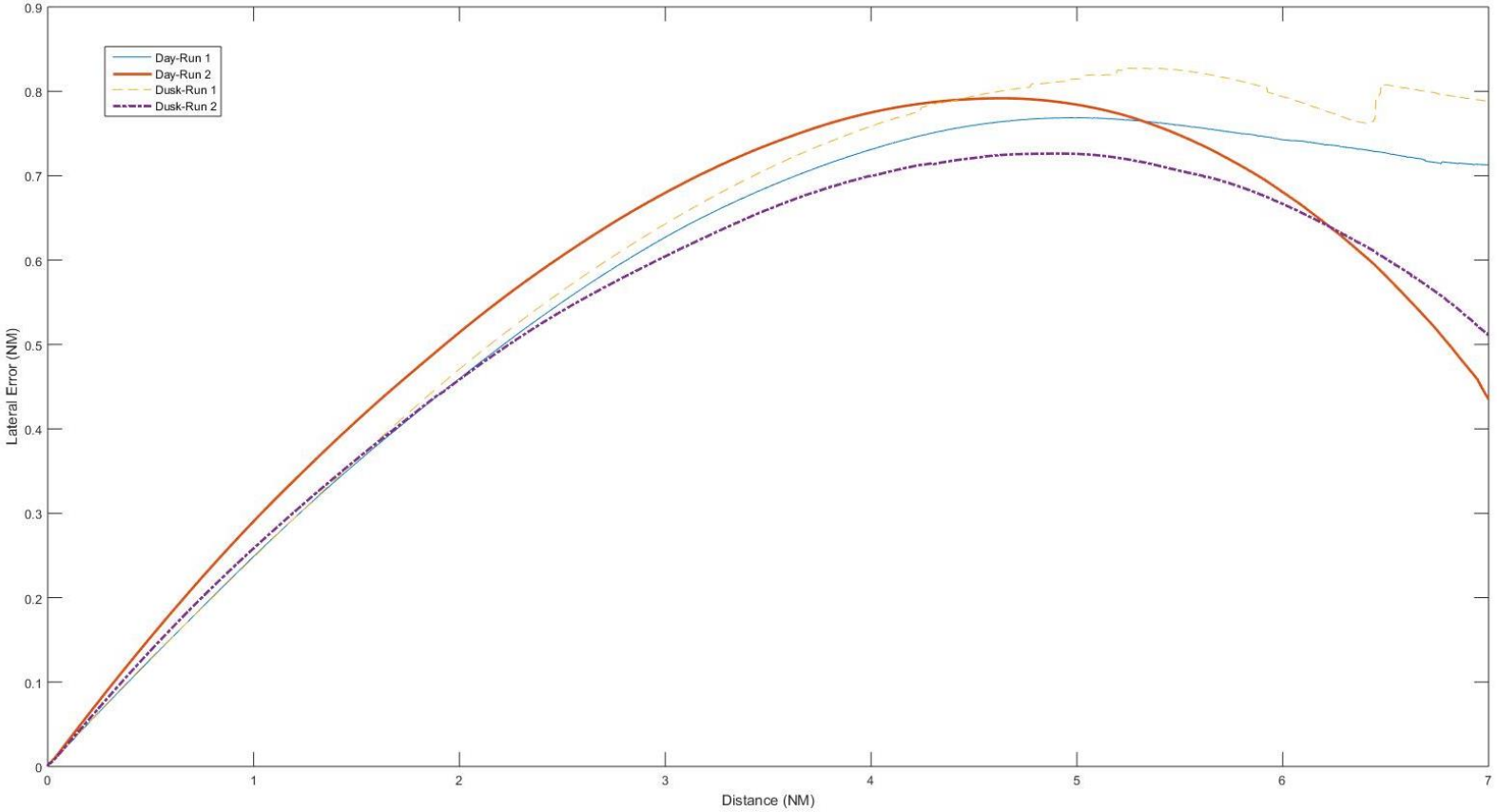

Figure B15 Dusk Lighting Effect on Lateral Position Error Over 7 NM Run

Estimation Lateral Velocity Error from Representative Runs

LOSR: Medium
HAT: 4,000 ft ± 500 ft
KGS: 300 ± 30

Test Dates: 10 Sep – 18 Sep 2020
Run Length: 7 NM
Terrain: Sagebrush

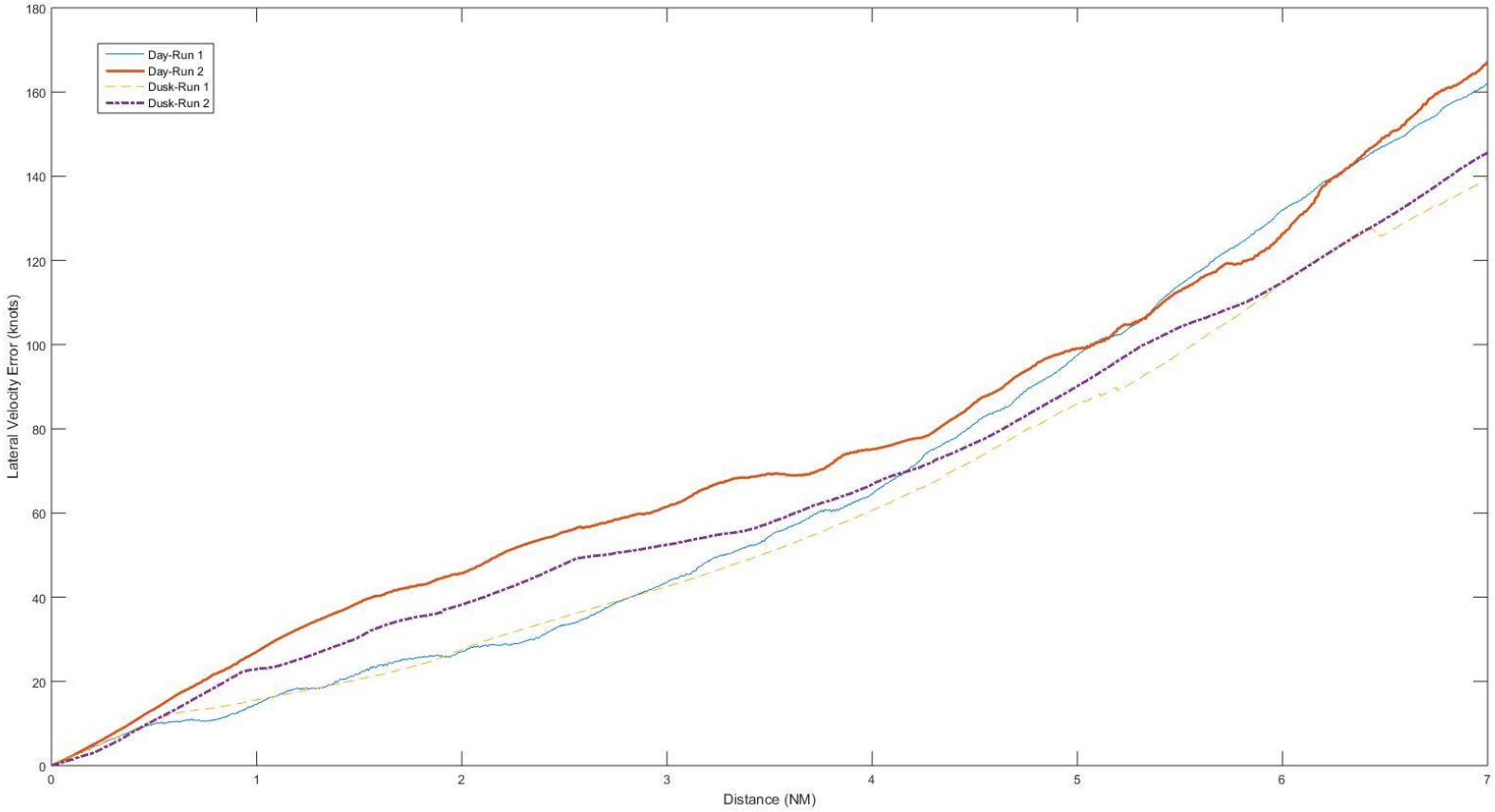

Figure B16 Dusk Lighting Effect on Lateral Velocity Error Over 7 NM Run

Estimation Pitch Angle Error from Representative Runs

LOSR: Medium
HAT: 4,000 ft ± 500 ft
KGS: 300 ± 30

Test Dates: 10 Sep – 18 Sep 2020
Run Length: 7 NM
Terrain: Sagebrush

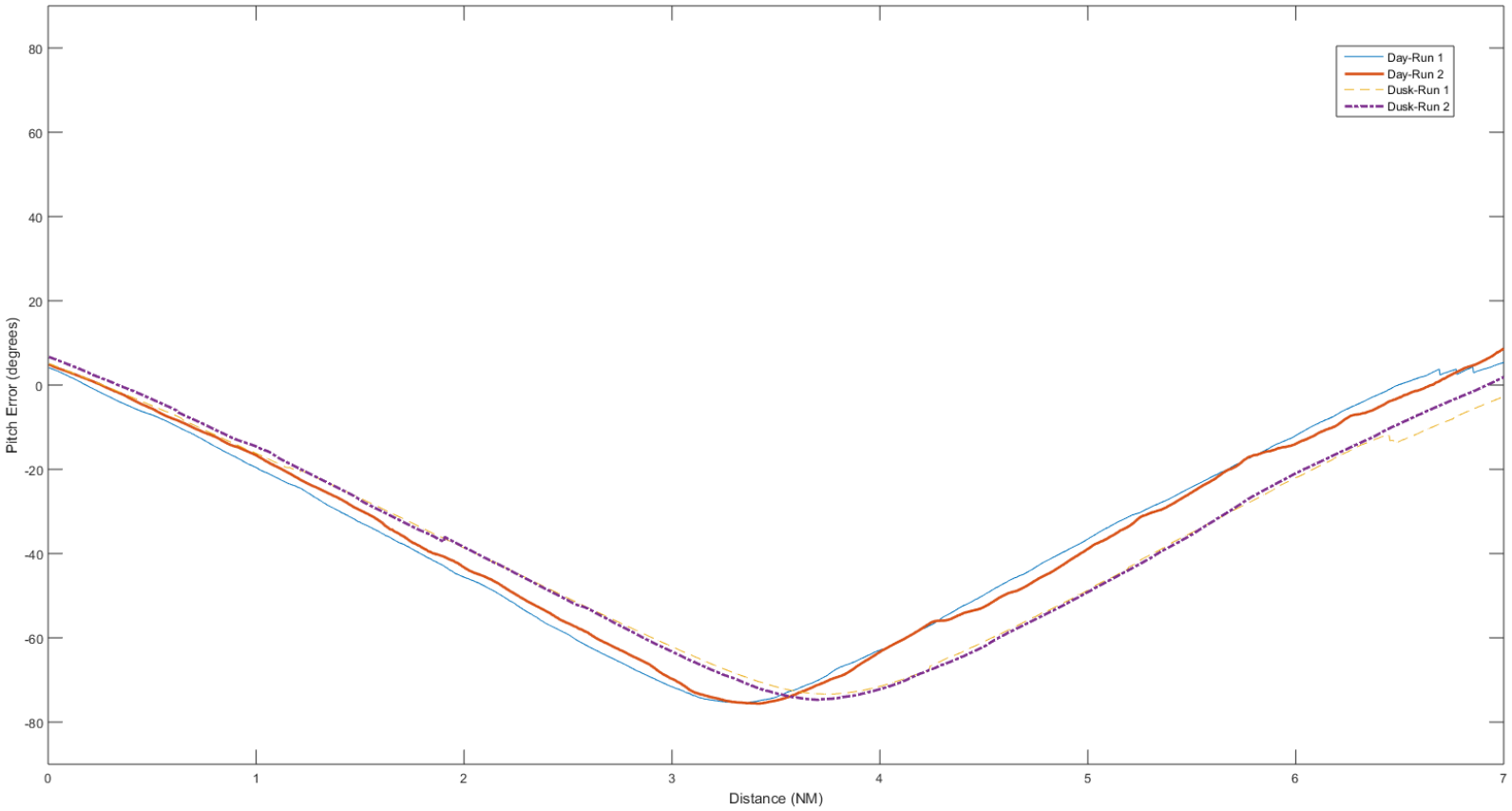

Figure B17 Dusk Lighting Effect on Pitch Angle Error Over 7 NM Run

Estimation Roll Angle Error from Representative Runs

LOSR: Medium
HAT: 4,000 ft ± 500 ft
KGS: 300 ± 30

Test Dates: 10 Sep – 18 Sep 2020
Run Length: 7 NM
Terrain: Sagebrush

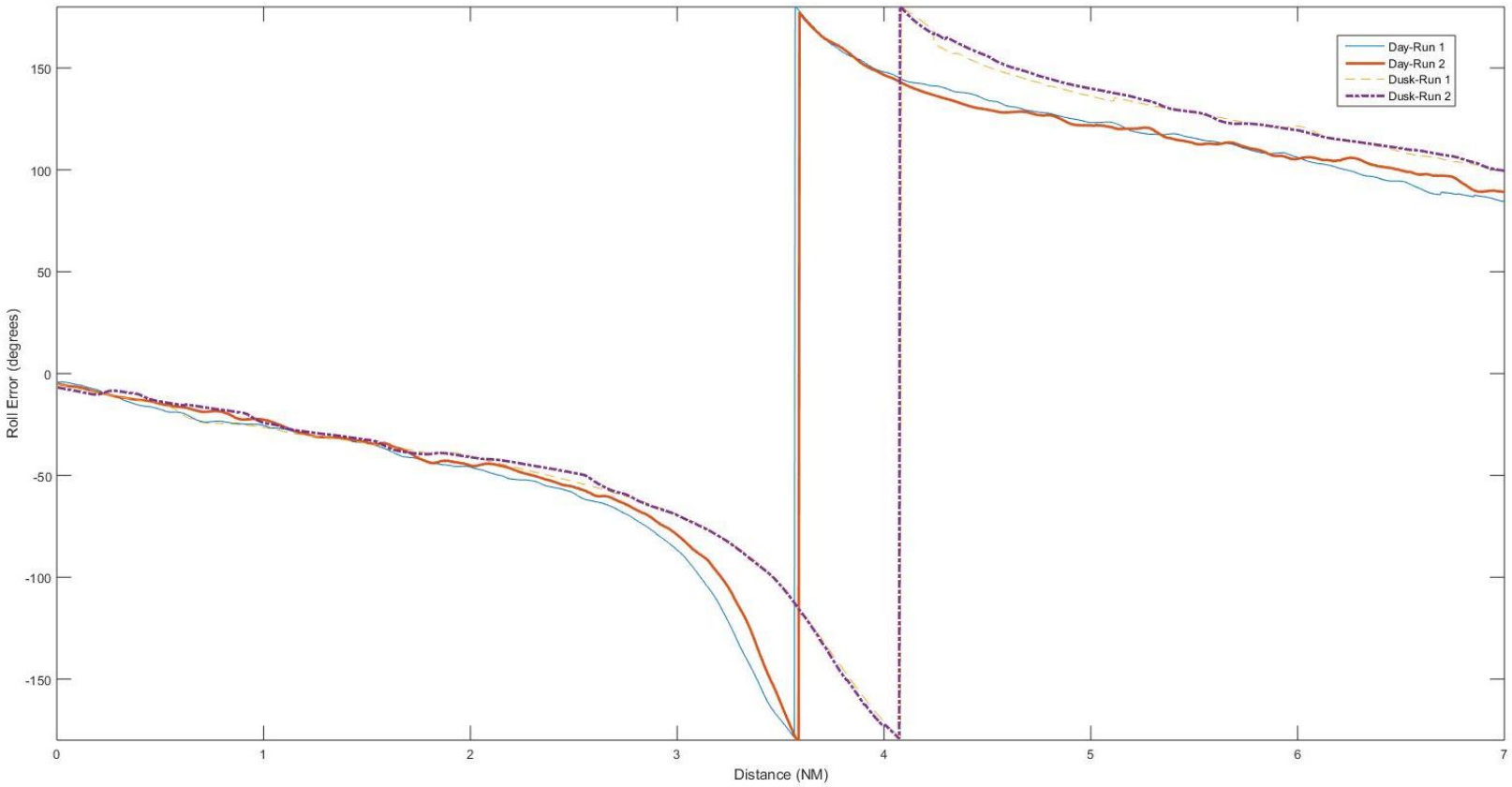

Figure B18 Dusk Lighting Effect on Roll Angle Error Over 7 NM Run

Estimation Yaw Angle Error from Representative Runs

LOSR: Medium
HAT: 4,000 ft ± 500 ft
KGS: 300 ± 30

Test Dates: 10 Sep – 18 Sep 2020
Run Length: 7 NM
Terrain: Sagebrush

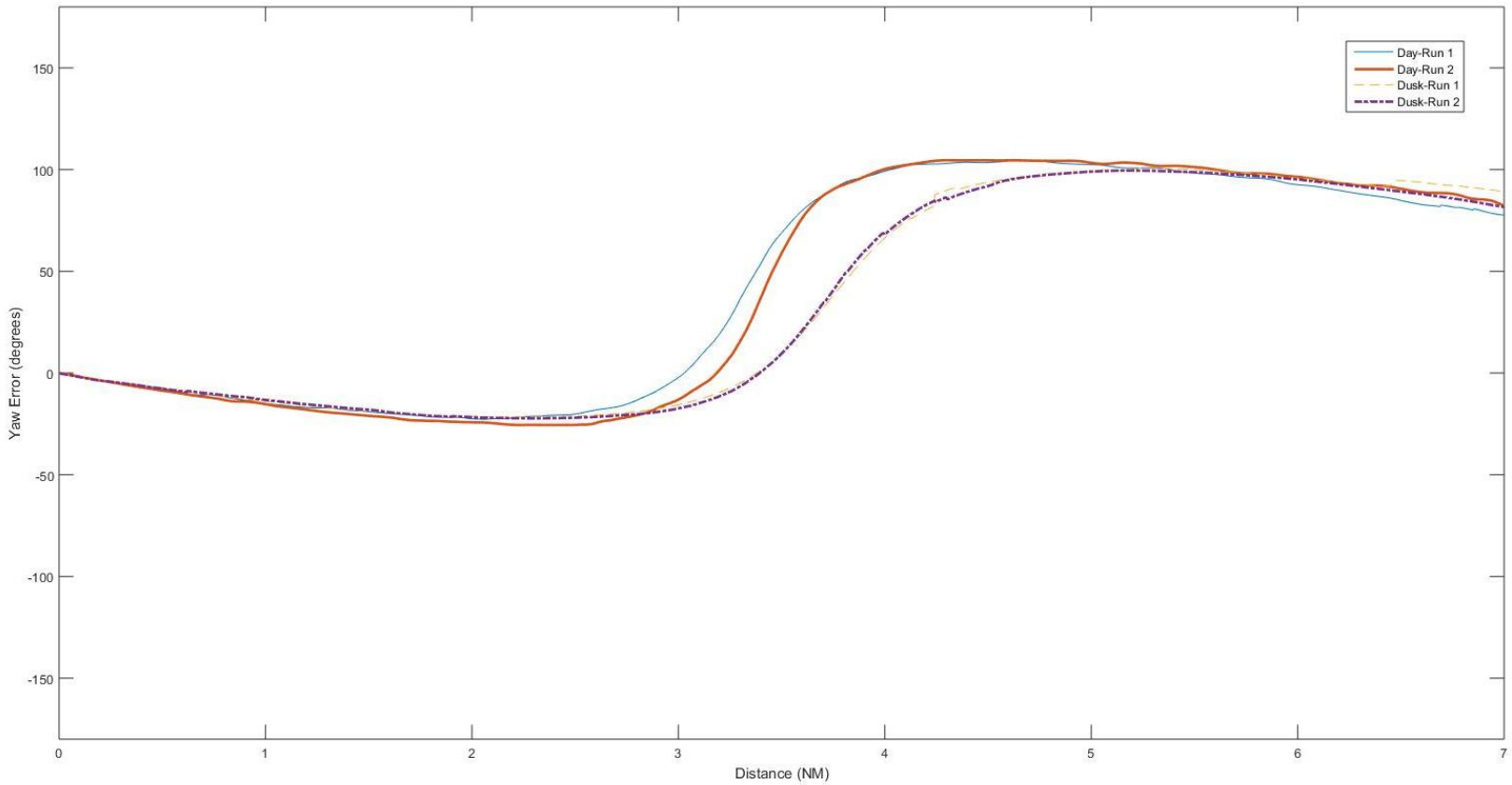

Figure B19 Dusk Lighting Effect on Yaw Angle Error Over 7 NM Run

Estimation Vertical Position Error from Representative Runs

LOSR: Medium
HAT: 4,000 ft ± 500 ft
KGS: 300 ± 30

Test Dates: 10 Sep – 18 Sep 2020
Run Length: 7 NM
Terrain: Sagebrush

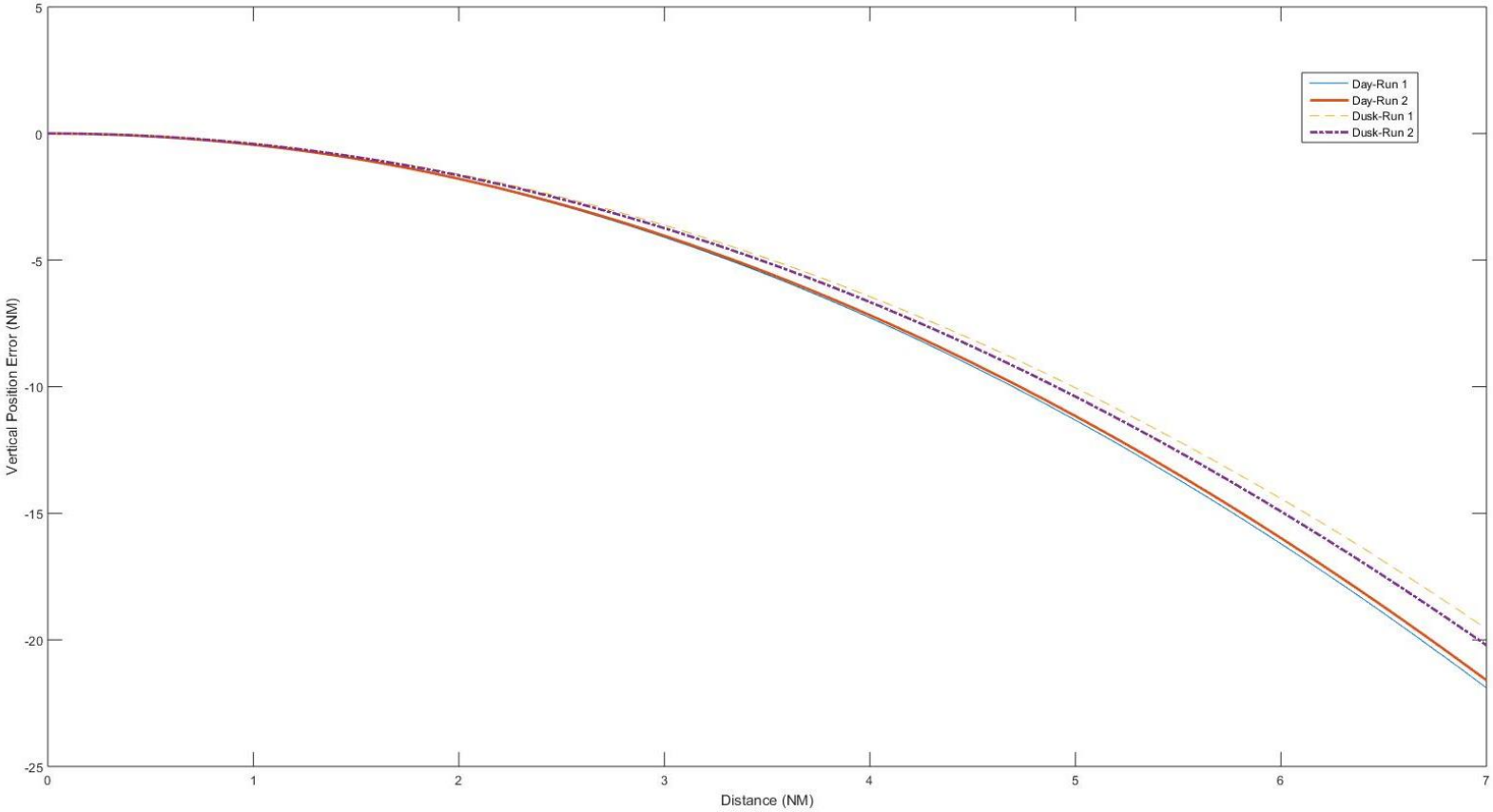

Figure B20 Dusk Lighting Effect on Vertical Position Error Over 7 NM Run

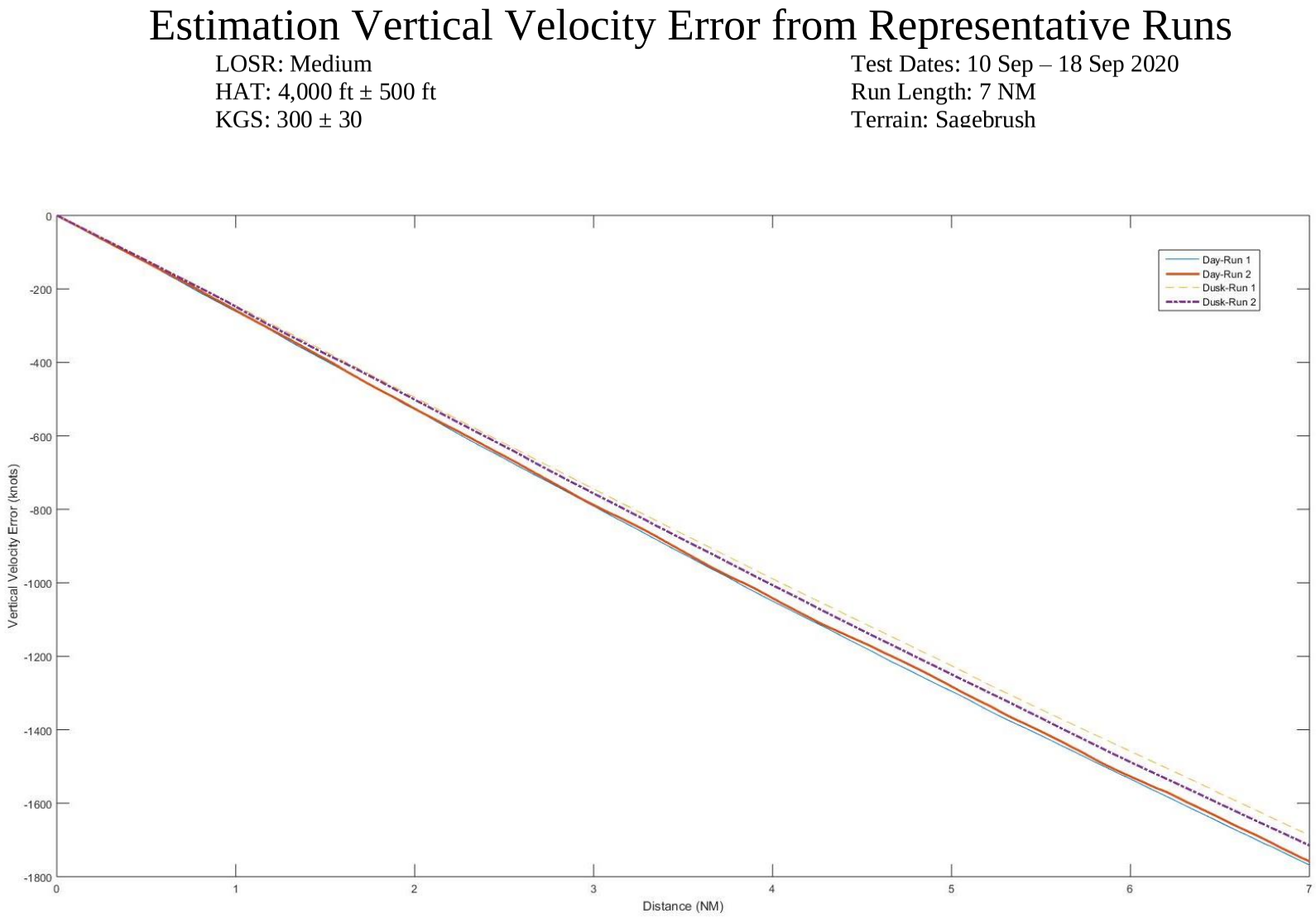

Figure B21 Dusk Lighting Effect on Vertical Velocity Error Over 7 NM Run

Estimation Lateral Position Error from Representative Runs

LOSR: Medium
HAT: 4,000 ft ± 500 ft
KGS: 300 ± 30

Test Dates: 9 Sep – 18 Sep 2020
Run Length: 7 NM
Terrain: Urban

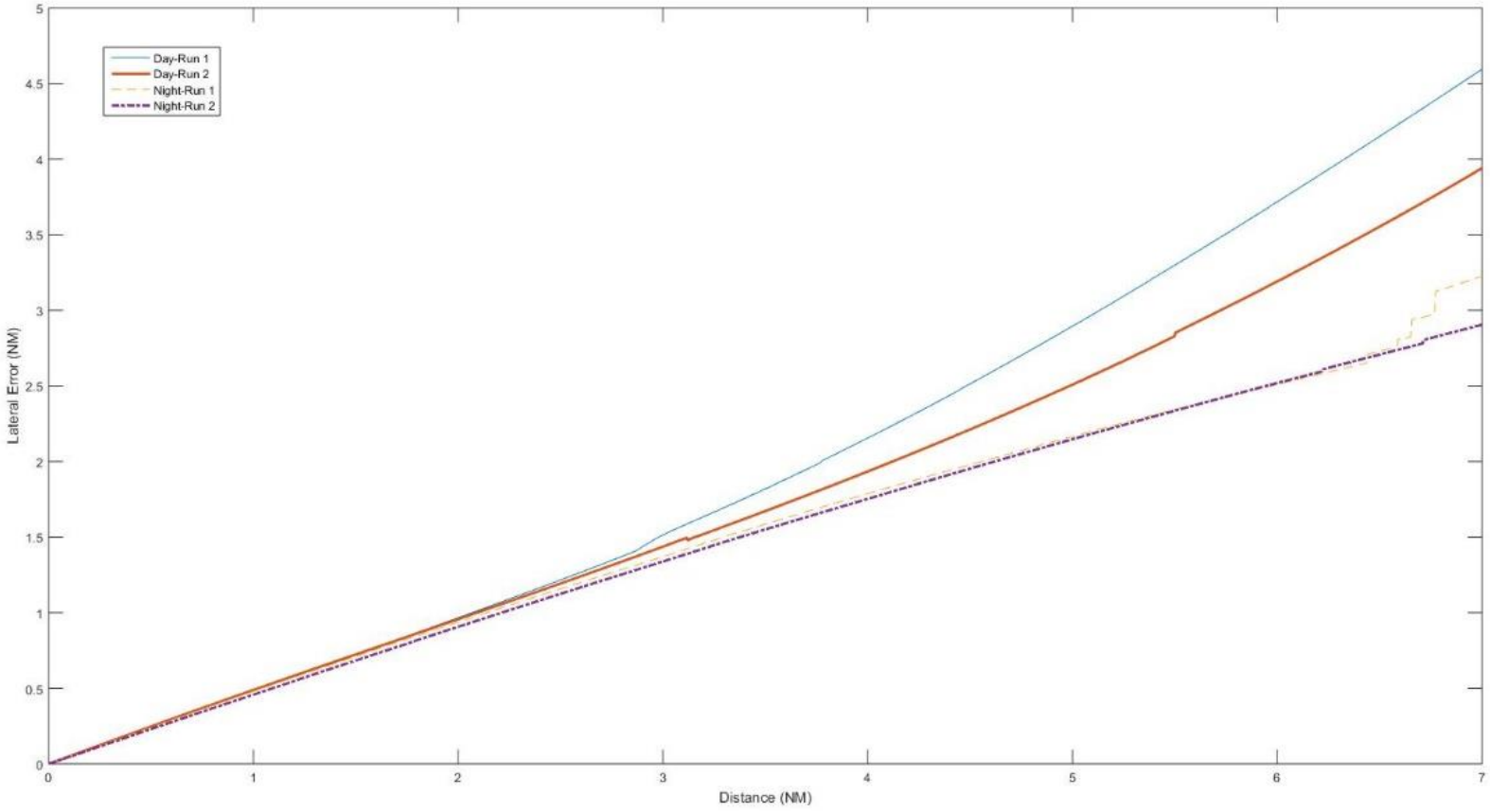

Figure B22 Night Lighting Effect on Lateral Position Error Over 7 NM Run

Estimation Lateral Velocity Error from Representative Runs

LOSR: Medium
HAT: 4,000 ft ± 500 ft
KGS: 300 ± 30

Test Dates: 9 Sep – 18 Sep 2020
Run Length: 7 NM
Terrain: Urban

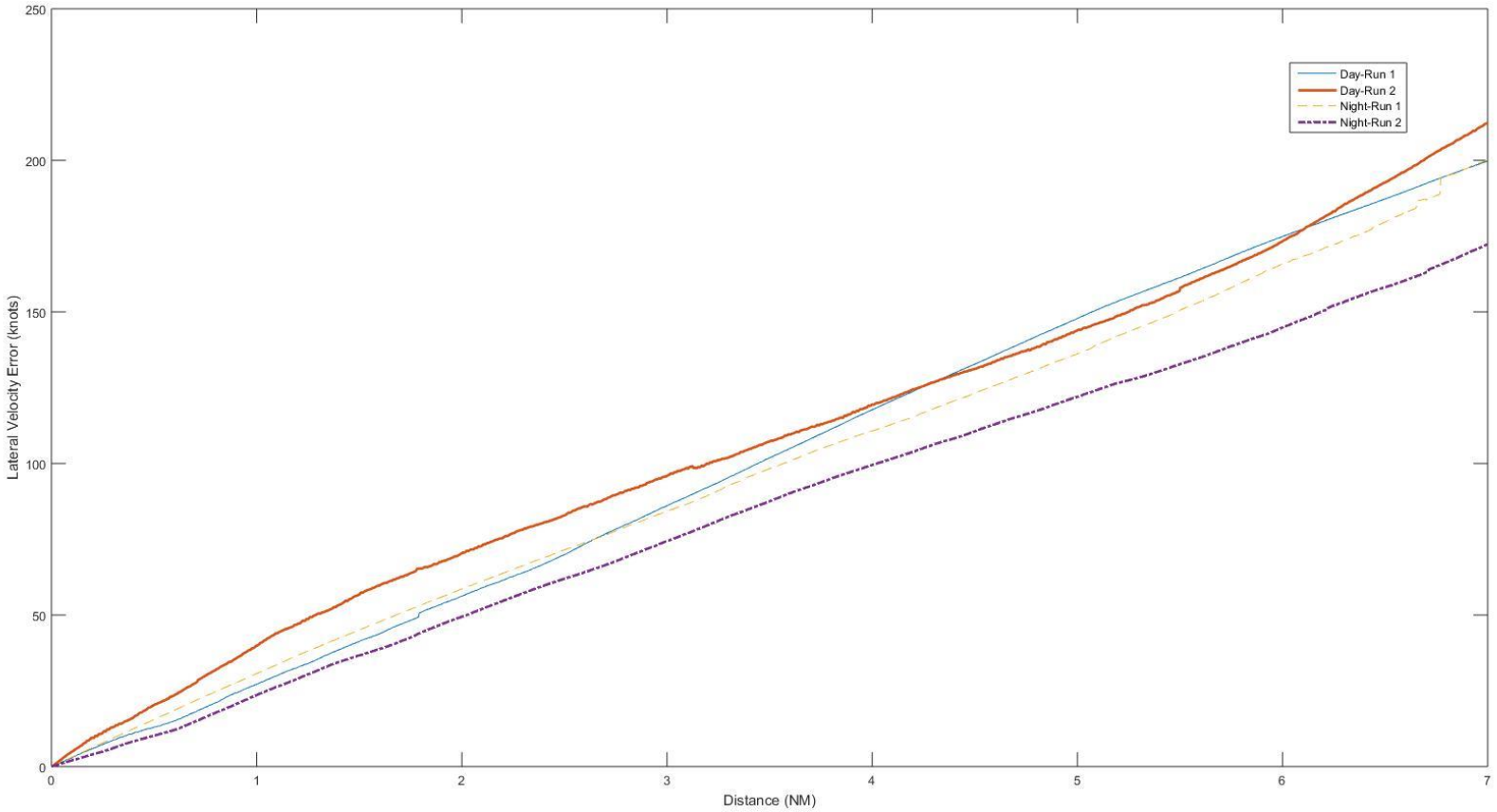

Figure B23 Night Lighting Effect on Lateral Velocity Error Over 7 NM Run

Estimation Pitch Angle Error from Representative Runs

LOSR: Medium
HAT: 4,000 ft ± 500 ft
KGS: 300 ± 30

Test Dates: 9 Sep – 18 Sep 2020
Run Length: 7 NM
Terrain: Urban

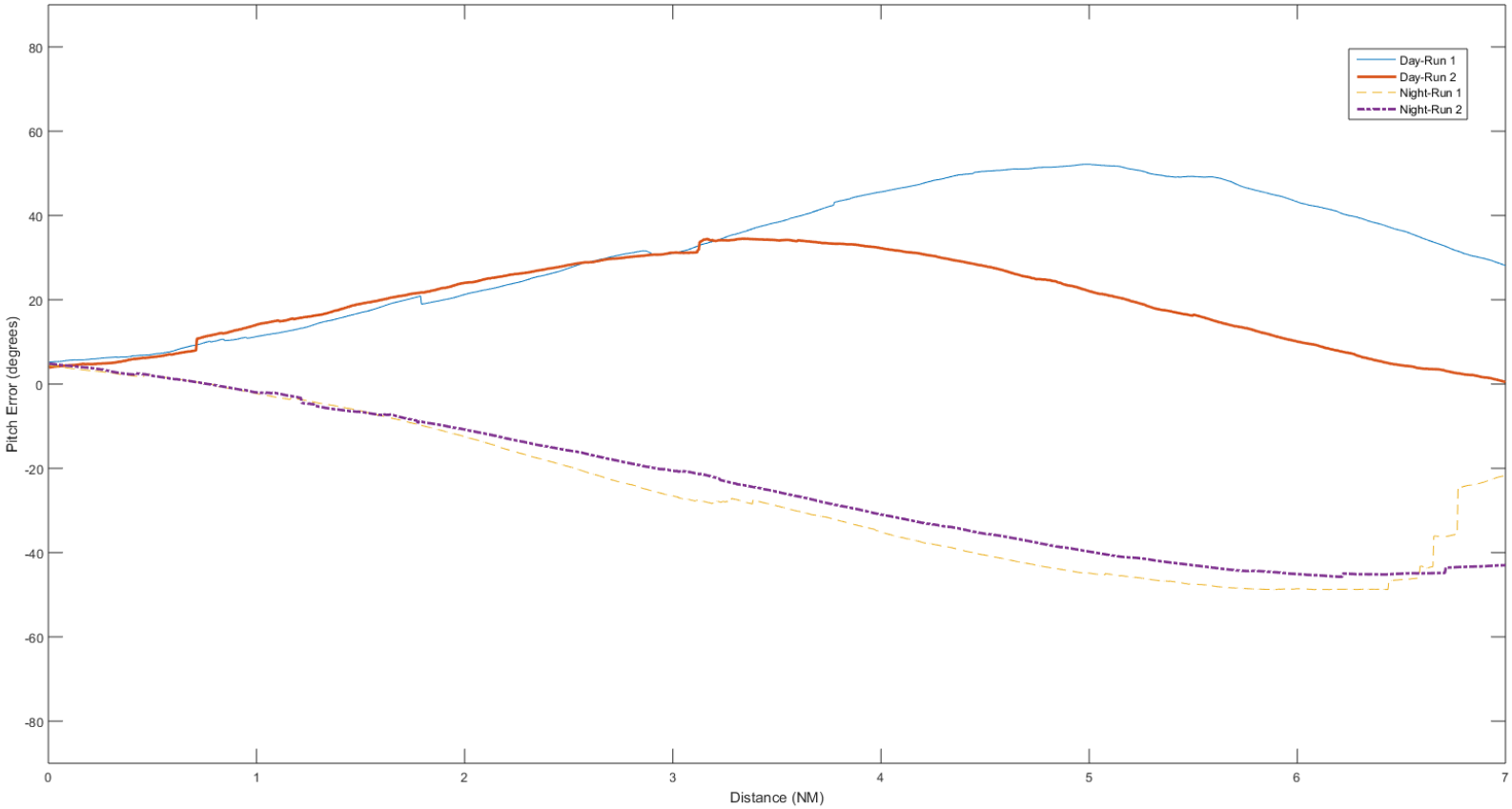

Figure B24 Night Lighting Effect on Pitch Angle Error Over 7 NM Run

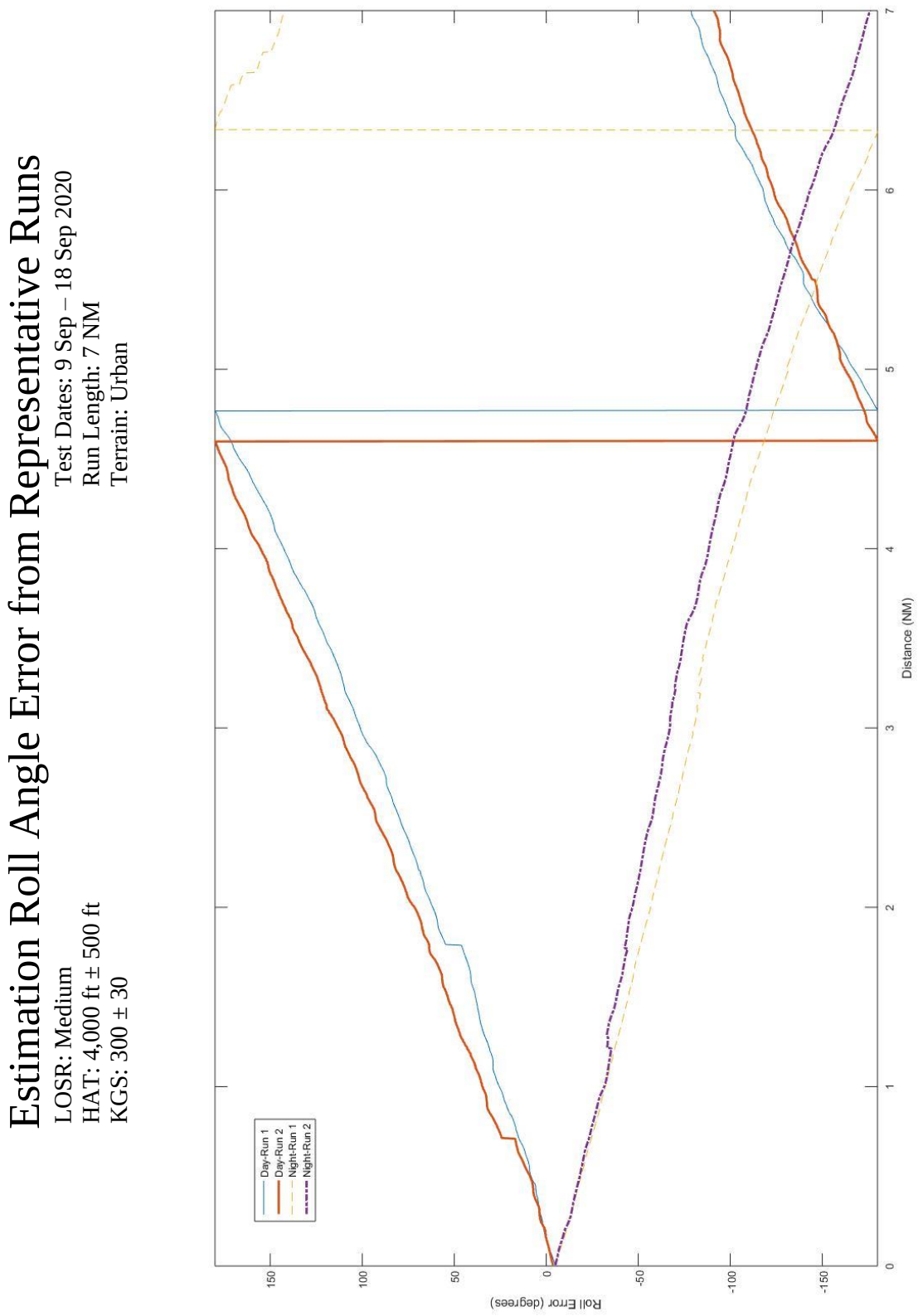

Figure B25 Night Lighting Effect on Roll Angle Error Over 7 NM Run

Estimation Yaw Angle Error from Representative Runs

LOSR: Medium
HAT: 4,000 ft ± 500 ft
KGS: 300 ± 30

Test Dates: 9 Sep – 18 Sep 2020
Run Length: 7 NM
Terrain: Urban

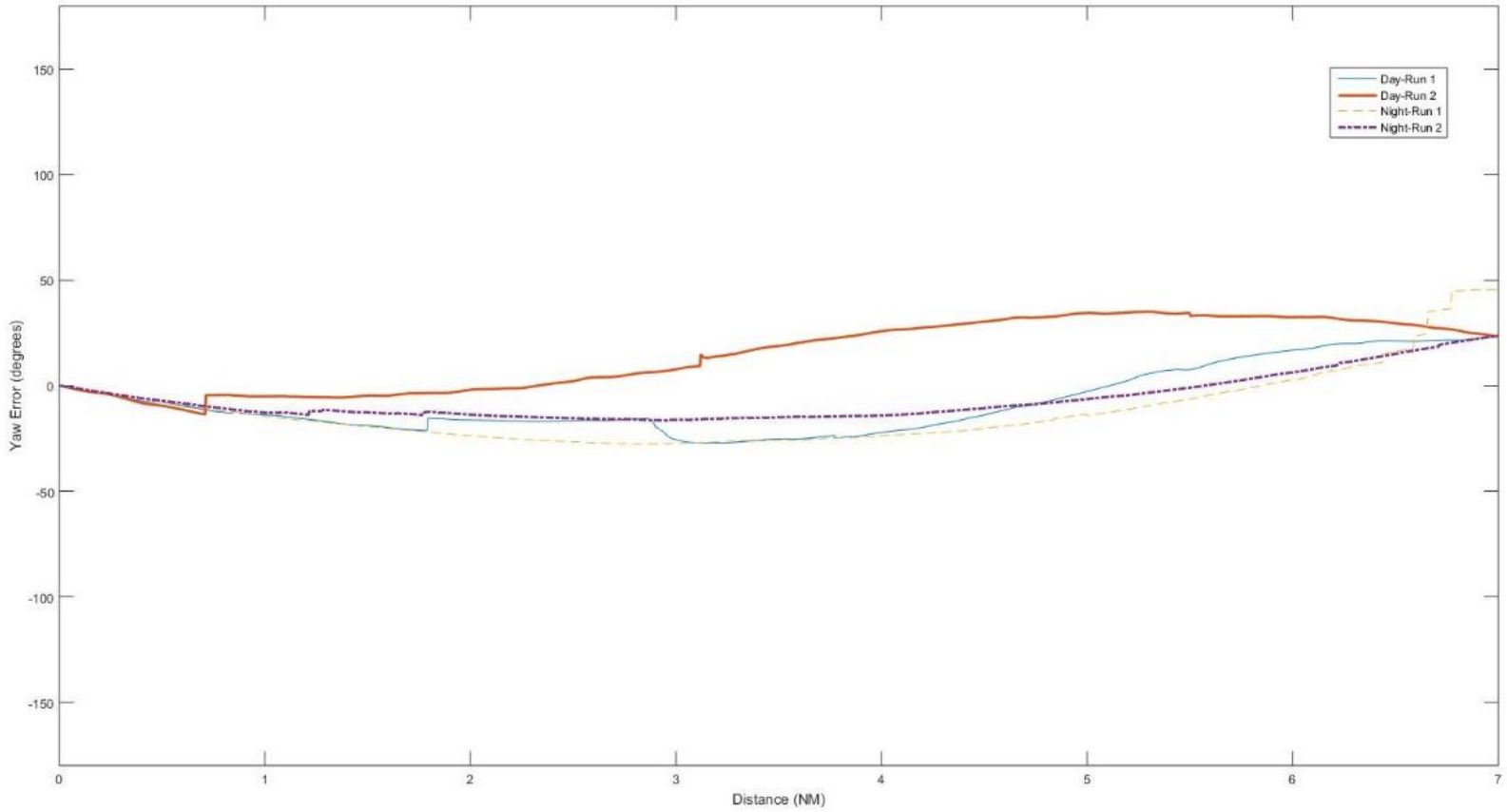

Figure B26 Night Lighting Effect on Yaw Angle Error Over 7 NM Run

Estimation Vertical Position Error from Representative Runs

LOSR: Medium
HAT: 4,000 ft ± 500 ft
KGS: 300 ± 30

Test Dates: 9 Sep – 18 Sep 2020
Run Length: 7 NM
Terrain: Urban

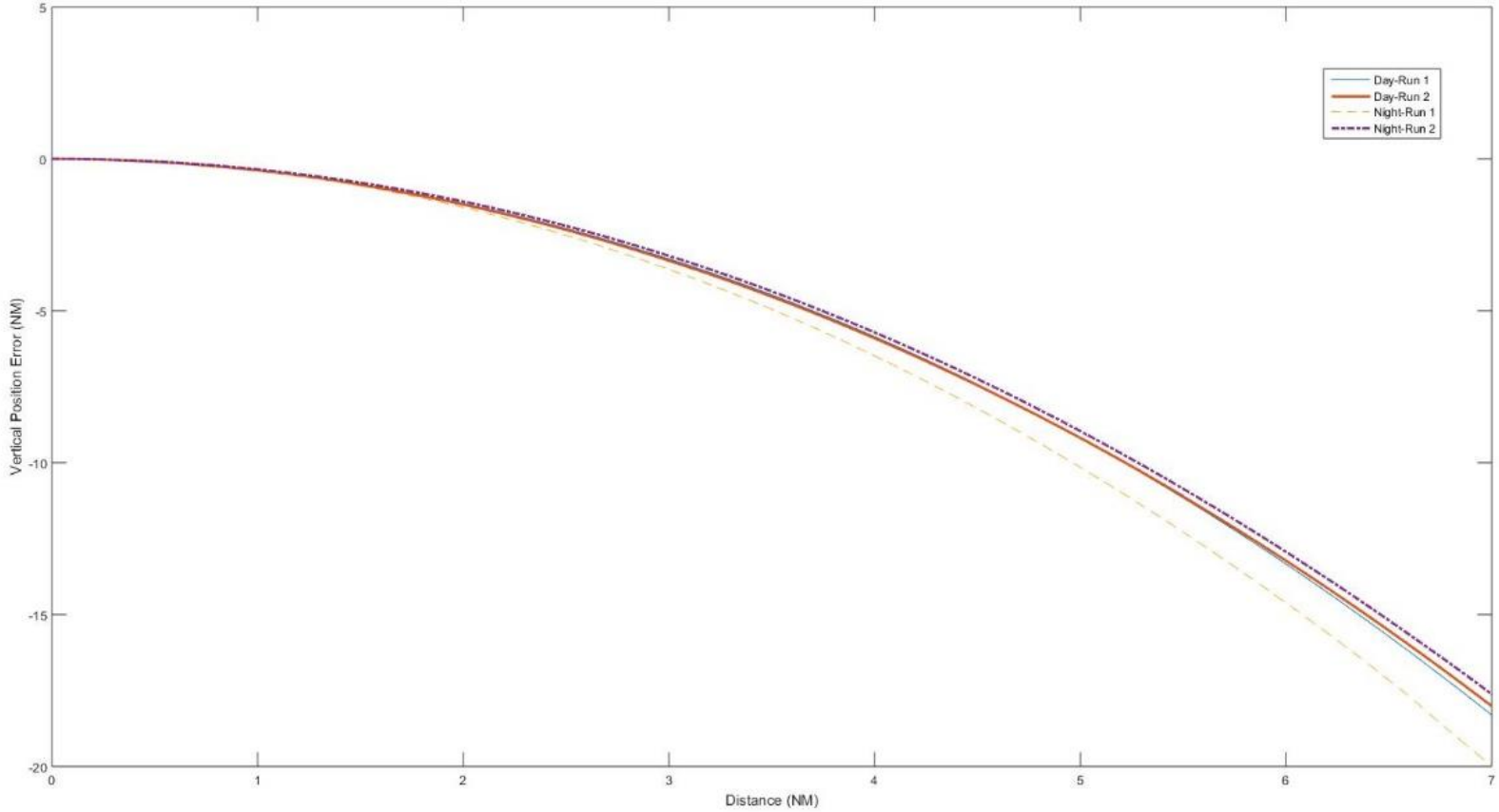

Figure B27 Night Lighting Effect on Vertical Position Error Over 7 NM Run

Estimation Vertical Velocity Error from Representative Runs

LOSR: Medium
HAT: 4,000 ft ± 500 ft
KGS: 300 ± 30

Test Dates: 9 Sep – 18 Sep 2020
Run Length: 7 NM
Terrain: Urban

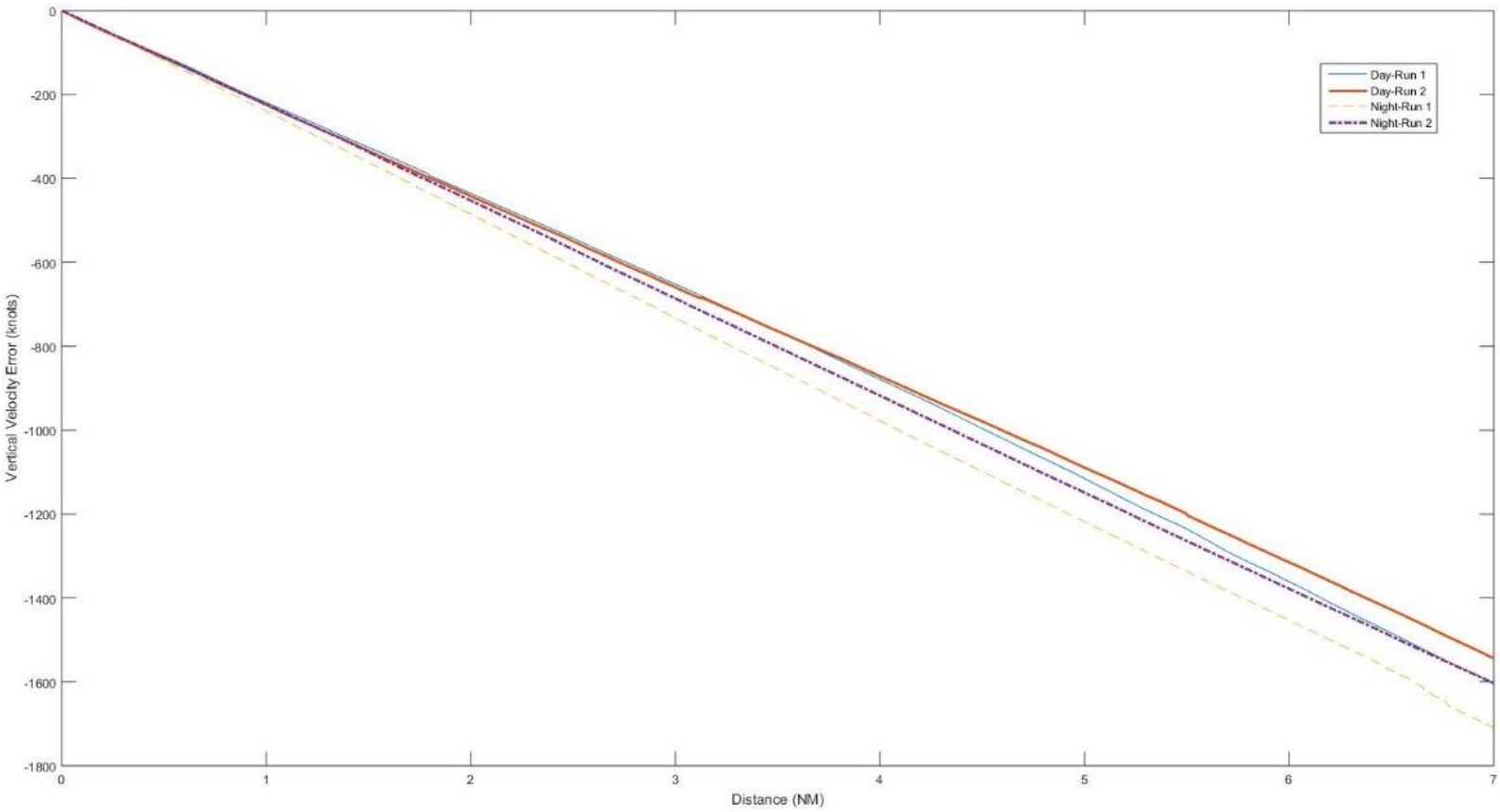

Figure B28 Night Lighting Effect on Vertical Velocity Error Over 7 NM Run

Estimation Lateral Position Error for Operationally Representative Scenario

Run Length: 43 min Test Date: 11 Sep 2020

Airspace: Sidewinder Low-Level Route

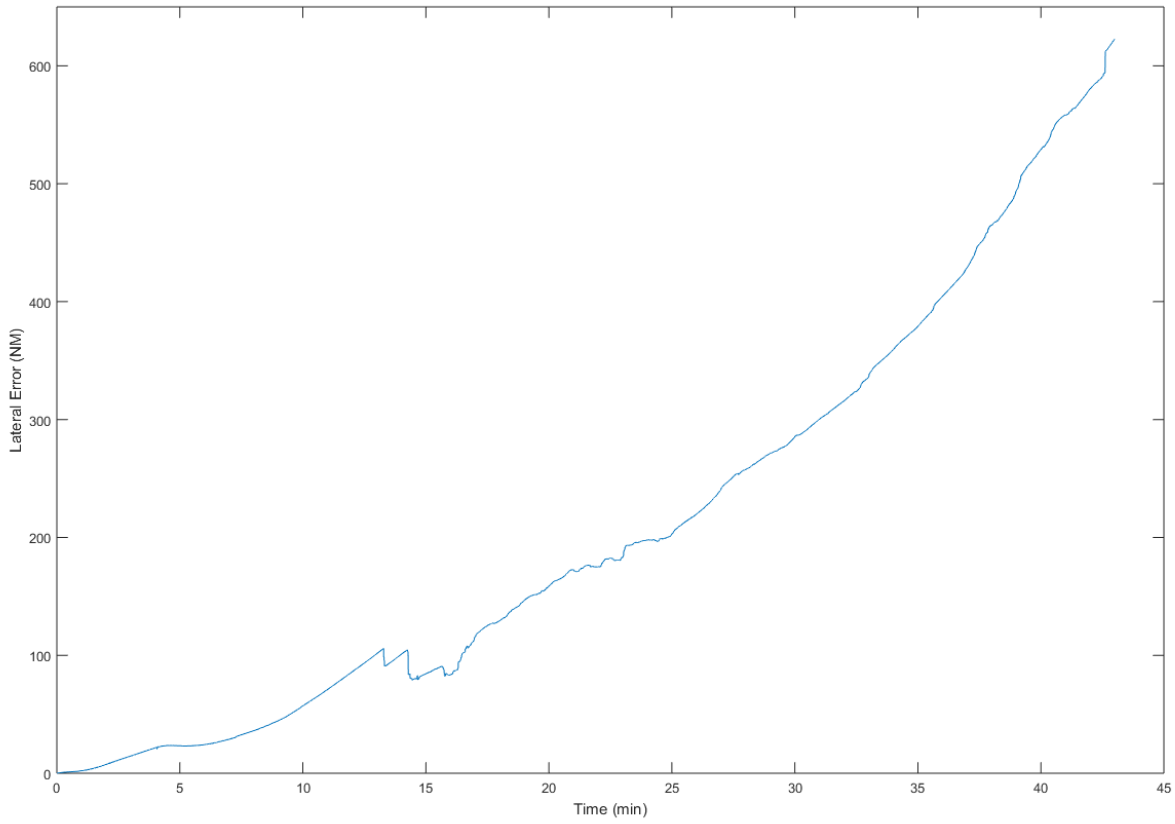

Figure B29 Operational Profile Lateral Position Error

Truth and Estimation Position for Operationally Representative Scenario

Run Length: 43 min Test Date: 11 Sep 2020

Airspace: Sidewinder Low-Level Route

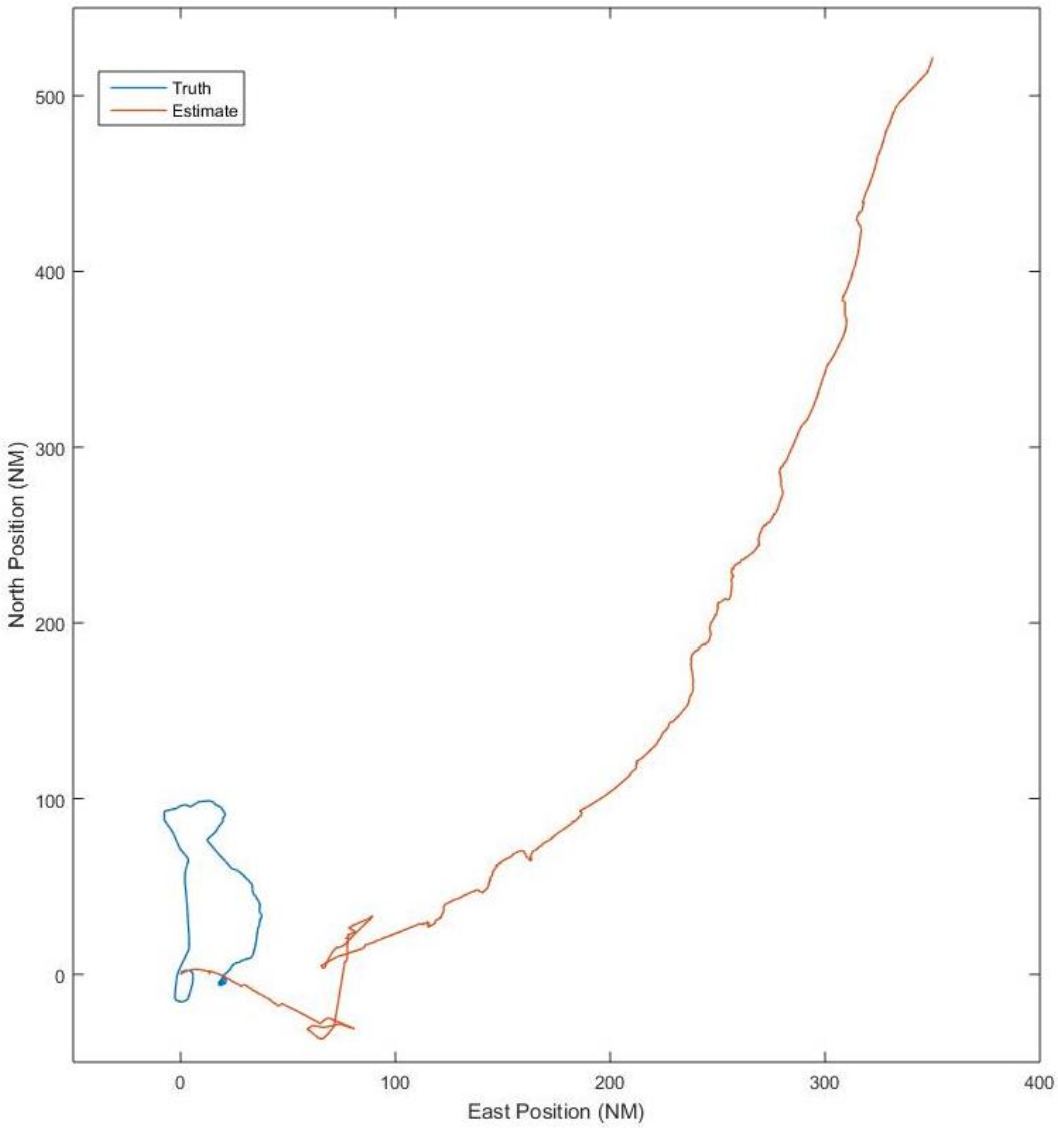

Figure B30 Approximate Position Truth (blue) and Estimate (red) for 43 min Operationally Representative Scenario

APPENDIX C – LESSONS LEARNED

Have a spare aircraft plan. If the initial plan only sources one aircraft, prepare a backup contingency option due to the very limited fly window. For projects with SUT connections to the F-16 cockpit, only two tails had Ethernet to the cockpit. The Getac tablet was planned for FTE control and status monitoring of the pod, but when aircraft maintenance issues drove the project to a different tail the contingency plan to startup of the sensors and verify IMU alignment by connecting to the pod externally was executed.

Plan ground checkout with the customer on site. The customer likely knows the system better than the test team and will provide value added during the ground checkout/EMIC that may prevent additional work from having to be accomplished.

Our RASCAL pod required a complete reconstruction when it arrived from the customer and increased the cost from SI four-fold. This was primarily driven by customer inexperience with airworthiness requirements, leading to inadequate wiring shielding and internal hardware mounting. If a customer is going to build the pod inner workings offsite, send example pod configurations and airworthiness requirements.

A standard TPS SI removable media tray for RASCAL pod should be included on all RASCAL pod builds. Since the SUT hard drive was not removable data download required ~30 mins of ground power after each flight to transfer via Ethernet. This delayed data processing as well as kept maintenance from working on the jet for 30 minutes after each flight.

If using CRIIS - CRIIS requires control room contact, include a frequency (dedicated mission or TPS ops) in scheduling load. Work with the schedulers to include this on the daily schedule.

The TSPI office delivers data via physical disc. Include all team members on the email requesting pickup; otherwise, the CD may be inaccessible until the single member who emailed TSPI can check for the lockbox code, delaying data processing.

Air-to-ground communications via handheld VHF radio requires extra coordination with frequency management for civil band frequency and communications quality was extremely poor with an F-16D on this test. A UHF radio may be preferable for direct aircraft communication to ground targets, if required.

Processing time was a huge factor for this project. Data intensive projects should invest in solid state disks for analysis lab computers as traditional hard drives were a computational bottleneck.

The time source format was inconsistent between data sources. Find out what time the system is using (Unix vs. GPS vs. UTC) so your post-processing data is appropriately synchronized.

Incorporate 3D modeling (e.g. Google SketchUp) for field of view analysis and flight test technique planning. This was extremely valuable for predicting flight paths and test points/orientations needed for field of view checks.

The SUT algorithm generated intermediate outputs which were useful in collecting information which was useful for SUT diagnosis. The area without intermediate outputs was the feature tracking within the Kalman filter. This limited the ability to diagnose system performance. Intermediate information outputs should be collected between each step of the data processing flow to gain diagnostic insight.

This page was intentionally left blank.

APPENDIX D – RASCAL POD/HAVE T-REX CONFIGURATION

The photos below were taken of the Have T-Rex RASCAL pod during Special Instrumentation rebuild. The photos show how the RASCAL pod was rebuilt into an airworthy condition and demonstrate the camera(s), processors, and data transfer modules were put together.

Figure D1 Have T-Rex on SI stand

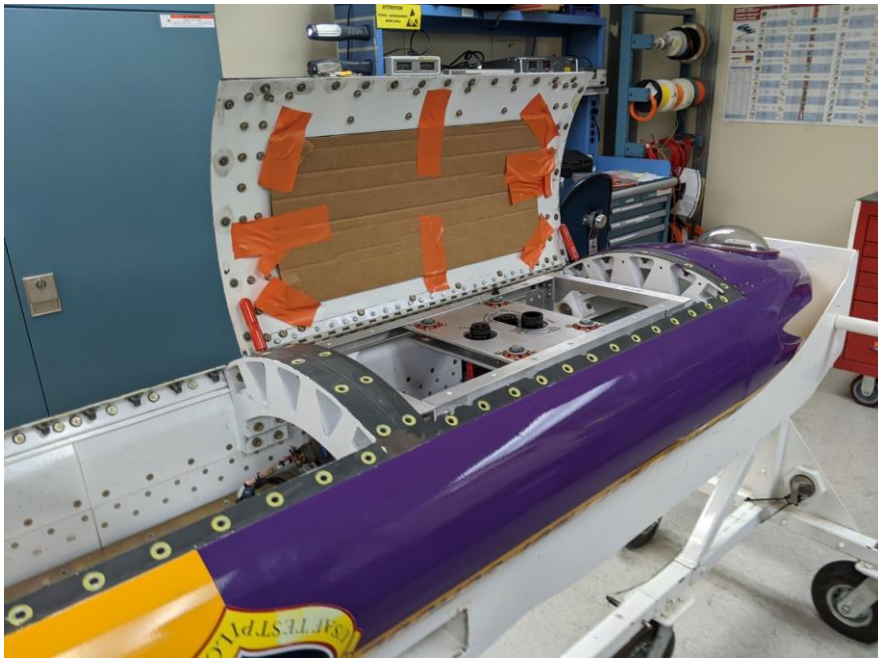

Figure D2 Have T-Rex with Panels Removed

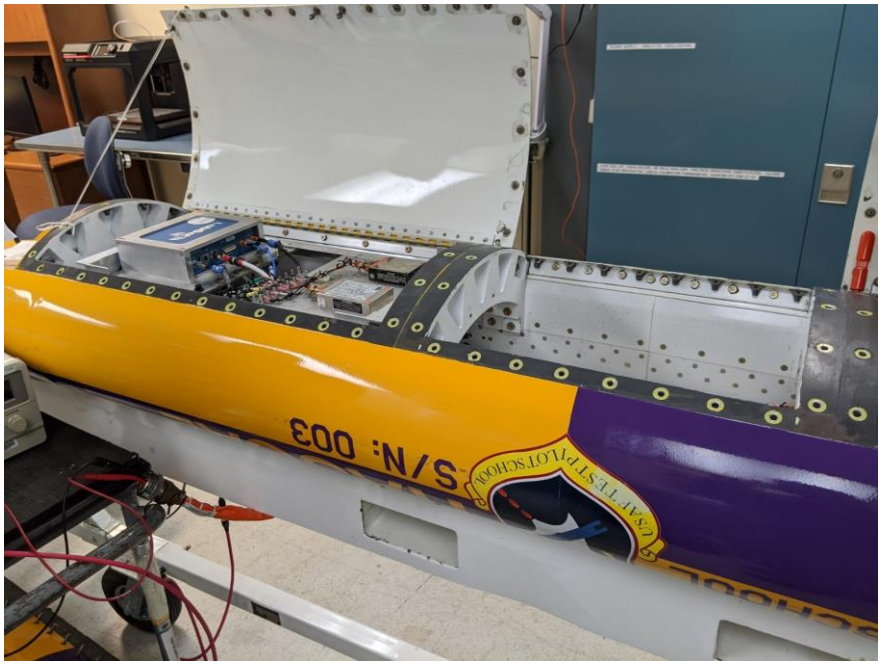

Figure D3 Have T-Rex Panel Removed LabSat

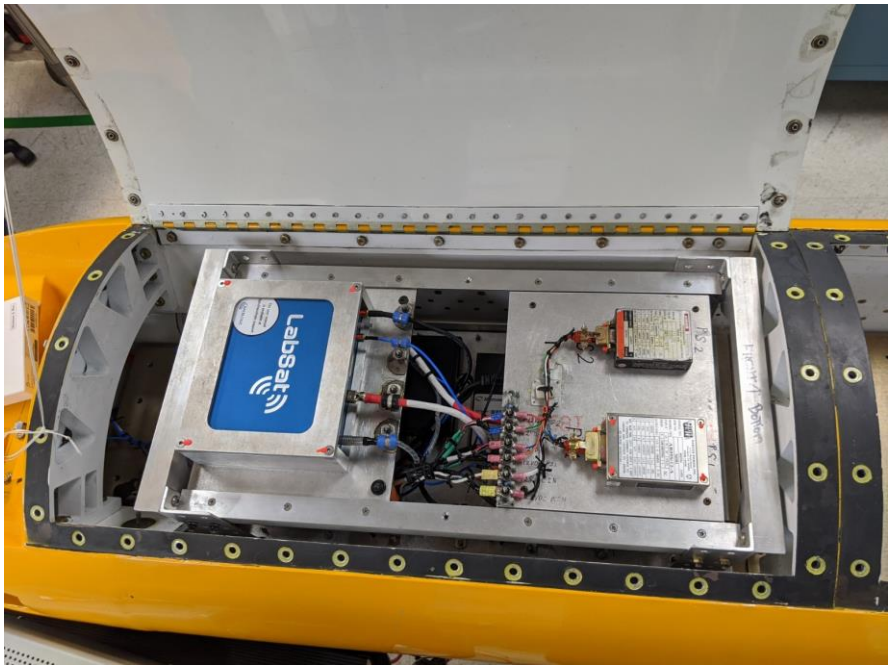

Figure D429 LabSat Top View

Figure D5 LabSat Side View

Figure D6 LabSat and Power Overhead

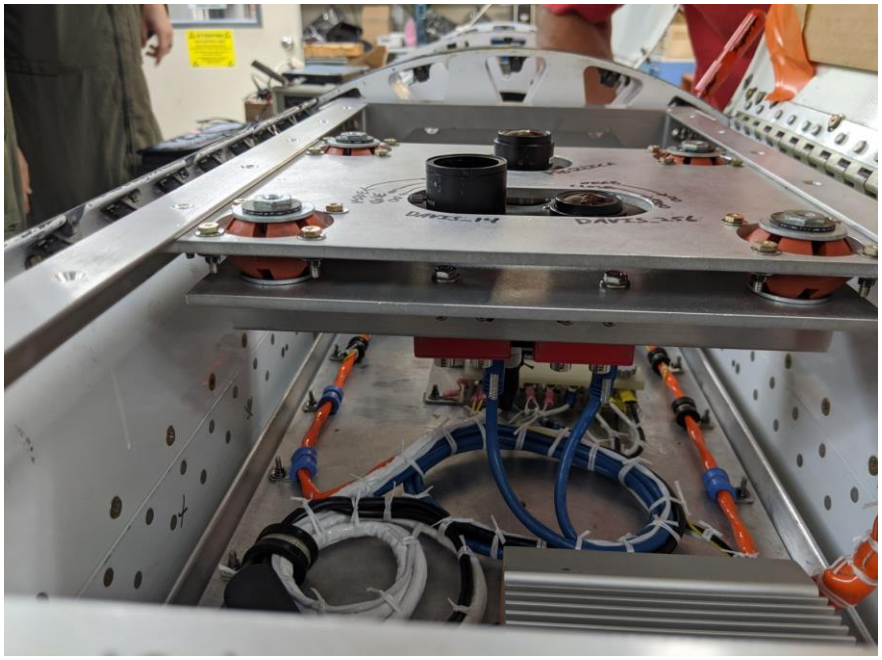

Figure D7 Camera Side Views

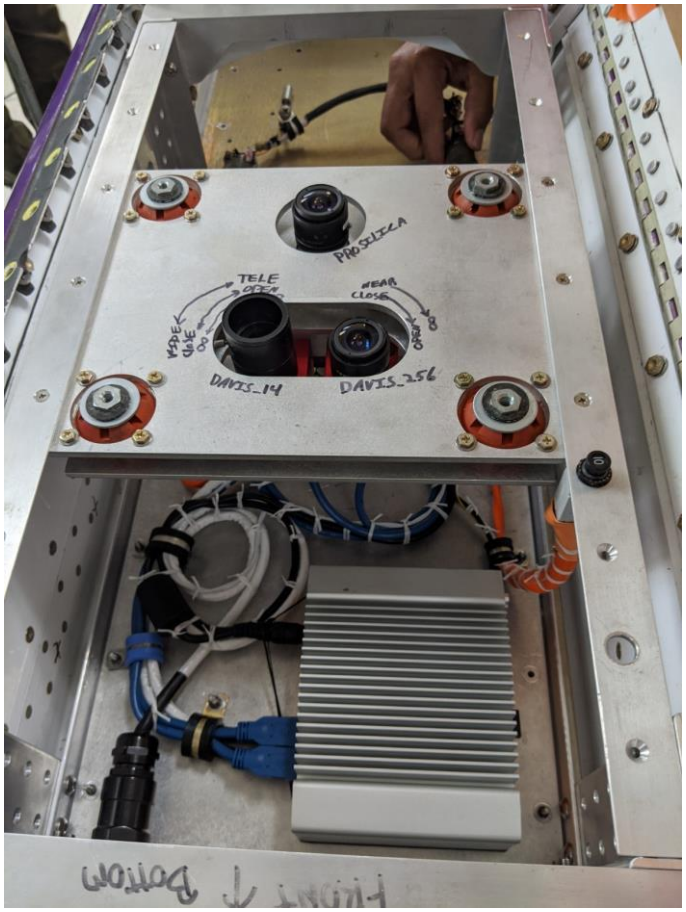

Figure D8 Cameras Overhead View

Figure D9 Camera with Rest of Pod in View

Figure D10 Processor

Figure D11 Power Supply Units

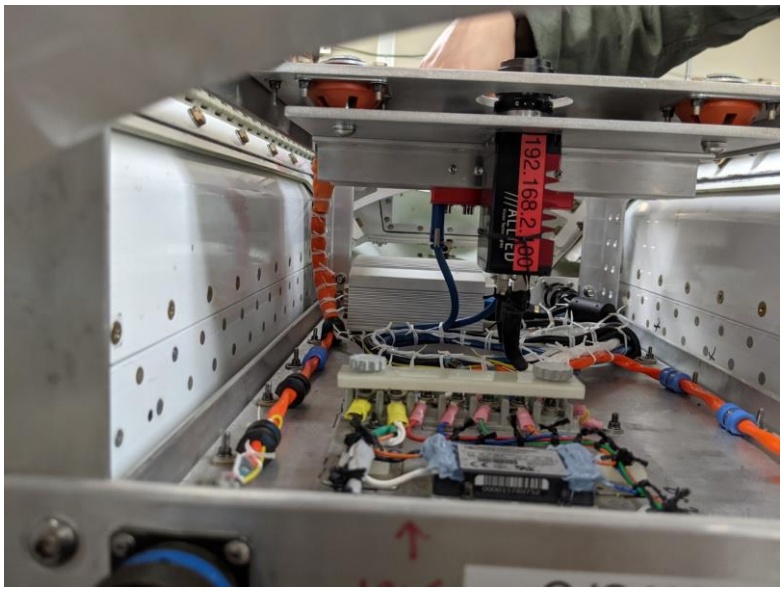

Figure D1230 Camera Bottom Views

APPENDIX E - DIGITAL APPENDIX

Actual test flight data are available on three external hard drives located at AFIT in the ANT Center, with mirrored backups existing locally at TPS. The files are compiled within a folder hierarchy as defined below, with specific test point runs grouped by flight number, test point number, and sequential numbering of similar runs. Each hard drive also contains a master spreadsheet for quick look-up of flight data specific run information. Folder structure for each external hard drive consisted of:

havetrexX/ (X: hard drive #2-4, #1 used for transfer only)
- Master Data Log V2.xlsx (master data log copy and flight data summary)

↳ flightXX/ (XX: flight #1-13)
- ↳ flightXX_TPYY_RunZ/ (YY: test point profile run # 1-27; Z: sequential)
  - ↳ out/ (result files required for plotting data)
  - ↳ reconstruction/ (reconstructed .png frames)
    - eventvideo.txt (log of all EBS events)
    - flightXX_TPYY_RunZ (run-specific trimmed LCM log file)
    - imu.csv (run-specific trimmed SUT IMU data)
    - truth.csv (run-specific trimmed TSPI data)
  - tps_lcm_log_# (2GB LCM log files)
  - flight# (concatenated 2GB LCM log files for full flight)
- flightXX.csv (log of Unix event timestamps/quicklook)
- Flt#_ARDS_Date_377.csv (supplied ARDS TSPI data)
- Date TRex Flight XX.csv (DAS data)
- flightXXdyn.csv (log of Unix event timestamps for dynamic runs)
- novatel*.* (IMU/GPS status message log)

Table E1 Data Location and Availability

Flight	Hard Drive Location	DAS	ARDS TSPI	Tgt TSPI	Unix Event Timestamps	LCM Logs	Data Comments
1	havetrex2	X	X	NR	X	X	
2	havetrex2	X	*	NR	X	X	
3	havetrex2	X	X	X	X	X	
4	havetrex2	X	X	NR	X	X	
5	havetrex3	X	X	NR	X	X	
6	havetrex3	X	X	NR	X	X	
7	havetrex3	X	X	NR	X	X	SUT hard drive ran out of space, several runs missed
8	havetrex3	X	X	NR	X	X	
9	havetrex4	X	X	X	X	X	
10	havetrex4	X	X	NR	X	X	
11	havetrex4	X	X	NR	X	X	

12	havetrex4	X	X	NR	X	X	
13	havetrex4	X	X	**	X	X	Narrow FOV EBS camera obscured and not available

X - data available
* - data not available post flight (corrupted or inoperative)
NR - data not required

Lightweight Communications and Marshalling (LCM) Data Structure Description:
The SUT recorded sensor data in the LCM log file format as described at https://lcm-proj.github.io/log_file_format.html. Data streams from various sources are combined in a single file with individual time tagged channels described below in table D2.

Table E2 LCM Channel Descriptions

Channel Name	Channel Description
/NOVATEL/imu	IMU lateral and angular accelerations **(used for SUT navigation estimate)**
/NOVATEL/observables	GPS status, time, satellites in the field of view
/NOVATEL/position	GPS latitude, longitude, altitude
/NOVATEL/pva	Novatel GPS/IMU blended position/velocity/acceleration solution
/NOVATEL/velocity	Novatel IMU derived velocities
SDM://RASCAL_POD/DAVIS_14/0000.0/EVENTS	Narrow field of view EBS event stream **(used for SUT target data collection)**
SDM://RASCAL_POD/DAVIS_14/2002.0/IMU	Narrow field of view EBS accelerometer data
SDM://RASCAL_POD/DAVIS_14/2004.0/GRAYSCALE_IMAGE	Narrow field of view EBS camera traditional frame-based image
SDM://RASCAL_POD/DAVIS_256/0000.0/EVENTS	Wide field of view EBS event stream **(used for SUT navigation estimate)**
SDM://RASCAL_POD/DAVIS_256/2002.0/IMU	Wide field of view EBS accelerometer data
SDM://RASCAL_POD/DAVIS_256/2004.0/GRAYSCALE_IMAGE	Wide field of view EBS camera traditional frame-based image
SDM://RASCAL_POD/PROSILICA_GT1290/2004.0/image	Wide field of view traditional frame-based camera

APPENDIX F – SUT HARDWARE SPECIFICATIONS

DAVIS Specifications

Camera Specifications – Current Models

	DAVIS346
Picture	
Resolution	346 x 260
Time resolution	1 µs
Frames	Greyscale, simultaneous output
Optics	CS-mount
Host Connection, Power source	USB 3.0 micro
Bandwidth	12 MEPS
Software	jAER and cAER
Power consumption	with/without APS: 130/120 mA
Dimensions [mm]	H 40 x W 60 x D 25
Weight	100 g without lens
Hardware camera sync	Yes
IMU	Yes
Special features	4 side mounting points, Anodized aluminum casing
Tripod mount	Whitworth 1/4"-20 female

Sensor Specifications – Current Models

	DAVIS346
APS / shutter type	Yes – global or rolling shutter
CMOS technology	0.18 µm 1P6M MIM CIS
Chip size [mm]	8 x 6
Pixel size [µm]	18.5 x 18.5
Array size [mm]	6.4 x 4.8
Fill factor	22%
Pixel complexity	48 transistors, 2 capacitors, 1 buried photodiode with micro-lens
DVS Interface[2]	10-bit word-serial AER
Supply voltage	1.8 V and 3.3 V
Power (chip only) [3]	High activity: 30 / 170 mW Low activity: 10 / 150 mW
Dynamic range	DVS: 120 dB (~1 lux[4]); APS: 56.7 dB
Min. contrast sensitivity	14.3% (on), 22.5% (off)
FPN	APS: 4.2 %
Max. bandwidth	DVS: 12 MEPS (CPLD) APS: 40 FPS (higher in bright lighting)
Min. latency	~ 20 us[5]
Photodiode dark current at room temperature	2.88 fA (3.8nA/cm^2)
APS dark signal	18000 e^-/s
APS readout noise	55 e^-

[1] Frame output for DVS240 devices available in calibration mode only: this mode operates independently to event mode

[2] Device AER pin-outs are no longer available for current device models

[3] Power is quoted for a standard set of biases; it is possible to increase or reduce these figures according to biasing needs. In general, faster responses require higher current usage.

[4] Minimum functional scene illumination is complex to quantify – enquire for more details

[5] Nominal figure; can be improved with strong lighting/optimised biases

Document version: 2019-10-16
Definition: EPS = Events per second

IMU-IGM-A1™

SPAN SYSTEM PERFORMANCE[1]

Horizontal Position Accuracy (RMS)

Single point L1/L2 NovAtel CORRECT™	1.2 m
» SBAS[2]	60 cm
» DGPS	40 cm
» PPP[3, 4]	4 cm
» RTK	1 cm + 1 ppm

Data Rates

IMU measurement	200 Hz
INS solution	Up to 200 Hz
Time Accuracy[5]	20 ns RMS
Max Velocity[6]	515 m/s

IMU PERFORMANCE[7]

Gyroscope Performance

Input range	±450 deg/sec
Rate bias stability	6 deg/h
Angular random walk	0.30 deg/√hr

Accelerometer Performance

Range	±18 g
Bias stability	0.1 mg
Velocity random walk	0.029 m/s/√hr

PHYSICAL AND ELECTRICAL

Dimensions	152 x 137 x 51 mm
Weight	475 g

Power

Input voltage	10-30 VDC
Power consumption[8]	2.5 W

Connectors

Main port and AUX port DB-HD15

COMMUNICATION PORTS

1 RS-232/RS-422 IMU data port
1 Wheel sensor port

Status LEDs

Power
GNSS status
INS status

ENVIRONMENTAL

Temperature	
Operating	-40°C to +65°C
Storage	-50°C to +80°C
Humidity	MIL-STD-810G 95% Non-condensing
Vibration (operating)	
Random	MIL-STD-810G (7.7 g)
Sinusoidal	IEC 60068-2-6 (5 g)
Bump	IEC 60068-2-27 (25 g)
Shock	MIL-STD-810G (40 g)
Immersion	IEC 60529 IPX7
Compliance	FCC, CE marking, Industry Canada

INCLUDED ACCESSORIES

- Combined power and data cable

OPTIONAL ACCESSORIES

- I/O and wheel sensor accessory cable
- Inertial Explorer post-processing software

OPTIONAL CONFIGURATION

Stackable with FlexPak6™ for a SPAN solution (shown)

For the most recent details of this product: www.novatel.com/products/span-gnss-inertial-systems/span-imus/span-mems-imus/imu-igm-a1/

novatel.com

sales@novatel.com

1-800-NOVATEL (U.S. and Canada) or 403-295-4900

China 0086-21-68882300

Europe 44-1993-848-736

SE Asia and Australia 61-400-883-601

PERFORMANCE DURING GNSS OUTAGES[9]

Outage Duration	Positioning Mode	POSITION ACCURACY (M) RMS		VELOCITY ACCURACY (M/S) RMS		ATTITUDE ACCURACY (DEGREES) RMS		
		Horizontal	Vertical	Horizontal	Vertical	Roll	Pitch	Heading
0 s	RTK[10]	0.02	0.03	0.020	0.010	0.035	0.035	0.150
	SP	1.00	0.60	0.020	0.010	0.035	0.035	0.150
	PP[11]	0.01	0.02	0.020	0.010	0.012	0.012	0.074
10 s	RTK[10]	0.46	0.13	0.100	0.021	0.072	0.072	0.210
	SP	1.41	0.70	0.100	0.021	0.072	0.072	0.210
	PP[11]	0.02	0.02	0.020	0.010	0.012	0.012	0.074

Version 8 Specifications subject to change without notice.

D17520 May 2016

Printed in Canada.

Statements related to the export of products are based solely on NovAtel's experience in Canada, are not binding in any way and exportability may be different with respect to the export regulations in effect in another country. The responsibility for re-export of product from a Customer's facility is solely the responsibility of the Customer.

1. Performance obtained when using an OEM6 Family receiver (contact NovAtel Sales for purchase information). For detailed receiver specifications, see NovAtel's OEM615 product sheet and Receiver brochure.
2. GPS-only.
3. Requires subscription to TerraStar data service. Subscriptions available from NovAtel.
4. An OEM628, OEM638, FlexPak6 or ProPak6 receiver is required.
5. Time accuracy does not include biases due to RF or antenna delay.
6. Export licensing restricts operation to a maximum of 515 metres/second.
7. Supplied by IMU manufacturer.
8. Typical, 12 V, 25°C, IMU only. System with FlexPak6 requires 5 W.
9. Outage performance information is applicable for firmware version OEM060240RN0000 and up.
10. 1 ppm should be added to all values to account for additional error due to baseline length.
11. Post-processing results using Inertial Explorer software.

APPENDIX G – ABBREVIATIONS, ACRONYMS, AND SYMBOLS

Abbreviation	Definition	Units
AFB	Air Force Base	---
AFIT	Air Force Institute of Technology	---
AGL	above ground level	ft
ANG	Air National Guard	---
ANT	Autonomy & Navigation Technology	---
AOB	angle of bank	°
ARDS	Advanced Range Data System	---
CRIIS	Common Range Integrated Instrumentation System	---
CD	compact disk	---
DAF	Department of the Air Force	---
DAS	Data Acquisition System	---
DGA	Délégation Générale pour l'Armement	---
DTIC	Defense Technical Information Center	---
EBS	event-based sensor	---
EMIC	electro-magnetic interference clearance	---
ETO	executing test organization	---
EVIO	event-based visual-inertial odometry	---
FOV	field of view	°
ft	feet	---
FTE	flight test engineer	---
G	acceleration due to gravity	m/s^2
GB	gigabyte	---
GPS	global positioning system	---
GUI	Graphical User Interface	---
HAT	height above terrain	ft
Hz	Hertz	---
IAW	in accordance with	---
IMU	Inertial Measurement Unit	---
IR	infrared	---
JON	job order number	---
KCAS	knots calibrated airspeed	---
KGS	ground speed	knots
LCM	Lightweight Communications and Marshalling	---
LDTO	Lead Development Test Organization	---
L_{long}	longitudinal distance in FOV	---
LOS	line of sight	---
LOSR	line of sight rate	---
m/s	meters per second	---
MTT	moving track target	---
NM	nautical mile	---
NR	not required	---
OPIR	overhead persistent infrared	---
PVI	Pilot-Vehicle Interface	---
RASCAL	Reconfigurable Airborne Sensor, Communications, and Laser	---
RCAF	Royal Canadian Air Force	---
RMSE	root mean square error	---
SALT	system altitude	ft

SI	Systems Integration	---
SRB	Safety Review Board	---
SUT	system under test	---
TFR	temporary flying restriction	---
TIM	Technical Information Memorandum	---
TMP	Test Management Project	---
TP	test plan	---
TPS	Test Pilot School	---
TSPI	Time, Space, Position Information	---
UAV	unmanned aerial vehicle	---
UHF	Ultra High Frequency	---
U.S.	United States	---
USAF	United States Air Force	---
USB	universal serial bus	---
UTC	Coordinated Universal Time	---
VHF	very high frequency	---
VO	visual odometry	---

APPENDIX H – FUTURE CONSIDERATIONS

This appendix offers some test team insights and informed speculation of relevant future considerations for an EBS-based SUT. This test program collected a rich data set of raw EBS imagery, TSPI, and IMU data that could support significant future development efforts without new or additional flight tests. The data and truth could be used to analyze new or improved algorithm performance. Additionally, sufficient data exists to train/re-train neural networks and still possess segregated data to be used for analysis.

The Microsoft Common Objects in Context 2014 computer vision dataset was inappropriate training for the SUT neural networks. As the SUT was exposed to almost entirely overhead aerial imagery, a more specific training dataset consisting of aerial imagery and feature imagery from overhead perspectives would be more appropriate. This may have led to significant error in the image reconstruction by the front end neural network. This may have been a contributing factor to the large navigation solution accuracy errors.

The SUT EBS cameras had fixed apertures that needed to be manually adjusted during different times of flight (day versus night). Highly recommend the use of a camera/lens that incorporates an automatic aperture. This would further increase camera performance and eliminate the need to open the pod while installed on the aircraft before and after night testing to ensure the sensor is not saturated at higher ambient lighting conditions.

Test planning originally focused on classifying LOSR into various bins for comparison, using combinations of HAT and GS to determine LOSR. This, however, may be limited by sensor resolution. During carriage on future platforms, and barring platform operating speed restrictions, varying LOSR solely by GS (i.e., at constant HAT across the LOSR spectrum) would minimize resolution factors.

MILITARY UTILITY

In its tested state, this system has no utility for current operations as a navigational source. The system accuracy did not provide a reliable source of navigation in any environment tested and showed significant error in position, velocity, and orientation. The system did not compute a navigation solution real-time, and required greater than 3:1 processing time (e.g. approximately 5 minutes was required to process 90 seconds of flight data). This system would not meet the warfighter's navigational requirements until real-time processing can occur and the accuracy can be improved significantly. Improvements to the algorithm and real-time processing must be completed before the utility can be re-evaluated.

The system under test collected data for future moving target tracking algorithm development. The system in its current state does not provide utility for any MTT capabilities due to the lack of a target tracking algorithm and the very close ranges required due to the camera/optics resolution; however, a higher resolution EBS could provide cueing for tracks further in range. This capability would allow for passive tracking of moving targets throughout the entire field of view. Infrared (IR) EBS would enable the same capabilities in the IR spectrum.

This page was intentionally left blank.

APPENDIX I – DISTRIBUTION LIST

Onsite Distribution	Number of Copies		
	E-mail	Digital	Paper
AFTC/HO 305 E Popson Ave Edwards AFB CA 93524-6502 Email: AF.HO.Mailbox@us.af.mil	1	0	0
Edwards AFB Technical Research Library Attn: Mr. Darryl Shiplett 307 E Popson Ave Edwards AFB CA 93524-6600	0	1	0
Air Force Test Center Executive Director Attn: Ms. Eileen Bjorkman 1 S Rosamond Blvd Edwards AFB CA 93524 Email: eileen.bjorkman.1@us.af.mil	1	0	0
USAF TPS/CT Attn: Mr. David Vanhoy 220 S Wolfe Ave Edwards AFB CA 93524	0	0	1
Offsite Distribution			
Defense Technical Information Center Attn: DTIC-O 8725 John J. Kingman Rd, Ste 0944 Ft Belvoir, VA 22060-6217 Email: Jackie.L.Rike.civ@dtic.mil	1	0	0
Air Force Institute of Technology Attn: Dr. Robert Leishman 2950 Hobson Way Wright-Patterson Air Force Base, OH 45433-7765 Email: robert.leishman@us.af.mil	1	0	0
Total	4	1	1

This page was intentionally left blank.